RUSSIAN ACADEMY OF SCIENCE
FEDERAL AGENCY ON EDUCATION OF RUSSIAN FEDERATION
RUSSIAN NATIONAL COMMISSION FOR UNESCO
COMMITTEE ON SCIENCE AND HIGHER EDUCATION OF THE GOVERNMENT OF SAINT-PETERSBURG
COUNCIL OF RECTORS OF SAINT-PETERSBURG HIGHER EDUCATION ESTABLISHMENTS
SAINT-PETERSBURG STATE UNIVERSITY OF AEROSPACE INSTRUMENTATION (SUAI)
UNESCO CHAIR “DISTANCE EDUCATION IN ENGINEERING” OF SUAI
RUSSIAN SECTION OF THE INTERNATIONAL SOCIETY OF AUTOMATION

ИЗВЕСТИЯ КАФЕДРЫ UNESCO ГУАП «ДИСТАНЦИОННОЕ ИНЖЕНЕРНОЕ ОБРАЗОВАНИЕ»

Сборник статей
Выпуск 2

BULLETIN OF THE UNESCO DEPARTMENT “DISTANCE EDUCATION IN ENGINEERING” OF THE SUAI

Collection of the papers
Issue 2

РОССИЯ, САНКТ-ПЕТЕРБУРГ 2017 SAINT-PETERSBURG, RUSSIA

УДК 378.1
ББК 74.58
И33

И33 Bulletin of the UNESCO department “Distance education in engineering” of the SUAI: Collection of the papers. St. Petersburg, Issue 2.- SPb.:SUAI,2017. - 124 p.
ISBN 978-5-8088-1174-4

ISA District 12 (The International Society of Automation) and SUAI (Saint-Petersburg State University of Aerospace Instrumentation) have organized the Thirteenth ISA European student paper competition (ESPC-2017). Papers of professors and the best students were included into this issue of the Bulletin of the UNESCO department “Distance education in engineering” of the SUAI. Papers can be interesting for students, post-graduated students, professors and specialists.

ISBN 978-5-8088-1174-4

Setting the Standard for Automation™

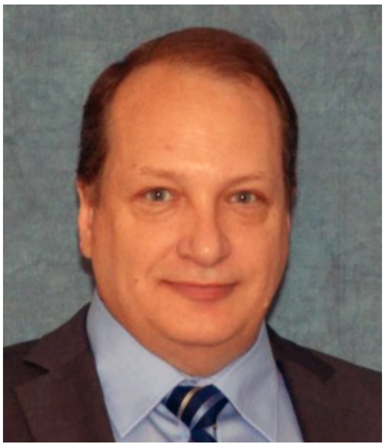

On behalf of the International Society of Automation, I congratulate the ISA Russia Section, ISA District 12, and the St. Petersburg State University of Aerospace Instrumentation (SUAI) on successfully completing the 13th ISA European Student Paper Competition.

ISA needs the commitment of students to advance the Society's mission and set the standard for automation.. The potential of these talented students is enormous and I am confident their contributions will improve the quality of life and security of our world in the years ahead. No matter which career path they choose, we hope ISA will have a place in their continuing education and professional development.

The papers published in this volume, selected by the advisory committee, represent the best contributions from among an excellent group of papers. I commend the students who committed their time to prepare a paper and on having their work selected for this publication.

Sincerely,

Steven W. Pflantz
2017 ISA President

ISA
67 Alexander Drive
P.O. Box 12277
Research Triangle Park, NC 27709
PHONE (919) 549-8411
FAX (919) 549-8288
E-MAIL info@isa.org
www.isa.org

Setting the Standard for Automation™

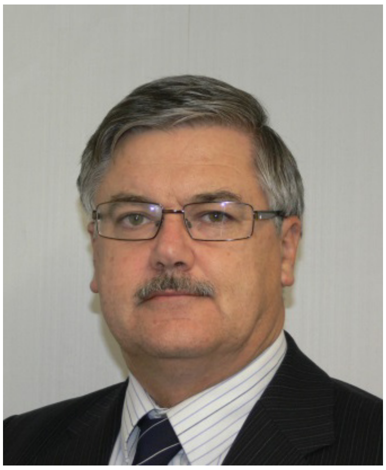

On behalf of the International Society of Automation, I extend congratulations to the ISA Russia Section and the St. Petersburg State University of Aerospace Instrumentation (SUAI) on successfully completing the thirteenth ISA European Student Paper Competition.

Students are the future for our Society We are all excited about these talented individuals who will be instrumental in "setting the standard for automation" that will enhance our lifestyle in the 21st century.

The students who committed their time to prepare a paper should be very proud to be selected for this publication. To the lecturers you are also playing an important part in shaping the future and you should feel proud of the standard that is visible in this publication.

On behalf of ISA may I extend my best wishes to all students and attendees in the 2017 ISA European Student Paper Competition.

Sincerely,

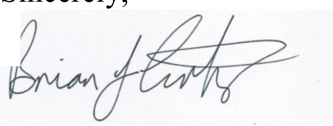

Brian J. Curtis
2017 ISA Vice-President elect Secretary

Standards

Certification

Education & Training

Publishing

Conferences & Exhibits

International Society of Automation
67 Alexander Drive
P.O. Box 12277
Research Triangle Park, NC 27709
PHONE (919) 549-8411
FAX (919) 549-8288
E-MAIL info@isa.org
www.isa.org

Setting the Standard for Automation™

I would like to extend congratulations to the ISA Russia Section, ISA District 12, and The Saint Petersburg State University of Aerospace Instrumentation (SUAI) for successfully organizing the Thirteenth ISA International Student Paper Competition.

As an educator and a member of ISA for over 30 years, I never tire of the opportunity to share with students the amazing challenges and personal rewards that a career in automation can bring. ISA is proud to have the opportunity to nurture the next generation of automation professionals.

We look forward to continuing the close relationship we have established between ISA, the Russia Section, District 12, and the SUAI. Through distance learning classes on project management and ongoing international online forums, we are developing new understandings in the technical, cultural, and personal arenas.

Congratulations to those who developed papers for this volume and to the advisory committee who had the difficult task of making paper selections.

Sincerely,

Gerald W. Cockrell

Gerald W. Cockrell
ISA Former President

ISA
67 Alexander Drive
P.O. Box 12277
Research Triangle Park, NC 27709
PHONE (919) 549-8411
FAX (919) 549-8288
E-MAIL info@isa.org
www.isa.org

PRODUCTION OF CEA CASINGS BASED ON COMBINED FDM TECHNOLOGY

Chabanenko Alexandr

Saint-Petersburg State University of Aerospace Instrumentation,
Saint-Petersburg, Russia
E-mail: Chabalexandr@gmail.com

Abstract

The article discusses aspects related to the evaluation of high production of electronic equipment (CEA), based on combined FDM technology.

Key words: Science intensive production, radio electronics, industry, evaluation, additive technologies.

Electronic electronics equipment requires special casings. Only with a special chassis can you create a safe and efficient instrument. Chassis cannot be universal, each requires its own unique design. Electronics production is now coming to a new level.

With the development of the electronic industry, which is known to be very turbulent in our time, the elemental base, which has a clear trend towards miniaturization, is being updated particularly rapidly. The compactness and availability of electronic components and parts has resulted in a marked recovery in the development of new and high-R and D e-devices.

The industry-based economy is characterized by an indicator of intensity production, measured by the ratio of R and D expenditure (VNIOKR) to the gross output of the industry (VVP):

$$(Vниокр\,/\,Vвп)\bullet 100\%\,, \quad (1)$$

It is believed that for knowledge-based industries, this figure should be 1.2-1.5 times higher than the average manufacturing industry.

Manufacturing CEA This is a very time-consuming and professional work that process a long time. And the number of parts is measured not by tens, hundreds and thousands, but, quite the contrary, things. And for such a "boxed" order doesn't want to take any manufacturer.

The constructs of unique chassis parts sometimes affect their complexity, the saturation of geometric elements, and the variety of forms.

The construction of the chassis part defines the manufacturing technology. In view of the technology to manufacture very small parties or even experienced products in a single instance, the use of FDM technology should be seen.

Most often, the casings of the fixtures are made from sheet metal (carbon, galvanized and stainless steel, as well as aluminium). But unlike sheet metal, plastic casings have a number of undeniable advantages: high strength, resilience to deformation, climatic effects, solid appearance. Also, the undeniable advantage of produced of FDM technology is the possibility of series production.

For CEA shells, an important indicator is the static safety of the protection object, subject to the ratio of [2.3]:

$$W \le K \le W_{\min}\,, \quad (2)$$

where $W_{\min}$ – is the power of the level that may arise within or from the object, J; K – safety factor selected from the terms of a valid (secure) according to GOST 12.1.004, GOST 12.1.010 probability of ignition or accepted equal to 0, 4; $W_{\min}$ – minimum ignition energy, J.

Also in production, you must consider the value of abrasion calculate by formula:

$$U = \frac{G_1 - G_2}{F}(г\,/\,см^2)\,, \quad (3)$$

where: G_1 – the dry weight of the sample to abrasion; G_2 – the dry weight of the sample after abrasion; F – area of abrasion.

In low production, it is necessary to use FDM technology to replace molding, which helps reduce production costs.

Before you start the serial production of CEA, you need to design a technical job and design the best structure for the CEA.

Stages of construction of the batch of shells for CEA:

1. The production of a technical task for the development and manufacture of the CEA.

2. Creation of a technology design and the design of the CEA;

The application of this technology allows the reduce process of production of small production of CEA casings.

The parts from the ABS plastic are gluing, drilling, paint. It is also possible to smooth the surface with an acetone bath.

In the processing of acetone, items become smooth and glossary, similar to ceramic products.

Model Requirements:

- minimum wall thickness: 1 mm;
- minimum thickness of convex or engraved part: 0.5 mm;
- standard thickness of the print layer: 200 µm;
- the maximum model size for the printer picaso3d Designer: 200 x 200 x 210 mm;
- The minimum model size: 3 x 3 mm;
- the minimum distance between two parts or walls: 1 mm;
- file format: STL, obj;

Multiple models in the same STL; file, connected parts, or part in parts are not allowed.

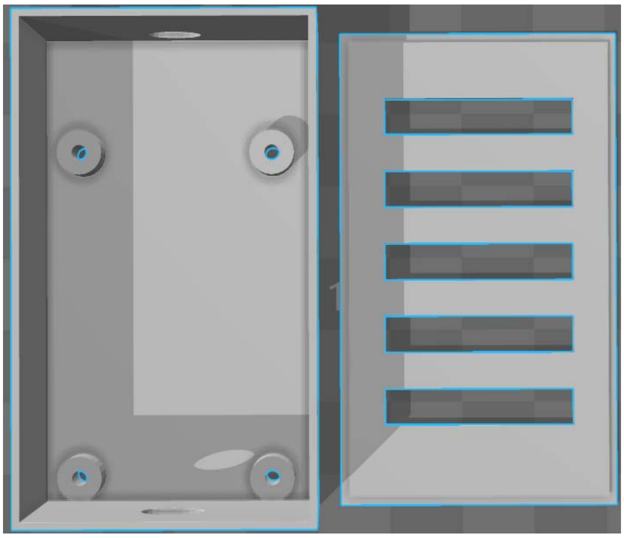

Figure 1
Design for CEA

3. Launch the process of the printing of the chassis with the production of CEA casing technology based on combined FDM technology.

4. Cleaning of the CEA.

The application of this technology allows the reduce process of production of small production of CEA casings.

The parts from the ABS plastic are gluing, drilling, paint.

Table 1

Main methods of FDM technologies

Method	**Technology**	**Materials used**
Extrusion	Simulated by layered melting (FDM and FFF)	Thermoplastics (such as polylactic acid (PLA), acrylonitrile butadiene styrene (ABS), etc.)
wire	Production of arbitrary forms of electronic-ray smelting (Ebf3)	Almost any metal alloys
Powder	Direct laser sintering of metals (DMLS)	Almost any metal alloys
	Electronic-ray melting (EBM)	Titanium alloys
	Selective Laser melting (SLM)	Titanium alloys, cobalt-chromium alloys, stainless steel, aluminium
	Selective thermal sintering (SHS)	Powder-thermoplastics
	Selective laser sintering (SLS)	Thermoplastic, metallic powders ceramic powders
inkjet	Inkjet 3D printing (3DP)	Plaster, plastics, metal powders, sand mixtures
Lamination	Production laminating method objects (LOM)	Paper, metal foil, plastic film
Lamination	Stereolithography (SLA)	Photopolymers
	Digital led projection (DLP)	Photopolymers

The Process matrix (table 2) is evaluated in order to determine the significance of the characteristics depending on the types of plastic.

Table 2

Assessment of relevance in the process matrix

Characteristic	Ranked value on demand					Mul'tiplikant	Gained weight%
	Deformation temperature	Electrical safety	Deformation	Wear resistance	Price centimeters cubic		
ABS-ESD7	10	10	10	4	3	12000	7,97321001
ABSi	6	7	4	8	4	5376	3,57199809
ABS-M30	9	10	5	6	9	24300	16,1457503
ABS-M30i	10	10	9	10	8	72000	47,8392601
ABSplus-P430	2	5	8	6	10	4800	3,18928401
PC	3	8	9	7	10	15120	10,0462446
PC-ABS	5	8	9	4	7	10080	6,69749641
PC-ABS	1	2	10	6	8	960	0,6378568
PC-ISO	9	7	9	1	4	2268	1,50693669
PPSF	10	6	10	2	3	3600	2,391963
Total value						**150504**	100

The design of the new CEA Corps can be defined as the process of creating a construction document, which is a graphical, textual or digital model of a future product built on the results of research, processing of technical information, using scientific knowledge that is characteristic of the research processes. Technological, material and planning-organizational preparation of production is a set of work related to the technical and information management of the production processes of direct production of designs, prototypes or a series of constructed products. (Figure 2) shows the relationship between the selected elements and the process of its creation according to the final product (ultimate goal) of each stage [1].

The production period is characteristic of the serial and mass production type where the product item is stable for some time. The duration of this period may vary from several weeks to several years.

Calculation of the period for the development of new products. During the period of development, labour-intensive production is significantly reduced [4]. It has been established that the pattern of change labor during the period of development is described by the equation

$$y_i = a \times x_i \,, \tag{4}$$

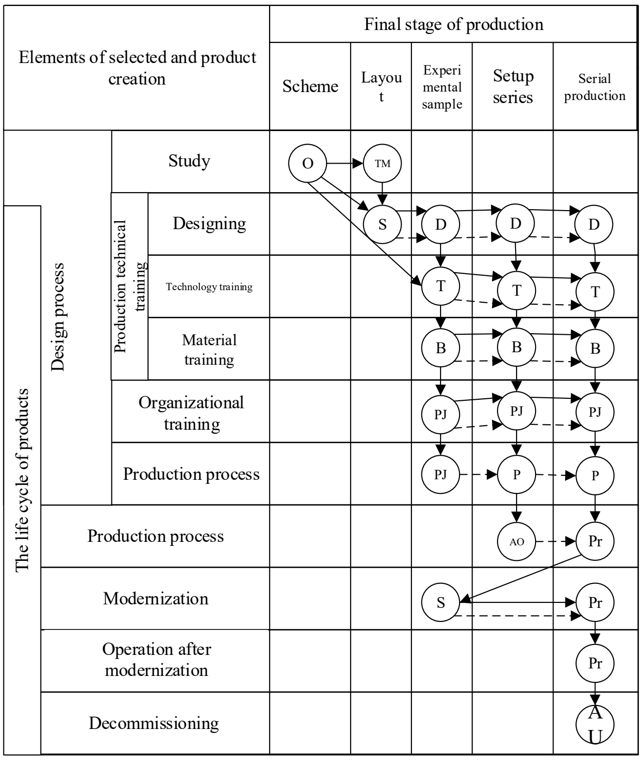

O-the beginning of selected TM-Technical mission, S-Sketches, D-drawings, t-processes, material resources, PJ-Plans and jobs, P-Production, Pr-product, AO-advanced operation, AU-decommissioning and recycling.

Figure 2

Structure of the selected new product

The "x" argument can be used both as a time parameter (starting from the beginning of the development) and in the natural (sequence number). In the latter case the equation will be:

$$T_i = T_н \times N_i \,, \tag{5}$$

Where is

T_i – the complexity of manufacturing the 1st number of the product, n-h;

$T_н$ – elementary complexity products, n-h;

b – the exponent, reflecting the intensity of reduction of expenses in the period the product development (0<b<1).

The use of these calculations will allow for a reasonable planning of techno-economic indicators during the period of development: labour-intensive and cost-consuming, acceptable product prices, expected profits, required the number of workers, necessary wage funds, etc.

CONCLUSION

The production of shells CEA very labour-intensive and professional work, process a long time. And the number of parts is measured not by tens, hundreds and thousands, but, quite the contrary, count.

The construction of the chassis part defines the manufacturing technology. In view of the technology to manufacture very small parties or even experienced products in a single instance, the use of FDM technology should be seen.

Chassis production Electronics is an integral part of the high-tech production in the mind of a significant proportion of research and development, and complex technical solutions aimed at ensuring an adequate level of physical-mechanical properties of the shell that protects the internal components.

REFERENCES

1. Improving the management of intensive production and assessing its potential for Semyonova E.G., Chabanenko A.V. Radio. 2016. No. 4. C. 38-43.
2. GOST 12.1.018-93 fire-explosion safety of static electricity: general requirements.
3. GOST R. 51898-2002 security aspects. Rules for inclusion in the standards.
4. GOST R. ISO 12100-1-2007 machine safety. Basic concepts, general design principles. Part 1. Basic terms, methodology.

SOLUTION OF THE PROBLEM OF INCREASING CAPACITY NETWORK WITH A FIXED MONTHLY RADIO CODE SEPARATION OF CHANNELS

A. F. Kryachko[1], K.V., Antonov[1], Y. Y. Levin[1], V.K. Losev[1], K.P. Shchegoleva[1]
[1]Saint-Petersburg State University of Aerospace Instrumentation, 190000 St. Petersburg, Russia

The paper considers a variant of network planning on the optimal use of hardware-software tools existing on the telecommunications market of this standard. In this case, the installation of additional repeaters is used. At the same time, it is necessary to determine the composition of the equipment and to revise the territorial plan for the deployment of the network.

Keywords: capacity, radio channel, base station, repeater, electro-magnetic compatibility.

INTRODUCTION

When planning user radio access networks using the CDMA standard, it is necessary to take into account the features typical for such networks in general, and the specific conditions of Russia. First of all, they should include a small number of base stations in the network (up to one), a correspondingly small amount of intra-network interference (co-channel interference), low mobility of subscribers (some subscriber phones are stationary).

Consider the option of choosing a cdmaOne subscriber radio access network - using base station signal repeaters (repeaters). This option can be applied starting from the stage of territorial planning, and contains a number of additions to the territorial plan and the hardware of the communication network.

MAIN PART

The practice of developing wireless cellular and personal communications shows that the method of extending the service area by increasing the height of the antenna suspension and increasing the power of the transmitters operating the BS (base station) has significant limitations due to terrain (relief, vegetation, etc.). The method of installing additional repeaters of BS repeater signals is more expedient, providing the following advantages:

- BS service areas are formed with the required spatial and energy parameters;
- the number of subscribers and the level of subscriber load on the BS are reduced to the required range of values;
- the requirements of intersystem and inter-system EMC (electro-magnetic compatibility) are facilitated. The hardware-technical solution underlying this option is illustrated in Fig.1. The main functional elements of the cellular communication system - the Switching Center (MSC) and the Base Station Controller (BSC) provide management and support of the operation of the subscriber radio access network, its interaction with the public telephone network (PSTN).

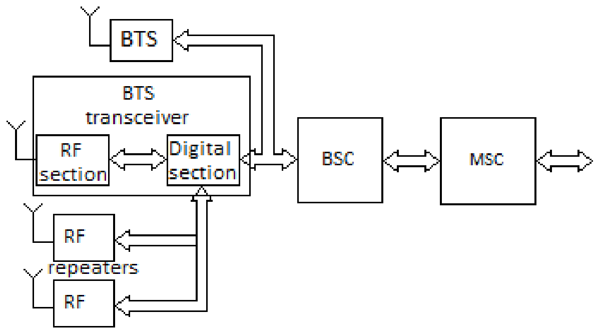

Fig.1 Architecture of the subscriber radio access network.

The base station transceiver (BTS) interacts with the BSC, performs data routing functions, code modulation-demodulation of messages transmitted over the radio channel, processes signals at the intermediate and radio frequencies, provides time synchronization of signals and generation of reference frequencies. Functionally and constructively, the transceiver consists of two main units - the digital signal processing section (Digital) and the signal processing section at the radio frequency (for example, the base station transceiver Qcell 2508i BTS from Qualcomm [1]). The digital processing section performs the operations of code modulation and conversion to the intermediate frequency of messages transmitted in the forward channel, as well as digitization and code demodulation of messages transmitted in the reverse channel. The radio frequency processing section, in turn, converts signals from the intermediate frequency to radio frequency, power amplification and band-pass filtering of signals transmitted in the forward channel, as well as amplification, band-pass filtering and conversion from radio frequency to the intermediate frequency of signals received in the reverse channel.

Thus, the base station repeater must have equipment equivalent in its functional characteristics to the radio base station transceiver processing section. The connection between the repeater and the digital processing unit of the transceiver of the base station can be carried out using fiber-optic and radio-relay lines. The positioning of the antenna equipment of the repeater is determined by the requirements for providing radio coverage in the calculated service area.

Let's consider some technical aspects of the proposed option. To simplify the analysis, we will consider non-partitioned cells, considering that, if necessary, the analysis can be easily extended to the case of sectored cells.

Case 1. The base station has K-1 repeaters (K≥ 2) with disjoint zones.

Verification of the level of real subscriber load should be carried out taking into account the "spatially-distributed" structure of the cell. The total traffic of the BS should be calculated as the sum of the traffic of all K stations connected to one digital processing unit of the transceiver BS:

$$A_{BS} = \sum_{j}^{K} \int\limits_{(S_{lightt\,j})} p_j\left(\vec{r}\right) A^{'}\left(\vec{r}\right) dr. \qquad (1)$$

Since each of the repeaters emits the same group signal on identical orthogonal code subcarriers. Intra-system interference in the forward channel is close to zero and is due only to those components of the multipath profile that are not involved in the RAKE process.

The interference in the reverse channel is created by subscribers of all K stations, since the signals from the outputs of the radio sections of the individual repeaters are added at the input of the digital processing section of the BTS:

$$E_{\text{int}}^{UL} = \sum_{j}^{K} E\left[\int\limits_{S_{\text{int}\,j}} \frac{P_{MS\,i}^{TX}\left(\vec{r_i}\right) A_{K-1}^{'}\left(\vec{r_i}\right)}{L_{BS} PL\left(\vec{r_{ij}}\right) F_L\left(\vec{r_i}\right)} d\vec{r_i} \right] =$$

$$= \sum_{j}^{K} E\left[P_{Int}^{UL}\left(\vec{r_j}\right) \right]. \qquad (2)$$

The signal-to-noise ratio at the output of the code RAKE demodulator of the BS receiver:

$$q^{BS}\left(\vec{r_j}\right) = \sqrt{\frac{2E_s}{\frac{1}{\Delta F} \sum_{j}^{K} E\left[P_{Int}^{UL}\left(\vec{r_j}\right) \right] + I_{0OUT}^{MS} + N_0^{BS}}}. \qquad (3)$$

Due to the spatial diversity of the service areas and the interference zones of individual repeaters, the additive interference level at the input of the digital processing section of the BTS will be determined only by the current number of subscribers in the service areas.

Case 2. The base station has K-1 repeaters (K≥2), the service areas of which intersect.

In the return channel there is a spatially separated reception by repeaters with overlapping service areas, which causes interference of the received copies of signals at the input of the digital processing unit BTS. In systems with frequency and time division of channels using signals with low time resolution, this would lead to failures and a sharp deterioration in the quality of communication, since intersymbol interference and frequency-selective fading of signals have a disastrous effect on the operation of such systems. In a CDMA system, complex signals having a high resolution are applied, which allows for diversity of time processing, and as a consequence, stable communication under multipath conditions.

It should be noted that the apparent similarity of the described communication principle to the principle of soft handover of a mobile subscriber in a cellular CDMA network is only external. In soft handoff, the signal to the MS transmits various BS on different code subcarriers.

In fact, with soft handover, various BS transmit different physical signals over different forward traffic channels. When organizing a repeater connection need: each of the repeaters in the same traffic channel transmits the same physical signal, but with an individual delay time. Thus, the subscriber station receiver does not perform code detection and separate signal processing of different repeaters, as would be the case with soft handover, but produces a time-separated reception of one total signal on one code subcarrier.

The introduction of artificial multipath can provide the following advantages in the CDMA system.

1. The average level of the received signal increases.

2. The probability of confident reception under the influence of slow signal fading increases.

3. The energy gain from the time diversity of the signals is increased when receiving with a fixed multiplicity of time diversity. This effect is due to the increase in the number of received beams with

uncorrelated fading of the signal. In this case, the radio multipath profile, the base station - the subscriber station represents a superposition of the multipath profiles of the radio channels, the repeater-subscriber station:

$$P_{\Sigma}(l) = \frac{1}{\sum_{j}^{K}\left[PL\left(\vec{r}_{ji}\right)F_{L}\left(\vec{r}_{ji}\right)\right]^{-1}} \sum_{j}^{K} \frac{P_{j}(\tau-\tau_{ji})}{\left[PL\left(\vec{r}_{ji}\right)F_{L}\left(\vec{r}_{ji}\right)\right]}, \quad (4)$$

When $\dfrac{\left[PL\left(\vec{r}_{ji}\right)F_{L}\left(\vec{r}_{ji}\right)\right]^{-1}}{\sum_{j}^{K}\left[PL\left(\vec{r}_{ji}\right)F_{L}\left(\vec{r}_{ji}\right)\right]^{-1}}$ - normalizing

factor, τ_{ji}- The delay of the first ray on the j repeater track ***r_{ij}* (fig. 2).**

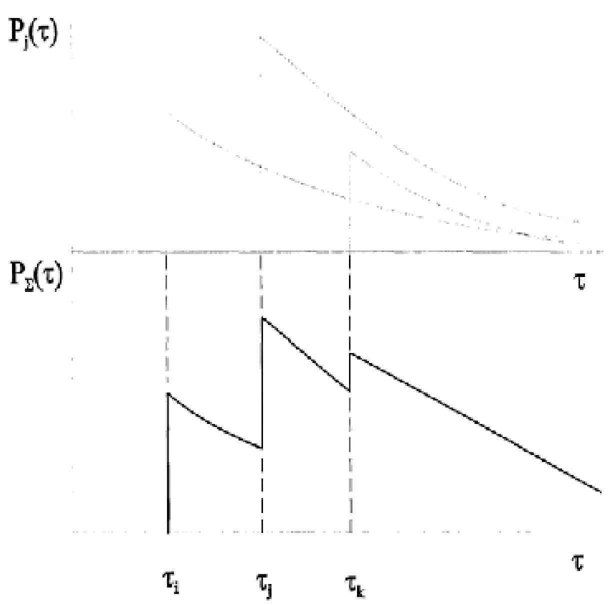

Fig.2. Addition of multipath profiles in the area of intersection of service areas of repeaters of a base station.

Analyzing the intersystem interference situation in the forward link, it should be taken into account that all repeaters retransmit one group signal on identical orthogonal code subcarriers, and the level of the noise background is mainly determined by the interfering copies of the signal that are not used in RAKE processing. Thus, in the first approximation, it can be assumed that repeaters connected to one digital processing unit BTS do not create in the forward interference channel the subscribers of this BS.

CONCLUSION

The considered method of network planning, involving the use of repeaters, is particularly effective. It allows you to:

• Expand the capacity of base stations, approaching the capacity of an isolated base station;

• Do not correct the previously developed network frequency plan, since in the case of the CDMA standard, communication is performed in a single frequency band;

• Ensure crossing of service areas of several repeaters and thereby improve the quality of radio coverage;

• Use a single section of digital processing, which reduces the cost of network selection;

• Convert repeaters to base stations, if necessary, by retrofitting them with digital signal processing sections.

• The additive interference level at the input of the digital processing section of the base station is determined only by the current number of subscribers in the service areas;

• Subscribers located in the intersection of service areas of different repeaters have an improved signal-to-noise ratio at the cost of deteriorating communication conditions in the coverage area of only one repeater.

REFERENCES

[1] Qualcomm Inc. Wideband spread spectrum digital cellular system. Proposed EIA/TIA Interim Standard.-1992.

[2] Babkov V.Ju., Voznjuk M. A., Dmitriev V.I. Sistemy mobil'noj svjazi/Pod red. M.A. Voznjuka. SPb.: VUS, 1998.

[3] Babkov V.Ju., Voznjuk M.A., Nikitin A.N., Sivere M.A. Sistemy svjazi s kodovym razdeleniem kanalov/SPbGUT.-SPb, 1999.

[4] Babkov V. Ju., Nikitin A. N., Sivere M. A., Osennij K. N. Sistemy mobil'noj svjazi s kodovym razdeleniem kanalov/Pod. red. V. Ju. Babkova. SPb.: Itaka, 2003.

CONDITIONS FOR CHOOSING A MATHEMATICAL MODEL FOR SIMULATION OF PASSENGER PROCESSES

Maiorov N.N.

Saint-Petersburg State University of Aerospace Instrumentation, Russia
Sciencesuai@yandex.ru

Abstract

The problem of choosing an exact mathematical model for constructing an imitation model of passenger processes in transport systems is studied in the article. The choice of the model depends on the accuracy of the process, efficiency, and the resources required. Passenger processes are the most complex objects of research, since the passenger behaves in the system on the basis of his personal interests. The object of the research was the airport and a specialized simulation model combining a set of mathematical models was presented.

Keywords: airport, air terminal complex, passenger flows, mathematical models, analytical models, agent modeling, queuing systems, gas-kinetic model, model of social forces, cellular automata model.

INTRODUCTION

Plans for the development of the various components of the airport system depend to a large extent on the activity levels which are forecast for the future. Since the purpose of an airport is to process aircraft, passengers, freight, and ground transport vehicles in an efficient and safe manner, airport performance is judged on the basis of how well the demand placed upon the facilities within the system is handled. To adequately assess the causes of performance breakdowns in existing airport systems and to plan facilities to meet future needs, it is essential to predict the level and distribution of demand on the various components of the airport system. Without a reliable knowledge of the nature and expected variation in the loads placed upon a component, it is impossible to realistically assess the physical and operational requirements of such a component. For example, forecasting of passenger flows makes it possible to increase the safety of the transport facility, to carry out research on possible weak points in the passenger handling system, and to determine the number of personnel and equipment required.

THEORETICAL PROVISIONS FOR CHOOSING THE TYPE OF SIMULATION

Over the years, certain techniques have evolved which enable airport planners and designers to forecast future demand. The principal items for which estimates are usually needed include:

• The volume and peaking characteristics of passengers, aircraft, vehicles, and cargo;

• The number and types of aircraft needed to serve the above traffic;

• The number of based general aviation aircraft and the number of movements generated;

• The performance and operating characteristics of ground access systems.

Using forecasting techniques, estimates of these parameters and a determination of the peak period volumes of passengers and aircraft movements can be made. From these estimates concepts for the layout and sizing of terminal buildings, runways, taxiways, apron areas, and ground access facilities may be examined.

Forecasting in an industry as dynamic as aviation and airports is an extremely difficult matter. It is very important to remember that forecasting now is a precise science and that considerable subjective judgment must be applied to any analysis no matter how sophisticated the mathematical techniques involved. By anticipating and planning for variations in predicted demand, the airport designer can correct projected service deficiencies before serious deficiencies in the system occur. In practice, when researching airport passenger processes, analytical models, linear models, stochastic and simulation models are used. But they has different laboriousness of execution and varying accuracy. Figure 1 presents the dependencies of the accuracy of models on their complexity.

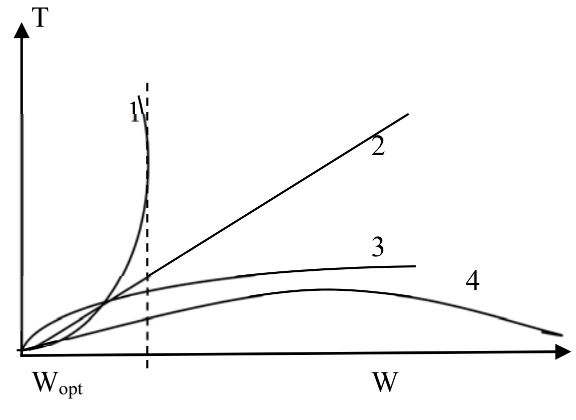

Figure 1. Dependence of the accuracy of the model on its complexity

Figure 1 shows: 1- analytical models; 2- linear models; 3- simulation models; 4- stochastic models. Figure 1 shows that the most attractive way is the use of simulation modeling.

PRACTICAL IMPLEMENTATION OF THE CHOOSING A MATHEMATICAL MODEL FOR THE STUDY OF PASSENGER FLOWS

The paper [1] presents practical implementation of the simulation model for Pulkovo Airport (Saint-Petersburg). In this paper, the developed information system is presented. But to improve the accuracy of its work, it is necessary to analyze the available mathematical models and determine which one will be more applicable to the study of passenger flows of the airport. In [1] presents how the use of an active terminal management, the passenger flow within the building is controlled for example through dynamic sign switchover. The terminal management itself is based on measurements of the current and forecasts for the future passenger traffic (fig.2).

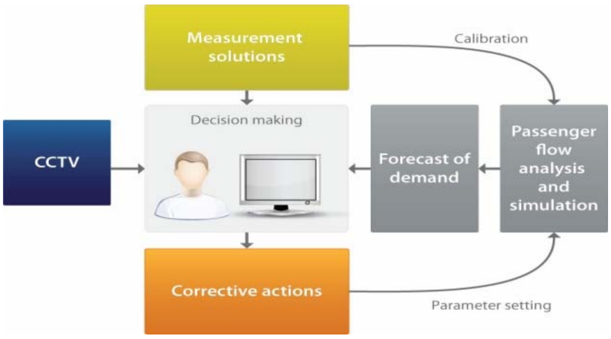

Figure 2. Passenger Flow Management

The effectiveness of modeling depends on mathematical models, each of which has its own characteristics. Let us consider in more detail.

The main problem of simulating pedestrian traffic is creating believable behavior of people. Sometimes they trying to get the final destination without colliding with other pedestrians, but it can be done by walking or rapid steps. In real life illogical behavior happens often. For example, it is a sudden stop in the busy traffic or sharp turns on the spot. However we can distinguish three stages of its behavior (fig 3.):

1. Choosing and making main aims. This is a strategic level, where the needs are forming.
2. Choosing of place and route modeling. This is a tactical level, where the connection of aims is realizing.
3. Executive action. This is operation level. At this level the movement and interaction with other members of stream is realized.

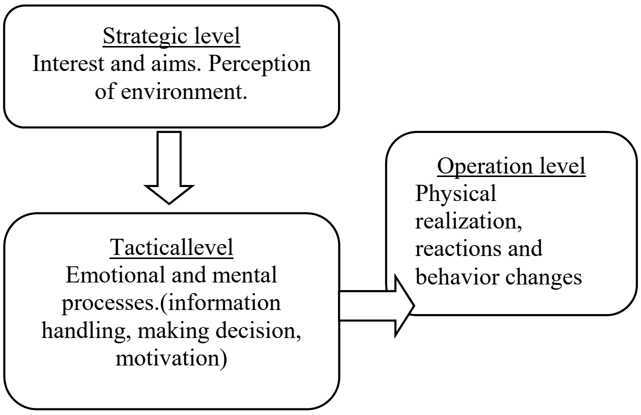

Figure 3. Levels of passenger behavior.

From all existing models of pedestrian streams the most popular are:

1.Model of pulling forces (based on Coulomb's law).

$$F = \frac{k \cdot q_1 \cdot q_2}{r^3}; \qquad (1)$$

where F – force of magnetic field; k – some constant; q_1 - intensity of magnetic pedestrian's load; q_2 - intensity of magnetic field; r - length of vector.

Pedestrians plays role of electronic charges located in magnetic field. Pedestrians and barriers are showed as positive charges, and moving targets as negative. [5,6]

2. Gas-kinetic model. At this model pedestrians are showed as molecules in liquefied gas. Separation of gas molecules to axes and speeds described by the Maxwell-Boltzmann distribution:

$$dn = const \cdot \exp\left(-\frac{m_r(V_x^2+V_y^2+V_z^2)}{2kT}\right) \cdot (2)$$
$$dV_x dV_y dV_z \cdot \exp\left(-\frac{U(x,y,z)}{kT}\right) dxdydz;$$

where dn - number of molecules, U - potential energy of a molecule at a point with coordinates x, y, z and speed projection. The Maxwell-Boltzmann distribution is showed as multiplication of two function of distributions: one of them is showing distribution for axes, another one for speeds [6]. Since this model is macroscopic and deterministic, then, as a result, it has low accuracy, especially at low pedestrian flow density.

3. Models that use the theory of queues with a probabilistic function to the description a pedestrian's moving. It is based on queueing theory [5,6,7].

The airport is a complex system, which is described by queuing systems. The arrival process starts when passengers land in the airport and finishes when they exit from the terminal. The transfer process includes operations of the departure and arrival process: passengers are involved in the procedures related to the departure process (security controls) and in some procedures connected to the arrival process. The passenger flow in the terminal can be subdivided in three sub-processes:

• departure;• arrival; • transfer.

The departure process starts when passengers enter the terminal and finish when they exit from the structure.

4. Model of social forces. It uses Newtonian mechanics to describe the motion of pedestrians, there fore it is considered the sum of all forces that acting on the pedestrian. For example, the driving force which impels to action and the sliding friction force, which prevents collision with other pedestrians. Forces arise from social interactions, displacements are anisotropic, it means that only matters what happens ahead of the passenger and that gets in his field of view.

6.Cellular automata. Model in which all the space is a grid, where each pedestrian can occupy only one cell. Such method is made for research fire evacuation, that's why it has special rules for calculating route and danger level, so the shortest route is chosen, but the farest to the fire [ ]. .For calculation can be used standart (GOST, Russia) 12.1.004-91, which offers a calculated method of estimates. This GOST gives an approximate idea of the effectiveness and safety of the layout of buildings and structures, but has several disadvantages:

1. Great dependence on predefined values (for example, only three types of people are considered - adult, adult in winter clothing and child).

2. Low modeling accuracy (for example, the decompaction of the human flow is not taken into account).

3. This model is used only in fire security (fig. 4) [8]

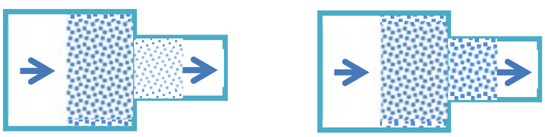

Figure 4. Example of passenger traffic according to GOST.

7. Agent simulation of passenger processes. An agent-based model is a feasible and effective approach to model passenger movements in airports. Unlike many models that treat passengers as individual agents, the proposed model in this thesis incorporates group behaviour attributes as well and evaluates the simulation performance of passenger movement within airports. Results from experiments show that incorporating group behaviour, particularly the interactions with fellow travellers and wavers can have significant influences on the performance and utilisation of services in airport terminals. The impacts can be seen in terms of dwell time at each processing unit, discretionary activity preference, and the level of service (LOS) at processing areas. Based on the airport passenger flow model that includes group dynamics, a case study of an airport evacuation event has been conducted. The simulation results show that the evacuation time can be influenced by passenger group dynamics. The model also provides a convenient way to design airport evacuation strategy and examine its efficiency. For airport designers and operators, the model also provides a convenient way to investigate the effectiveness of space design and service allocations, which may contribute to the enhancement of passenger airport experiences. The model was created using AnyLogic [4] software (fig 5).

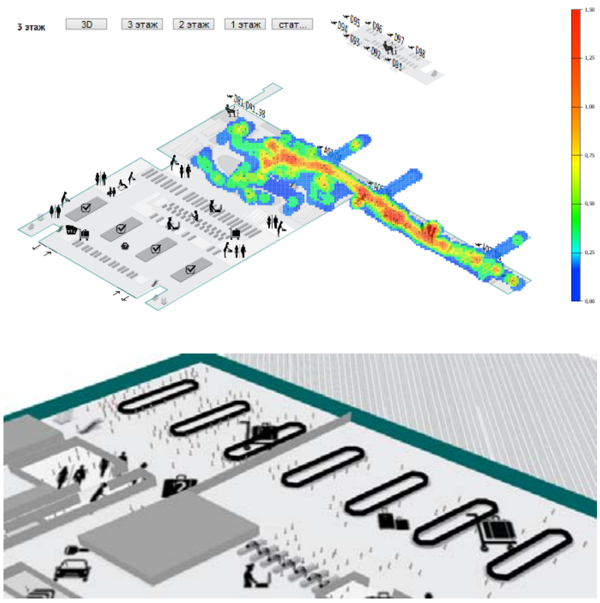

Figure 5. The window form of the created simulation model for the study of passenger flows based on the model of social forces and agent modeling

CONCLUSION

Thus, having the opportunity to analyze and compare different models, it is obvious to single out the model of social forces and agent base simulation. It should be noted that for a long time it was not considered, due to the complexity of processing a huge amount of information, but with the growth of computer performance it became possible to perform experiments with a large number of participants, that is, a full pedestrian flow on any object under consideration Currently, due to the integration of the social forces model into various software products, for example the PTV Vision VISSIM software package or the AnyLogic [4] simulation footbridge, designed for flow modeling, it is possible to analyze pedestrian flows that are actually produced at a sufficiently high level.

REFERENCES

1. Maiorov N.N., Fetisov V. Research and development special automated control system of passenger traffic at the airport using simulation. // The Novelity OF THE UNESCO CHAIR "Remote engeneering education" ,SUAI, 2015. – P. 7-11

2. Maiorov N. N., Fetisov V. A., Gardjuk A. N. Tehnologii i metody modelirovanija passazhirskih perevozok na vozdushnom transporte [Technologies and methods of modeling of passenger transportations by air transport]. — SUAI, 2014. — 215 p. (in Russian)

3. Malikov R. F. Praktikum po imitacionnomu modelirovaniju slozhnyh sistem v srede AnyLogic 6 [Practical work on simulation of complex systems in AnyLogic 6] – UFA:, 2013. – 296 p. (In Russian).

4. Anylogic Web. 10 March. 2017 .<www.anylogic.com >

5. Pravdin N. V., Negrei V. Ia., Podkopaev V. A. Vzaimodeistvie razlichnykh vidov transporta (primery I raschety) [The Interaction of Different Modes of Transport (Examples and Calculations)]. Moscow, Transport Publ., 1989. 208 p. (In Russian).

6. Litvin N. V. Teorija massovogo obsluzhivanija [Queuing Theory] M. 2014.– 47 p.

7. Gasnikov A.V. Vvedenie v matematicheskoe modelirovanie transportnyh potokov: uchebnoe posobie [Introduction to mathematical modeling of transport flows] M.: , 2013 - 426 p.

8. GOST 12.1.004-91.

RESEARCH OF SAW TAGS FOR IDENTIFICATION SYSTEMS

Zhezherin A.,Petrov A., Chugunov A.

Saint-Petersburg State University of Aerospace Instrumentation,
Saint-Petersburg, Russia

Abstract

This article intended to research cross correlation relation (CCF) of FSK signals with random symbol's frequencies within predefined frequency band. The techniques to increase a number of selected codes, whose correlation level located beneath predefined level A, were reviewed

.

GENERAL INFORMATION ABOUT THE SAW TAGS

RFID (Radio Frequency Identification) is a technology of contactless object identification by tags with mapped information on them. Our object of interest is a passive RFID transponders based on surface acoustic waves (SAW) elements. Such element is nonvolatile and radiation-resistant.

Identification system comprises reader (device which emitting and processing radio pulses reflected from tag) and passive SAW tags reflectors.

SAW tag backbone is piezoelectric substrate. The surface of substrate mapped with interdigital transducer and reflecting elements – gutters on the both sides of transducer. Interdigital transducer transform the energy received by stripline antenna into SAW which spreads in crystal to the reflecting structures.

Reflecting structures based on sections of reflectors. Part of the SAW energy drawback from reflectors towards interdigital transducer. Hence one emitted radio pulse generates a multiple return acoustic pulses. Each section of reflectors creates their own pulse in return transponder signal. Then the sequence of acoustic pulses received by interdigital transduces and transformed to the high frequency electromagnetic waves emitting by transponder's antenna. This waves can be received by reader. The number of pulses corresponds to number of reflecting structures on substrate.

Please note that delay time between separate symbols is proportional to the distance between reflecting sections on substrate. Distance between reflectors in section defines the pulse frequency in final signal. The length of signal describes by number of radio pulses (symbols) in sequence. Symbols frequencies arrangement defines signal's code.

Placement of reflectors can't be changed after tag production therefore transponders belong to "read only" devices class.

FSK SIGNALS AND THEIR SIMILARITY

Transponder code defines the parameters of M-ary FSK signal. Symbols frequencies described by spatial place of gutters in reflector.

In order to shrink size of substrate and achieve widespread FSK operating frequency $f_0 = 900\,MHz$ were selected. On this frequency significant attenuation of spreading across substrate SAW occurs. Hence we limit the length of FSK signal to $4\ \mu s$.

Active spectrum width of FSK signals restricted to bandwidth ΔF according to conditions of the problem.

Symbol's frequencies displaced relatively f_0 on different discrete frequency steps Δf. Let's name a number of possible frequency steps that can be assigned to the symbols as $K = \Delta F/\Delta f$. Suppose that symbol's frequencies can be described as $f_k = K\Delta f$ and possible values of f_k equally probable distributed within bandwidth ΔF. It's known from combinatorial analysis that number of possible code combinations of FSK signals in case K > M is equal $Q = K^M$.

Suppose that amplitude of FSK signal is constant hence maximum of autocorrelation function (ACF) is also constant despite the symbol's frequencies. We take the level of normalized CCF as the signals difference criterion in set Q, i.e. the less level of CCF signals has, the more different these signals are.

Hereby the problem is to form a family of FSK signals with predefined level of CCF. Let's name this family of signals as code's family. CCF of signals in code's family are satisfy the level A, i.e. their maximum of normalized CCF located beneath predefined level A.

Since increase of M for SAW tags isn't desirable only one way to increase code's family left. This way means to increase the number of available frequency steps K but we have to keep in mind predefined bandwidth ΔF. As soon as K depends on

Δf as $\Delta F/\Delta f$, the increase of K can be achieved by decrease of Δf.

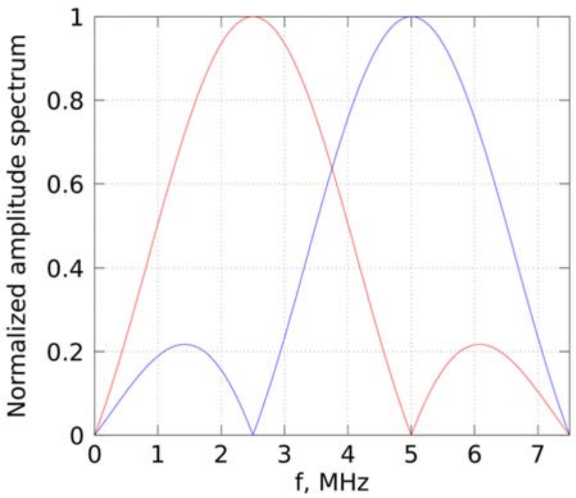

Fig. 1. Normalized amplitude spectrum of two symbols from FSK signal with rectangular envelope and $\boldsymbol{\Delta f = 1/t_s}$

To estimate this possibility consider a pair of symbols from FSK signal with frequency difference Δf. These symbols are radio pulses with rectangular envelope. Normalized amplitude spectrum of such symbols is shown in fig. 1.

Symbols are orthogonal if $\Delta f = 1/t_s$ (t_s – symbol's length) as it known from [1]. As it can be seen in fig. 1 the symbols have some area of intersection. This area defines the level of CCF of two symbols.

Symbols covariance is determined by normalized CCF level, which in this case (Δf=1/t_c) takes value equal to 0.31. As we can see from figure 2, the smaller Δf (or expanded spectrum intersection area) causes increase of the CCF level.

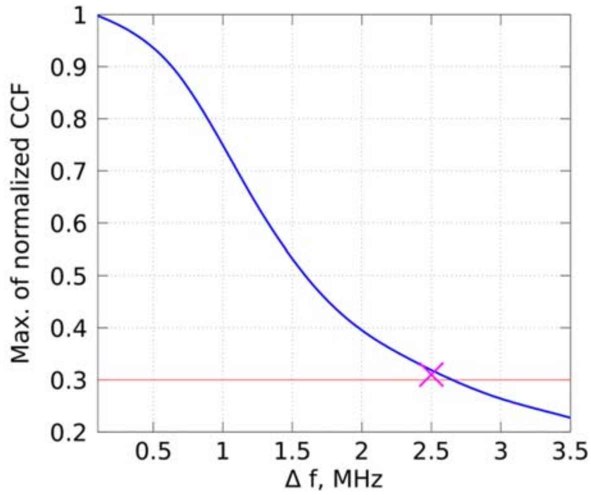

Fig.2. Normalized CCF for two rectangular symbols envelope depending on Δf. The red line shows level of CCF equal to 0.31. The crosshair shows CCF level at a val. of $\boldsymbol{\Delta f = 1/t_s}$.

It is known that decreasing Δf rises the frequency steps number K, however this will increase the CCF level between symbols and, probably, between FSK signals that are composed with these symbols.

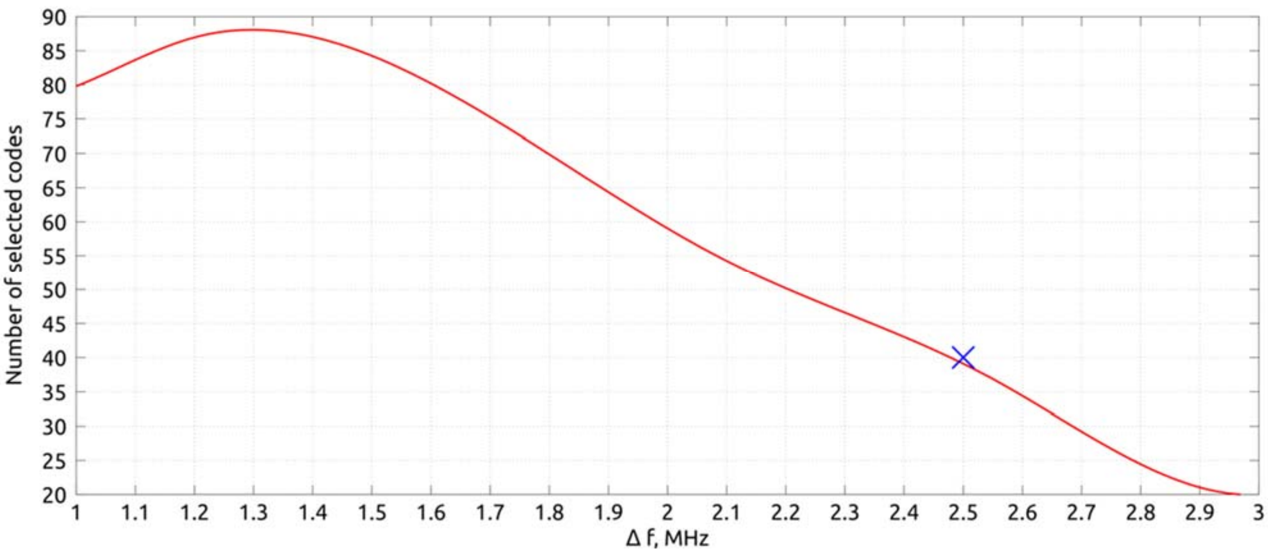

Fig 3 Number of selected codes depending from Δf for rectangular symbol envelope. Crosshair shows the number of codes at a value of $\boldsymbol{\Delta f = t_s}$

With these parameters the number of code variations is $Q = 10^8$. Calculating all of them will require large time and computing resources because from the set Q it is necessary to select a number of codes with predetermined normalized CCF level. The algorithm for calculating code combinations has already been developed [3].

To research the K number impact on CCF level between codes we consider FSK signals carrying these codes. The number of codes that have CCF level lower than predetermined level A we has named number N. We need to establish which of the factor will influence on number N stronger: increasing K number or rising CCF level. Consider the specific case: $K = 10$, $M = 8$, symbol duration $t_S = 0.4\ \mu s$, $\Delta f = 2.5\ MHz$, $\Delta F = 25\ MHz$.

For quick selection we limit the number of comparing codes to a sample $L = 5 \times 10^4 < Q$. Evaluation of the results for such small sample was interpolated to the whole set Q. The possibility was approved on series of applicative calculates. The results are shown on figure 3. The N number increases with decreasing Δf to 1.3-1.4 MHz (rising the number K accordingly). Number N does not exceed 90 codes. The calculation with $\Delta f = 1/t_s$ was made for comparing. [1]. Based on results obtained we can reduce Δf to a value that is smaller for achieving larger number of codes with predetermined CCF level [1].

INFLUENCE OF THE ENVELOPE

We decided to consider FSK signals with symbols having orthogonal rectangular spectra. Signals with such spectrum are impossible to be generated from the fact that symbols would represent themselves as signals with $\frac{\sin(x)}{x}$ *(sinc)* envelope and unlimited duration.

Main energy part of signal is concentrated at main leaf, so we limit duration of the symbol to the duration of main leaf. In that way the signal spectrum envelope will lose rectangular shape. The signals spectra with Δf = 2.5MHz are shown on figure 4. Compared with fig.1 we can see that spectrum intersection area of symbols with sinc envelope is smaller, but the duration of signal is doubled.

Consider the dependence of CCF for two symbols with sinc envelope. The dependence of CCF from frequency step is shown on figure 5. We can see that frequency step needed to reach CCF level equal to 0.31for sinc symbol envelope is less than for rectangular symbol envelope.

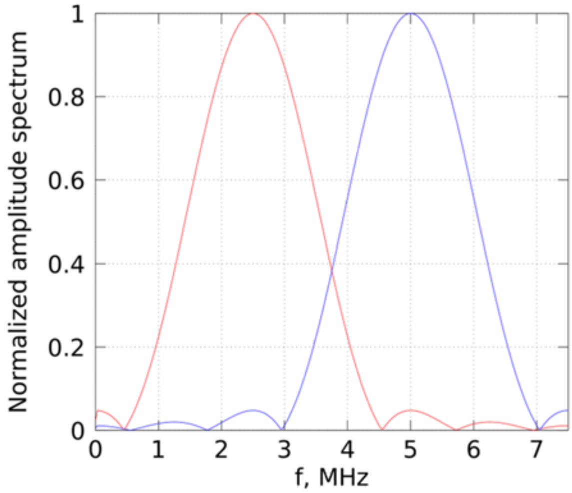

Fig. 4. Amplitude spectra of two FSK signal symbols for sinc envelope.

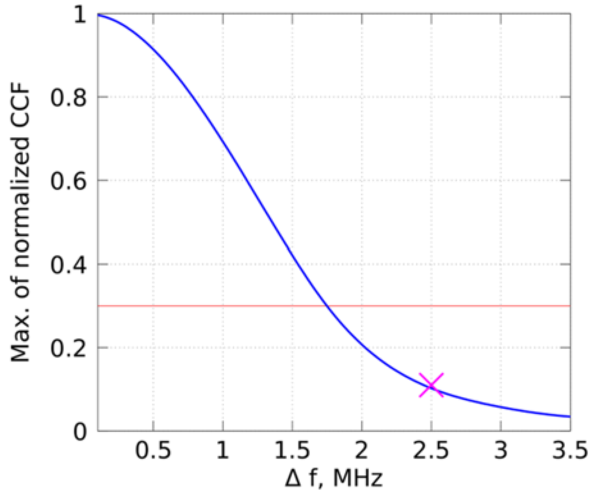

Fig. 5 Normalized CCF for two sinc symbol envelope depending on Δf. The red line shows level of CCF equal to 0.31. The crosshair shows CCF level at a val of $\boldsymbol{\Delta f = 1/t_s}$

.

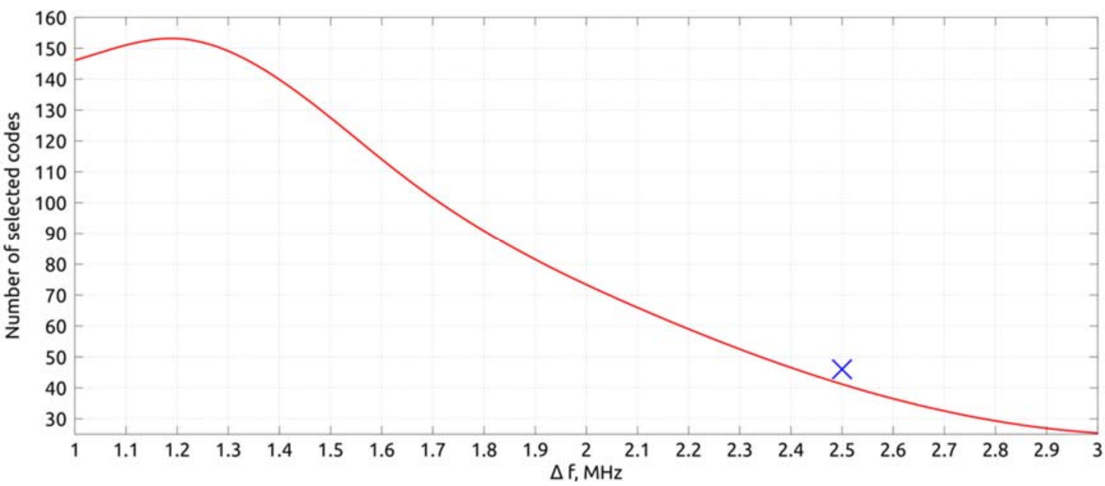

Fig.6. Number of selected codes depending on Δf for sinc symbol envelope. Crosshair shows the number of codes at a value of $\boldsymbol{\Delta f = 1/t_s}$

It is interesting to see how much frequency step can be reduced to reach CCF level as in case of rectangular symbol envelope. In this case frequency step takes value of 1.65MHz for reaching 0.31normalized CCF level. The smaller value of Δf for a constant active spectrum width gives a possibility of increasing the K number.

Examine the influence of K number on number of codes for the FSK signal with sinc symbol envelope. Results of calculation are shown of figure 6. The maximum number of codes can be seen at value of $\Delta f < 1.3\ MHz$. Based on Δf value we can calculate new K_1 number. K_1 number determined by the ratio ΔF/Δf in this case will take a value equal to 19. The number of codes has been increased up to 160 either.

CONSLUSION

The possible number of FSK signals with predetermined CCF level can be increased by changing the symbol envelope from rectangular to the shape repeating main leaf of $\frac{\sin(x)}{x}$ function.

REFERENCES

[1] B. Sklar, «Digital communications: fundamentals and application/ Bernard Sklar; 2007. - 1099 p.

[2] V. Ipatov. ”Spread Spectrum and CDMA: princi-ples and applications”, 2007. - 487 p.

[3] I. Ivanov, CODE SEQUENCES DEVELOPMENT FOR SAW TAGS IN THE SYSTEMS OF AU-THENTICATION / MODERN INFORMATION SOCIETY FORMATION -- PROBLEMS, PERSPECTIVES, INNO-VATION APPROACHES, XVI International forum 1 – 5 June 2015 – Saint-Petersburg: SUAI 2015

EFFECT OF RESTRICTED GEOMETRY ON THE ORDER PARAMETER AND COEFFICIENTS OF THERMAL EXPANSION OF NANO2

Alekseeva Olga

Peter the Great Saint-Petersburg Polytechnic University,
Saint-Petersburg, Russia

E-mail: alekseevaolga0@gmail.com

Abstract. The structural studies of ferroelectric nanocomposite materials (NCM) based on NaNO2 embedded into a porous glass with average pore size 20 and 46 nm are performed by diffraction of synchrotron radiation. It has demonstrated that both NCMs have ferroelectric phase transition of the first order as in bulk NaNO2. It has shown that layer with lack of long ordering exists on the surface of NaNO2 nanoparticles, its thickness has estimated. Anomalies of the temperature dependencies of anisotropic coefficients of thermal expansion have observed in NCMs.

INTRODUCTION

It is known that properties of nanostructured materials can significantly differ from those of bulk materials that determines a great interest to its study both fundamental and practical. The main causes of these differences are the proximity of lengths of the characteristic interactions and the nanoparticle sizes and the growth of effects of surface atoms on the physical properties of nanoobjects when their sizes reduce. Local symmetry and interactions of surface atoms with environment, walls of the matrix significantly differ from internal atoms.

One of the methods of producing of nanocomposite materials (NCM) is intrusion or synthesis of substance into the nanosized pores of pore matrixes. As a matrixes such structures as porous glass, chrysotile asbestos, artificial opals, zeolites, mesoporous matrix can be used [1-3]. In this work nanocomposites based on pore glasses are considered. For producing of such glasses alkali borosilicate glasses can be used. In alkaline borosilicate glasses during heat treatment phase separation occurs into the chemically resistant to acids SiO2 enriched phase and chemically unstable phase [4]. By selecting temperature treatment conditions and composition of initial melt the forming of two skeleton of the interpenetrating phases can be achieved [5]. After etching of the chemically unstable phase the three-dimensional (3D) random dendrite system of topologically interconnected nanopores forms. The size of nanopores can be modified in wide range from units to hundreds nanometers by varying temperature of the treatment. The spread of the pore sizes is small. NCM based on porous glasses are widely used in biotechnology, in the manufacture of membranes in medicine and pharmaceutics [6-7], for the manufacture of chemical sensors and gas sensors [8-9].

NaNO2 is a very convenient model object for a study of ferroelectric NCM based on pore matrixes due to its high wetting ability enabling ease penetration into the pores and filling of pore space, its bulk physical properties are studies very well. Sodium nitrite is a typical order-disorder ferroelectric, undergoes the first order phase transition at $T_C \approx 437$ K. At room temperature NaNO2 has a body centered orthorhombic lattice (a = 3.57 ˚A, b = 5.578 ˚A, c = 5.39 ˚A) with ***Im2m*** space group. In the low-temperature ferroelectric phase the spontaneous polarization appears due to a partial alignment of NO2 groups along b axis accompanied by the displacement of sodium ions. At high temperature (above T_C) a mirror plane perpendicular to the b-axis appears and the space group changes to ***Immm.*** In the narrow temperature range 437-438 K the incommensurate phase exists characterized by partial disordering of NO2 groups.

Dielectric studies of NaNO2 confined within artificial opals and pores glasses revealed significant rapid growth of dielectric permittivity of NCMs with NaNO2 above the temperature T_C of the ferroelectric phase transition (PT) (up to 10^8 at 100 Hz) [10] and some anomalies of dielectric response which can indicate change of temperature range where the incommensurate phase exists [11]. The goal of this work is the study of temperature evolution of crystal structure of NCMs based on NaNO2 embedded into pore glasses which is important for understanding of microscopic mechanisms leading to anomalous properties of NC comparing with the bulk material.

EXPERIMENT

The study of structural evolution of NCMs with NaNO2 was performed in the temperature region 100 - 460 K, *i.e.* below and above Curie temperature of bulk NaNO2 by synchrotron radiation diffraction (BM01A station, ESRF, France) at $\lambda = 0.703434$ ˚A. The temperature stability was better than 1 K. The temperature step was 2-5 K. The measurements were performed on heating and cooling. The experimental results were treated by the FullProf program. The samples were two NCMs of NaNO2 embedded into porous glass with average pore size of 20 (NCM-20) and 46 nm (NCM-46). In the same experimental conditions the diffraction patterns of bulk NaNO2 were measured.

RESULTS AND DISCUSSIONS

The information about evolution of the order parameter of NaNO2 were obtained. The physical realization of the order parameter in NaNO2 is the difference between the occupancies of the two equivalent crystallographic positions by anionic groups NO2. The intensity of diffraction peaks of NaNO2 [12] is proportional to

$$|\mathbf{F}|^2 = \mathbf{F}^2_{re} + \eta^2(\mathbf{T}) \times \mathbf{F}^2_{im}, \qquad (1)$$

where $\mathbf{F}_{re}$ and $\mathbf{F}_{im}$ are the real and imaginary parts of the structure factor F, and η is the order parameter for the ferroelectric phase.

Among all the Bragg peaks of NaNO2 two groups can be distinguished with significantly different values of F_{real} and F_{im}: for first ones $F^2_{real} >> F^2_{im}$ and the intensity of these peaks is independent of the order parameter, and for the second group $F^2_{real} << F^2_{im}$ and its intensity is proportional to the square of the order parameter η. Thus the information about the temperature dependence of the order parameter can be obtained directly from the diffraction data.

The temperature dependences of the order parameter η (T) NaNO2 for NCM-20, NCM -46 and bulk NaNO2 at heating and cooling are shown in Fig. 1. It can be clearly seen that the ferroelectric phase transition Tc differ significantly at the heating and cooling for both NCMs. At heating values of Tc are close to value of Tc of bulk NaNO2 (Tc≈ 437 K), while at cooling the phase transition into the ferroelectric phase occurs at ≈ 425 C in both NCMs. Thus, there is a significant temperature hysteresis (~ 10 K), the magnitude of which is comparable with hysteresis NaNO2 embedded in synthetic opals [13]. Crossover of the ferroelectric phase transition type from the first to the second is not observed. Obtained result is in agreement with results of previous neutron diffraction studies which also not revealed the crossover of PT for NCM at pore diameter 20 and 46 nm but observed it at pore diameter 3 and 7 nm [13,14]. So the critical size of NaNO2 nanoparticles within pores exists below which ferroelectric PT in NaNO2 nanoparticles become the second type. It should be noted that this average particle size does not coincide with average pore diameter because the particle can fill space of several neighbor pores. Average particle size can be estimated from width of Bragg reflections which significantly broaden when diffraction occurs on nanosized objects. For NCM-20 the average size of NaNO2 particles is 56 nm.

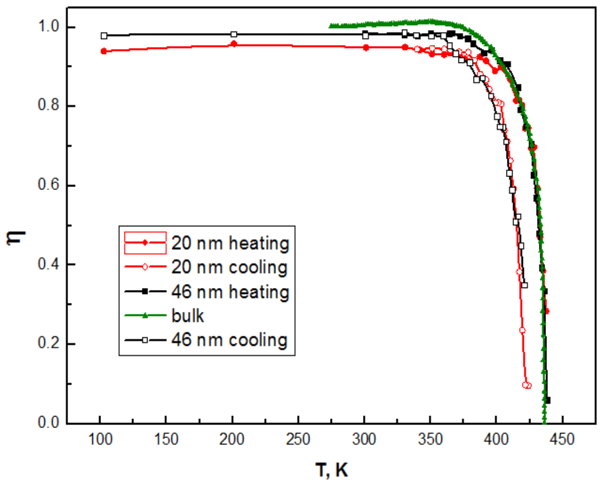

Figure 1
Temperature dependencies of the order parameter η(T) for NCM-20, NCM-46 and bulk NaNO2 at heating and cooling.

It is clearly seen from fig. 1 that even at low temperatures the order parameter in nanocomposites does not reach the unit value (for NCM- 20 its value is 0.94, for NCM-46 - 0.98). This fact can be related with the disordering of the surface layer of nanoparticles NaNO2. Knowing the average pore and basing on the model of cylindrical nanoparticle diameter the thickness of the surface layer with lack of long-range order can be estimated. For NCM-20 this thickness is approximately 6 ± 1 A, for NCM-46 - 5 ± 1 A.

The temperature dependence of the lattice parameters were obtained (Fig. 2). The pronounced temperature hysteresis is observed for unit cell sizes in NCMs. Small differences between heating and cooling temperature curves can be seen also for bulk NaNO2 which determine the possible instrumental errors. But they are significantly smaller than observed in NCMs. At heating the unit cell parameters are close to corresponding values of the bulk, at cooling the unit cell extends along the [100] and [010], and decreases in the direction of [001].

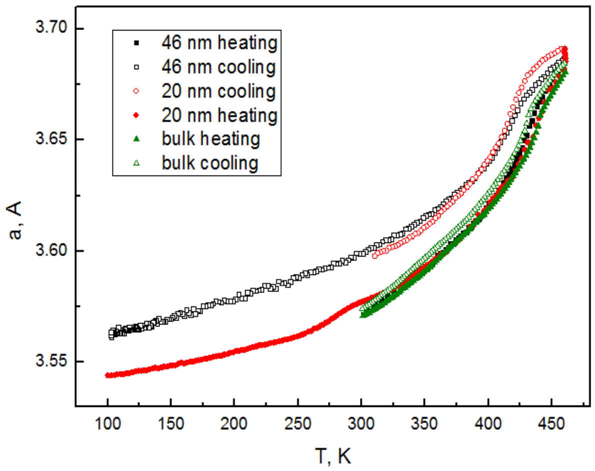

Fig. 2. Temperature dependencies of the lattice parameter a for NCM-20, NCM-46 and bulk NaNO2 at heating and cooling.

In general there is an increase of the unit cell volume. Based on these results the coefficient of thermal expansion (CTE) of NaNO2 was calculated. Increasing of CTE (about 2 times as compared with bulk material) in the direction [010] by heating and reducing of CTE along the [100] and [001] at cooling were found for both NCMs in temperature range corresponding to the paraelectric phase. In the ferroelectric phase noticeable differences between the CTE values of the NCMs and bulk NaNO2 are not observed.

CONCLUSION

The temperature evolution of crystal structure of NaNO2 embedded into the porous glass with average pore size 20 and 46 nm was studied. The pronounced temperature hysteresis of the order parameter was observed in NCMs. The crossover of the type of structure phase transition was not found. The size of disordered surface layer with lack of the order parameter of NaNO2 nanoparticles was estimated. The values of anisotropic coefficients of thermal expansion were found to differ in NCMs from corresponding bulk values in paraelectric phase.

REFERENCIES

[1] Levitz P. Porous vycor glass – the microstructure as probed by electron-microscopy, direct energy-transfer, small-angle scattering, and molecular adsorption / P. Levitz [et al.] // Journal of Chemical Physics – 1991. Vol.95, № 8 – P. 6151

[2] Pundsack F.L. The pore structure of chrysotile asbestos / F.L. Pundsack // Journal of Physical Chemistry – 1961. Vol. 65 – p. 30

[3] Breck D.W. Zeolite molecular sieves / A Willey-Interscience Publication Jonh Willey&Sons, New-York, 1974

[4] Mazurin O. Two phase glasses. Structure, properties, application / B. Varshall [et al.] //L. Nauka - 1991 - 276 pp.

[5] Vasilevskaya T. The study of the structure of nanoporous glassy matrices by X-ray small-angle scattering / T. Vasilevskaya, T. Antropova // Physics of the Solid State — 2009. Vol. 51, №12. — p. 2386

[6] Wu C. Bioactive SrO–SiO2 glass with well-ordered mesopores:Characterization, physiochemistry and biological properties / C. Wu [et al.] // Acta Biomaterialia - 2011. Vol. 7 - p. 1797

[7] Qian K. Application of Mesoporous Silicon Dioxide and Silicate in Oral Amorphous Drug Delivery Systems / K. Qian, R. Bogner // Journal of Pharmaceutical Sciences - 2012. Vol. 101, № 2 - p. 444

[8] Dorosz D. Porous glasses for optical sensors / D. Dorosz, B. Procyk // Photonics Applications in Astronomy, Communications, Industry, and High-Energy Physics Experiments IV - 2006 . Vol. 6159 - article ID 615923 (6 pp)

[9] Evstrapov A. Porous glasses as a substrate for sensor elements / A. Evstrapov [et al.] // Optica Applicata - 2010. Vol. 40, № 2 - p. 333-340

[10] Pan'kova S.V. The giant dielectric constant of opal containing sodium nitrate nanoparticles. / S.V. Pan'kova, V.V. Poborchii, V.G. Solov'ev // J. Phys. Condens. Matter - 1996. Vol. 8. - L203

[11] Kink M. Dielectric Properties of $NaNO_2$ and $NaNO_3$ Confined in Porous Glass /M. Kink, J. Bany, A. Naberezhnov. // Ferroelectrics - 2009. Vol. 390 - p. 160

[12] Lamas A. On the use of powder diffractometry in the study of phase transitions case of $NaNO_2$ / A. da Costa Lamas, S.-L. Chang, S. Caticha-Ellis // Phys. Stat. Sol. (a) - 1981. Vol. 68 - p. 173

[13] Bescrovny A.I.. Temperature dependencies of the order parameter of NaNO2 embedded into the porous glasses and opals / A.I. Bescrovny, S.G. Vasilovskiy [et al.] // Phys Sol. St. - 2010. Vol. 52 - p. 1021

[14] Naberezhnov A. Structure and properties of confined sodium nitrite / A. Naberezhnov [et al.] // Eur. Phys. J. E - 2003. Vol. 12 - p. s21

This work was supported by the Russian Science Foundation (project №14-22-00136).

IMPROVING LISTENING SKILLS IN LANGUAGE LEARNING WITH SPACED REPETITION TECHNIQUE

Baranov Yaroslav

Saint-Petersburg State University of Aerospace Instrumentation,
Saint-Petersburg, Russia

E-mail: kciray8@gmail.com

Abstract

Listening comprehension is one of the hardest skills for many people to develop in language learning. Developing listening skills is a long, slow and painful process for them. Nevertheless, we can significantly increase it with spaced repetition technique.

This article is about using the spacing effect for improving listening skills. The user extracts fragments from some video and repeats them later with increasing intervals. We have created the application that automates and simplifies this process.

INTRODUCTION

Thousands of people around the world are studying foreign languages. They spend many years to become fluent speakers. Listening comprehension is an ordeal for many of them even though they have access to thousands of high-quality videos on the Internet. We should develop a special learning technique because it is insufficient to watch those videos passively. People forgot words and their sounding too fast.

SPACED REPETITION

The spacing effect was reported by a German psychologist Hermann Ebbinghaus in 1885 [3]. He observed that we tend to remember things more effectively if we spread reviews out over time, instead of studying multiple times in one session. Since the 1930s there have been many proposals for utilizing the spacing effect to improve learning, in what has come to be called spaced repetition.

According to Ebbinghaus, we gradually forgot things if we do not repeat them (fig. 1). We should recall information if we want to maintain it in our memory.

We break information down into pieces (e.g., statements or video fragments). Each piece has the last repetition day and the next repetition day. We should increase the interval before these days. It is ineffective to do it manually. There are a lot of programs that can assist us. Anki [4] is one of the most popular. It is a free, cross-platform and general-purpose application.

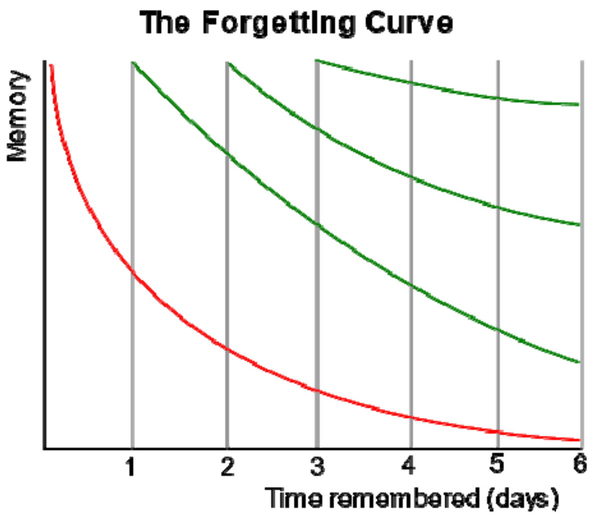

Figure 1
Figure 1 shows the Ebbinghaus forgetting curve

SPACING EFFECT IN LANGUAGE LEARNING

Many learners use spaced repetition for remembering new words. It is easy and natural to create a flashcard with a foreign word on the front side and the translation on the back, and then just review it with increasing intervals.

Pimsleur language learning system is also based on spaced repetition. It has been gaining popularity since 1967 when it was developed.

It seems appropriate to use the similar technique for listening comprehension. We can replace flashcards with video fragments. The user can extract these fragments from the video and review them later at increasing intervals. Spaced repetition can help retaining obtained listening skills and imprint the speech deeper in user's mind.

AUTOMATION OF VIDEO FRAGMENTS EXTRACTION

It is quite hard to extract video fragments without a special program, and it is even more difficult to organize the spaced repetitions of these fragments. We were unable to find any program that does and tried to write an Anki extension that would save video fragments as flashcards, but it was proved inefficient. Thus, it was necessary to create an application from scratch.

The special interface was created that allows the user to stop the video and extract a fragment alongside with the subtitles (fig. 2).

The application tries to guess the start time and the end time of the fragment. This prediction is based on subtitles accuracy and work well in the most cases.

The user can adjust the bounds of the fragment if subtitles timing is not good enough for him. The application has the convenient interface for it (green arrows in figure 2).

It is possible to attach a flashcard in case the subtitle contain a new word. The user can improve vocabulary at the same time with listening skills.

The program stores the information about all video fragments in the database. The user can repeat previously extracted fragments (fig. 3). He can slow the speed down if the speech is too fast or unclear. Pimsleur language learning system is also based on spaced repetition. It has been gaining popularity since 1967 when it was developed.

Figure 2

Figure 2 shows the user interface for video fragment extraction

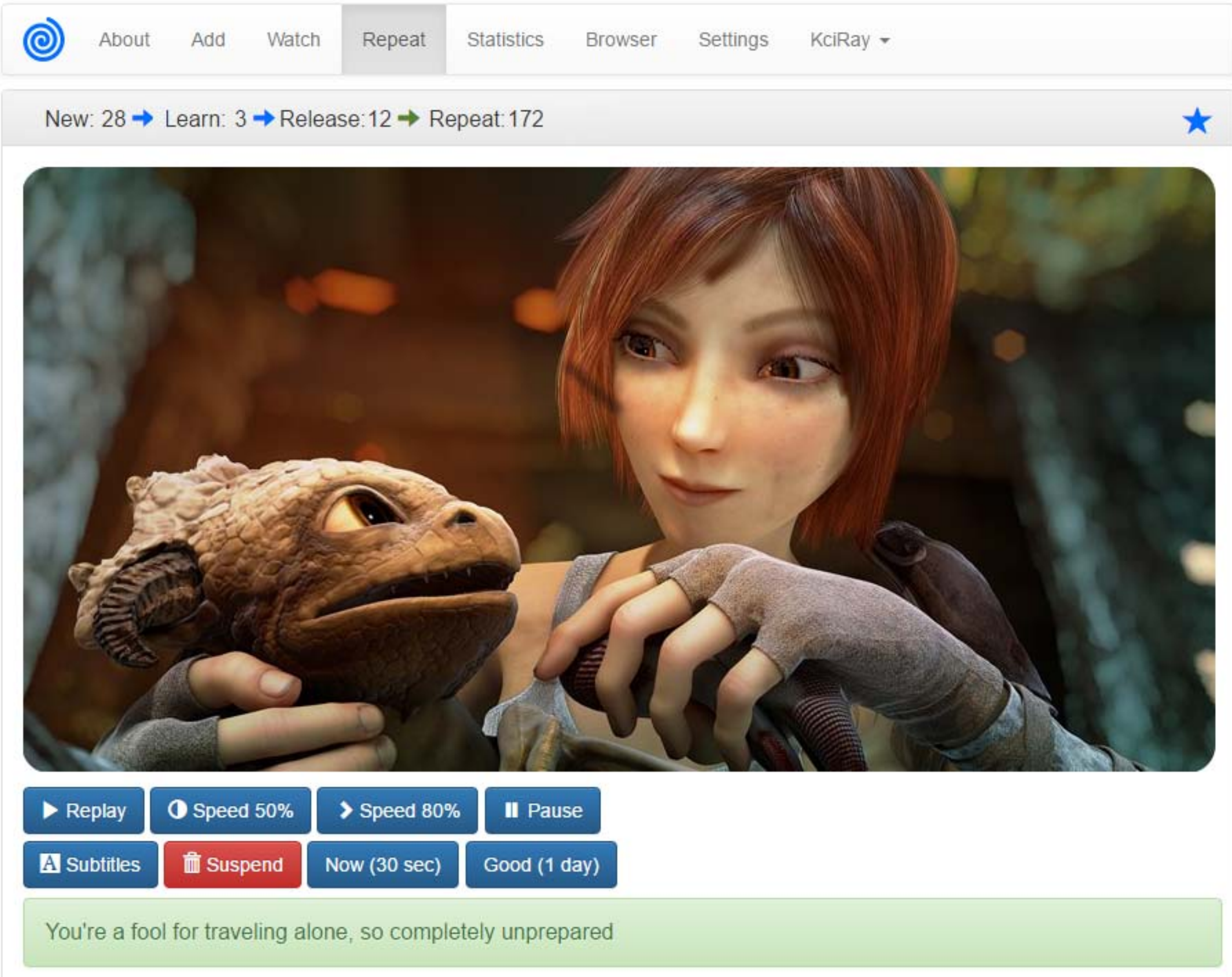

Figure 3
Figure 3 shows the repetition panel

WORK SEQUENCE

The user should stick to the special order while he is working with the application (fig. 4). There are three activities – the fragments extraction, the first repetitions and the spaced repetitions. The user should start with watching the video and extracting fragments from it. He should repeat them on the next day with care. The first repetition is usually more difficult than the next repetitions (the spaced repetitions).

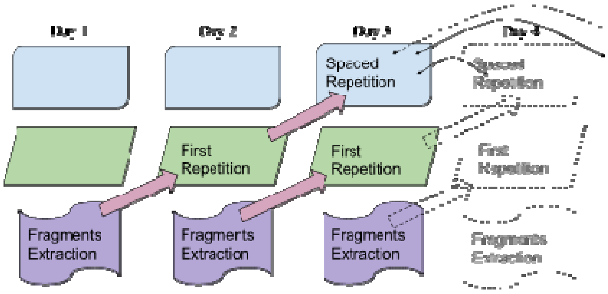

Figure 4
Figure 4 shows the work sequence

It is worth noting that the user should work with the application every day and spend about 2 - 2.5 hours. We presented estimated durations for each type of activity in table 1.

Table 1. Activities

Activity	Duration (min)	Efforts
The fragments extraction	40 – 60	Hard
The first repetitions	30 – 40	Middl e
The spaced repetitions	1 – 30	Easy

RESEARCH

When the user finished a season from some TV series, the application can calculate the average number of extracted fragments per episode. The user can estimate his skills by this value and track their development from season to season. This method is very precise because episodes tend to have the same length.

The assistant extracted about 7000 fragments during the three-month period (from April to June

2016) and processed four seasons from Friends (table 2). The average fragments decreased from 100.15 to 51.33. Thus, the assistant improved his listening skills twice. This is a very good result because many people spend years to achieve the same result.

Table 2. Statistics

Season	**5**	**6**	**7**	**8**
Episodes	24	25	24	24
Fragments	2404	2067	1367	1232
Average Fragments	100.15	82.67	56.96	51.33
Flashcards	260	270	245	202
Average Flashcards	10.83	10.80	10.21	8.42

TECHNICAL ASPECTS

The developer wrote the application in Java/Groovy and HTML5 mainly. It based on client-server architecture and uses Spring Framework on the server side and AngularJS on the client side.

The video player is based on HTML5 <video> element. Thus, there are three supported video formats: MP4, WebM, and Ogg. However, the user should check if his browser supports particular codecs.

The database is stored in a file. The application works through Hibernate Framework and uses H2 Database as an engine.

Many additional libraries and frameworks were used, such as Apache commons, Jsoup, Jetty, Twitter bootstrap and VTT JS.

CONCLUSION

We have proved that the spaced repetition technique is useful for improving listening skills. The user can use the application “IceMemo” [1] to automate this process.

We published the article on the Internet [2], and two hundred of users downloaded the application from our server and checked it out. Some of them contacted us a few months later and declared that their listening skills were improved significantly.

REFERENCES

[1] IceMemo - Improving listening skills in language learning with spaced repetition technique http://icememo.org/ (retrieved on 10 March 2017)

[2] IceMemo – studying foreign languages with TV series https://geektimes.ru/post/278382/ (retrieved on 10 March 2017)

[3] Ebbinghaus, Hermann (1885). Über das Gedächtnis. Untersuchungen zur experimentellen Psychologie [Memory: A Contribution to Experimental Psychology] (in German). Trans. Henry A. Ruger & Clara E. Bussenius. Leipzig, Germany: Duncker & Humblot.

[4] Friendly, intelligent flash cards. Remembering things just became much easier. http://ankisrs.net/ (retrieved on 10 March 2017)

[5] Human Memory: Theory and Practice", Alan D. Baddeley, 1997

AN ASSESSMENT STRATEGY TO MEASURE PROGRESS TOWARDS REALIZING A NATIONWIDE LEARNING HEALTH SYSTEM

Bryant Stephanie

Indiana State University
Terre Haute, Indiana

E-mail: s.bryant862@gmail.com

Abstract

Technology and digital communication system advances has made collection, storage and transmission of health information easier and faster. The US government has made electronic health information networks and health data systems a national priority by enacting legislation to develop a national health information infrastructure and encourage the meaningful use of electronic health records. Learning health systems seek to retrieve and analyze electronic health record data retrieved from nationally dispersed health information sources and develop new insights that will useful to various stakeholder groups, including individuals, clinicians, researcher, and health policy makers. This effort seeks to determine how much progress has been made in using connected health data systems to learn from collected electronic health record data on a nationwide basis. The proposed assessment strategy seeks examine progress toward realizing a national learning health system in terms of system operational concepts – system usage, data transformation capabilities, and sustainability; and progress measures in terms of system maturity, learning capabilities, and dissemination capabilities.

INTRODUCTION

Technology and digital communication system advances has made collection, storage and transmission of health data easier and faster. Healthcare is a key nationwide industry that addresses both individual and population level health concerns. According to a Centers for Medicare and Medicaid Services (CMS) report, in 2015 healthcare spending accounted for 17.8 percent of the US Gross Domestic Product (GDP), which measures the annual contribution of all goods and services of a country [1]. The US government has made electronic health information systems and networks a national priority by enacting legislation and creating a national health information technology office charged with establishing the foundations for a national health information infrastructure, as well as incentivizing the meaningful use of electronic health records.

Many stakeholders, including patients, clinicians, researchers, insurers, and policymakers are interested in health data collected in electronic health records (EHR). By analyzing EHR data, stakeholders can ascertain evidence-based implications of real life health issues, such as health outcomes and efficacies of treatment protocols, drugs, medical devices, and other health related topics. In a 2015 report, the Office of the National Coordinator (ONC), the federal organization charged with leading the digital conversion of health information and supporting health information infrastructure, reported that over 80% of doctors used an EHR system [2]. While electronic health record systems enable efficient collection, storage, and retrieval of health information, how can we develop insight from that electronic data on nationwide scale? A Learning Health System (LHS) integrates electronic health data networks with analytical components in order to analyze large sets of health data and develop evidence based insights of health topics supported by data from real patients.

A learning health system is envisioned as a system of systems that uses large scale (i.e., nationwide) health data networks to learn from collected electronic health data. This effort seeks to determine how much progress has been made in using connected health data networks to learn from collected electronic health record information on a nationwide scale. The proposed strategy examines the progress of selected early learning health system endorsers in extending their health data networks to include transformative capabilities that generate new knowledge or insights from existing electronic health data. The strategy also includes provisions to examine the experiences and variations of existing learning health system implementations and discover emerging patterns that may be applied in other organizations seeking to develop learning health system capabilities. The strategy seeks examine to progress toward realizing a national learning health system in terms of system operational concepts – system usage, data transformation capabilities, and sustainability; and progress measures in terms of system maturity, learning capabilities, and dissemination capabilities.

LEARNING HEALTH SYSTEM

The Institute of Medicine (now the Health and Medicine Division of the National Academies of Sciences, Engineering, and Medicine) recognizes the importance of health information and informatics. In 2007, the IOM developed a definition for a learning health system which represents a computational extension to existing health data networks [3]. A learning health system is an Informed decision making tool used for disseminating health knowledge generated from large and diverse health data sets and evidence based findings to clinicians, researchers, and other health stakeholder groups. The generated results are then used as input to next iteration of analysis in order to continuously learn from past information while incorporating new information. A learning health system's strength is achieving a continuous cycle of learning from existing and new information.

A nationwide learning health system requires the coordination and consensus of people and technology across local, regional and state boundaries. There are many challenges to realizing such an ultra large system. Some challenges can be categorized as governance, technology, and standards. Governance challenges include establishing general standards of operation, managing participation, codifying data use across multiple domains and organizations. Technology challenges include adoption of technology and processes, growing the system by interconnecting existing learning health system implementations, and integrating innovation. Standards challenges include gaining consensus on common system concepts of interoperability so that system can successfully exchange information in known formats.

Learning and analytical capabilities distinguishes a learning health system from health data system. Key activities in the knowledge generation or learning process of a learning health system consists of aggregation (gathering and prioritizing relevant data), analysis (mining data for patterns, and insights), and dissemination (transferring findings and insights to stakeholder groups for consideration). The stakeholder groups can be data generators as well as information users. The process forms a continuous loop of learning that benefits stakeholder groups by delivering timely evidence-based information.

As more organizations embrace the LHS vision, tracking progress toward realization of a nationwide inter-connection of learning health systems is important to understanding what work needs to be done in order to realize the vision of a nationwide learning health system. Sitting et al [4] constructed a framework of concepts to assess the progress of health information networks. The Learning Health Community developed a research agenda to identity relevant research questions pertaining to the development of a learning health system [5]. Morain, Kass, and Grossmann [6] studied challenges experienced by organizations in their transition to learning health care system and included recommendation for other organizations considering a similar transition. This assessment strategy combines concepts and findings from these previous efforts in health data network operation and learning health systems to assess the progress towards a national learning health system. This proposed assessment strategy seeks measure national learning health system progress in terms system operational concepts and progress measures.

OPERATIONAL CONCEPTS

System operational concepts focus on system usage, data transformation capabilities, and sustainability. The system availability and usability concepts seek to understand the essential health data network operation. System availability is the health data system's structure that enable users to access and interact with data over periods of time. Systems use addresses the frequency of system interaction by patient, provider, and other health information consumers.

The learning capability concepts address the learning health data networks ability to distill and transform health data in to information and insights. Nationwide health data transformation requires collection, analysis and sharing of information beyond the current organization, region, or legislative boundary. There varying degrees of data transformation, including aggregation, pattern finding, and insight development.

PROGRESS MEASURES

The proposed assessment strategy will be used a dissertation research effort. Data collected during research effort includes technology challenges, successful technology trends, and progress toward a nationwide (large scale) learning health system implementation. Assessment data will be gathered as part of semi-structured interviews with technologists familiar with an existing learning health system development and operation.

Measurement of progress is determined suing a set of measurement parameters supporting the assessment concepts. The author assigns each parameter a base line measure and progress is measure as demonstrated capabilities beyond the baseline.

To achieve nationwide operation, learning health must be mature enough to support large scale and continuous operation. Technology Readiness Level (TRL) will be used to gauge system maturity. TRL, a technology assessment approach originating from the Department of Defense, used to report the overall development stage of a technology or system as one of nine levels from basic technology research (level 1) to mission operation (Level 9) (Azizian, et al, 2011). The baseline TRL level for an operating learning health system is level 6 – the prototype system has been tested in relevant environment.

The learning capability parameter is expressed as a discrete set of category options describing the data transformation and dissemination abilities of the LHS. The categories are “aggregate”, “reason”, and “disseminate”. Aggregate is the capacity to extract and filter relevant data from local and external systems into a set for automated analysis. Reasoning implies the incorporation of an analysis process to examine input data as a group and produce set-based results. Dissemination is capability to export the set- based results to local and external systems. This research effort assumes that the learning capability is beyond descriptive statistical analysis of the set, such histograms, averages, etc. The base level for the learning capability parameter is “aggregate”.

The system connectivity parameter is expressed as one of a discrete set of category options describing the capability of the target LHS to exchange information with external systems. The categories are “No external contact”, “Plan for external contact”, and “Executed external contact”. A plan for external contract could be the existence or establishment of a data sharing agreement between the target organization and an external organization under a separate governing structure. This strategy assumes that an LHS in a multi-site organization where each site is under the same governing control are considered a single LHS system. An external system must be separate for all internal sites. The base level for the system connectivity parameter is “No external contact”.

Together the operational concepts and progress measures a target LHS address the system operational capability as health data system and extended capability necessary to operate as a learning health system and demonstrate some capability to participate in a large scale implementation of a learning health system.

CONCLUSION

The proposed assessment strategy seeks to determine how much progress has been made in using connected health data systems to learn from collected electronic health record data on a nationwide basis. The strategy seeks to examine national learning health system progress in terms concepts operational concepts and progress measure: systems availability and usability, data transformation, system maturity, and sustainability, system connectivity. The strategy measures progress from an established base line chosen by the research in terms of system maturity, analysis capability, and external system contact for a set of target learning health system implementations.

REFERENCES

[1] Center for Medicare and Medicaid Services (CMS). (2016). Historical – Centers for Medicare & Medicaid Services. Retrieved March 1, 2017 from https://www.cms.gov/research-statistics-data-and-systems/statistics-trends-and-reports/nationalhealthexpenddata/nationalhealthaccountshistorical.html

[2] Monegain, B. (2015). More than 80 percent docs use EHRs. Healthcare IT News. Retrieved March 1, 2017 from http://www.healthcareitnews.com/news/more-80-percent-docs-use-ehrs.

[3] Institute of Medicine (IOM). (2007). The Learning Healthcare System: Workshop Summary. Washington, DC: The National Academies Press

[4] Sitting, D, Shiffman, R., Leonard K., Friedman, C., Rudolph, B., Hripcsak, G., Adams, L., Kleinman, L., Kaushal, R. (2005). A draft framework for measuring progress towards the development of a national health information infrastructure. BMC Medical Informatics and Decision Making. 5(14). http://www.biomedical.com/1472-6947/5/14

[5] Friedman C, Rubin J, Brown J, et al. (2014). Toward a science of learning systems: a research agenda for the high-functioning Learning Health System. J Am Med Inform Assoc. doi:10.1136/amiajnl- 2014-002977

[6] Morain, S. R., Kass, N. E., and Grossmann, C. (2016), What allows a health care system to become a learning health care system: results from interviews with health system leaders, Learn Health Sys, doi: 10.1002/lrh2.10015

[7] Azizian, N., Mazzuchi, T., Sarkani, S., & Rico, D. F. (2011). A framework for evaluating technology readiness, system quality, and program performance of U.S. DoD acquisitions. Systems Engineering, 14(4), 410-426. doi:10.1002/sys.20186

8 TAKE-OFF

Caputo Salvatore, Vitale Stefano

Computer Engineering and Networks Laboratory – Kore University of Enna - Italy

Email: {salvatore.caputo;stefano.vitale}@unikorestudent.it

Abstract

This paper focuses on the implementation of a new mode of detection of the ideal parameters during take-off of an aircraft Airbus A319, through sensors installed inside the aircraft. The proposed system is composed of a wired network, with the IEEE 802.3 protocol and knitted or crocheted topology. The simulation has been implemented using Matlab/Simulink.

INTRODUCTION

Our project addresses an interesting issue in the aeronautical field. We want to outline what should be the ideal parameters necessary so that the takeoff of an Airbus A319 [1] can be done. The considered aircraft (Airbus A319), from technical specifications, has the following characteristics:

- wingspan 33.91 m;
- maximum height from ground 11.76 m;
- Fuselage length 33.84 m;
- max weight on takeoff 68,000 kg;
- autonomy at full load 4.908 km (2650 miles);
- cruise speed 841 Km.

In the context of aviation, instruments capable of giving to the pilot the feedback such as to be able to understand if the Takeoff is happening in the correct way or less already exist [2]. One of the instruments on board, which makes it possible to the pilot to understand the speed of the aircraft, is the anemometer. This tool, indicating the speed of the aircraft with respect to the surrounding air, is based on the measurement of the dynamic pressure obtained from tubes of Pitot. The anemometer has three arches of various colors: arc white, green and yellow.

The white arc is used generally for flaps and truck, the green arc for the cruising speed of operation of the aircraft, the yellow arc for the speed of the aircraft in the calm air. At the end of the yellow arc, there is a red line (VNE) which indicates the maximum speed aircraft structural.

The solution introduced in this paper is composed of several sensors that periodically communicate over the network with a central gateway, which is activated at irregular intervals [3]. Once the values have been received, the gateway will monitor the actual veracity of the above values and sends them to a physical output, i.e. to a soft computing system. The values are processed by means of specific and strict criteria calibrated on the basis of the technical data sheet of the aircraft, that help to decide whether the takeoff can take place safely or not.

Our project is more comprehensive and reliable because it is based not only on the speed of the aircraft but also takes into consideration other important parameters such as the fuel pressure and the speed of the wind. If their values become critical, the system will sound a specific or general alarm. Depending on the alarm, the system will activate 3 lights of different coloring, green, yellow and red; the pilot, looking at the light, is able to determine if the aircraft take off may or may not occur and what are the parameters to consider in adverse conditions.

THE PROPOSED APPROACH

In our approach a network, composed of the following functional blocks, each with a different task and set on the basis of the role it plays, is implemented.

1) SENSORS: devices that allow to measure the physical quantities which are considered relevant for the functionality of the system. In our network, there are the following sensors:

- Speed Aircraft SENSOR;
- Fuel Pressure SENSOR;
- Speed wind SENSOR.

2) GATEWAY: device installed and configured within a network, work at the network level or at higher levels of the model protocol ISO/OSI. It has the task of routing packets toward other gateways, until they arrive at their destination. Our gateway within the network has the function to check if the received packets are empty or less. Finally, if they are not empty, it forwards them to appropriate destinations, thus allowing the correct reception of the data that will be subsequently processed.

3) SOFT COMPUTING: techniques that are used to evaluate, to decide and to check in the approximate areas and various emulating and using the ability of humans to perform these activities on the basis of their experience. Soft computing has characteristics, depending of the application in which is used:

- possibility of modeling and control uncertain and complex systems, as well as to represent the knowledge in an efficient manner through the linguistic descriptions typical of fuzzy sets theory;
- ability of the optimization of the generic algorithms whose computation is inspired The laws of selection and typical mutation of living organisms;
- ability to learn complex functional relationships of neural networks, inspired by those of the brain tissues.

In our approach, there are two types of soft computing, i.e. fuzzy controllers, set differently depending on the technical data sheet of the aircraft concerned and with different functions.

4) STATEFLOW: environment for modeling the simulation on the base of a state machine and flow charts. It allows to combine graphical and tabular representations, including transition diagrams of state flow diagrams, to model the way in which the system reacts to events, temporal conditions and signals. In our project the StateFlow has been used to represent the logic for supervision applications for planning and management of actions or faults (fault management).

The sensors are activated periodically, they acquire the data received and send them through the network to the gateway (controller), which is activated at irregular intervals and, once received and verified, they are sent to their destinations, through physical outputs of the gateway. These data, in turn, will be received and processed by the soft computing (fuzzy logic controller), set according to the characteristics of the aircraft into consideration and, finally, will be sent to StateFlow, which will emit three different lights on the basis of the settings and the data received.

The choice of IEEE 802.3 [4] protocol and a star topology is justified by several needs:

- transfer data without having electromagnetic interference, since inside an aircraft are already present in the fields determined by the onboard instrumentation such as radar and transponder;
- transfer data in a safe and reliable way, ensuring an error probability close to zero, security that you may not have a wireless network, since the only medium is the ether and the data may suffer losses or numerous interference;
- the wired network allows a safer transmission data with respect to a wireless network, thus preventing intrusions, interception or alterations of unauthorized data.

SCENARIO

In this Section, we introduce our simulation scenario created in Matlab/Simulink, presenting illustrative figures and analyzing the various structural configurations.

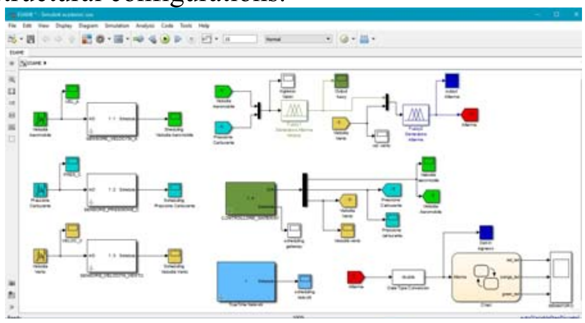

Figure 1: Matlab/Simulink scenario

Figure 1 shows the physical structure of our project, the network with its nodes, the three sensors for the detection of parameters, the gateway, the controllers to fuzzy logic appropriately set and finally the StateFlow. In detail, the Gateway, that receives the data (packets) sent by the sensors via the network, is positioned in the middle. Once received the data, it forwards them without the use of the network to the fuzzy logic controller. To the left of Figure 1, the 3 sensors are positioned. They detect data as aircraft speed, wind speed and fuel pressure. The StateFlow is positioned at bottom right. It receives, as an input, the signal and gives a luminous signal in output, on the basis of the preset settings.

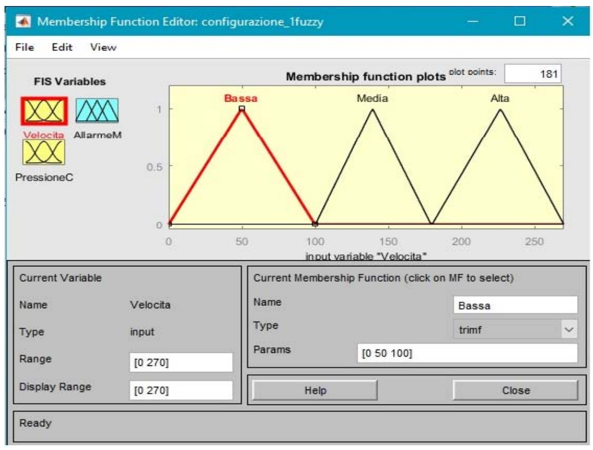

Figure 2: fuzzy configuration of aircraft speed

An example of used fuzzy controller is depicted in Figure 2. In this case, the fuzzy configuration of aircraft speed is shown.

INPUT: aircraft speed; Range [0 270]

The membership function plots have been set as follows:

- Low [0 50 100];
- Medium [100.1 139.3 180];
- High [180.1 226.8 270].

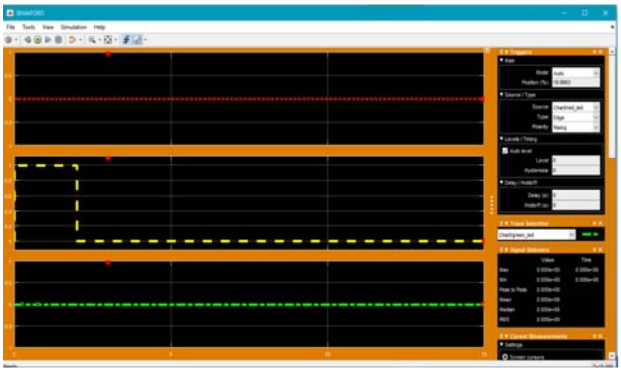

Figure 3: scheduling of the semaphore

Figure 3 shows the scheduling of the semaphore. As soon as the StateFlow receives the input of the alarm, it generates a light signal and it is the basis on which the takeoff may be completed or not:

- Red: takeoff denied;
- Orange: it is possible to carry out the takeoff, paying attention to the critical parameters detected by the sensors, then the pilot must evaluate the checklist;
- Green: it is possible to carry out the takeoff in complete safety.

PERFORMANCE ASSESSMENT

In this section, we present the correct functioning of our network. Therefore, we will include figures showing different scheduling of tasks.

Figure 4: scheduling of the network

Figure 4 shows the scheduling of the network, i.e. the activity of the sensors, deduced by different colors. The gateway has no activity because it is not a periodic task and then it is only active when it receives values from the sensors.

Figure 5 shows the scheduling of the semaphore, after the StateFlow has received the input of the alarm, it generates a light signal and it is the basis on which the takeoff can be made or not.

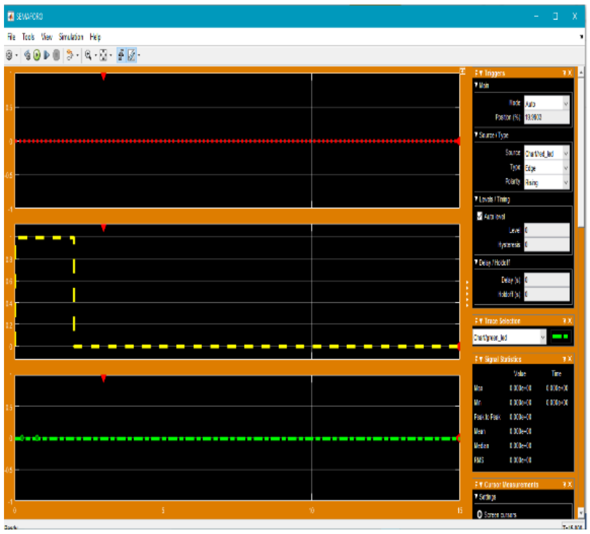

Figure 5: scheduling of the semaphore

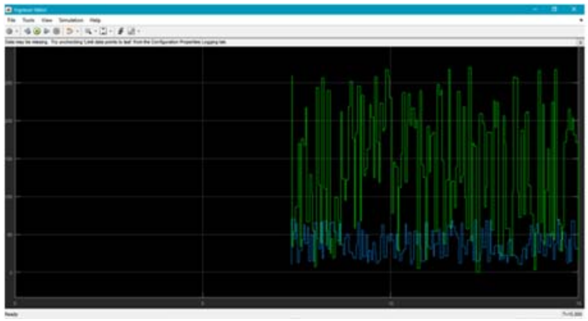

Figure 6: scheduling of the fuzzy logic controller

Figure 6 shows the scheduling at the entrance to the first fuzzy logic controller. In input, it receives the aircraft speed and the fuel pressure.

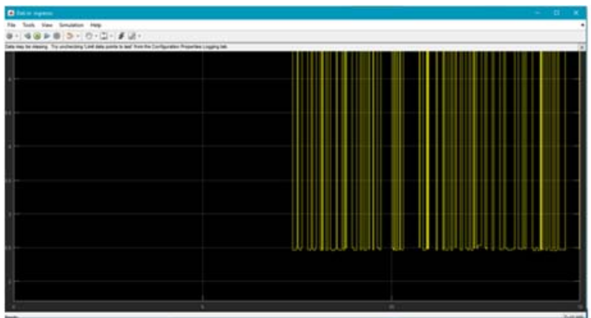

Figure 7: scheduling of the StateFlow

Figure 7 shows the scheduling at the entrance of the StateFlow that has the function of kindling the lights of the semaphore on the basis of the value of incoming alarm.

CONCLUSIONS

The proposed solution confirms that its implementation could be optimized and then tested on board of an aircraft. This project aimed to simulate a network in order to show what are the ideal parameters during the takeoff. The choice of implementing a wired network has been carried out because onboard of an aircraft a wireless connection may cause interference with the onboard instrumentation. In the aeronautical field, there are already similar projects, such as, for instance, the indicator to takeoff is based exclusively on a single parameter: the speed of the aircraft, acquired by means of an instrument of edge called anemometer. In this project, on the contrary, there are other essential parameters, such as wind speed and fuel pressure, which could improve and inform the pilot both on the condition of the aircraft and on climatic conditions, thus allowing a greater safety and awareness on the takeoff.

REFERENCES

[1] Official Manual Airbus A319.

[2] R. Trebbi, Theory of Flight.

[3] Carlo Brantolese, William Fornaciari, Embedded Systems (Hardware and Software Development for dedicated systems), Pearson.

[4] Andrew.S, Tanenbaum - David J. Wetherall networks of computers 5° Edition.

A WSN IMPLEMENTATION BASED ON ZIGBEE PROTOCOL IN A HOME AUTOMATION SYSTEM

Costanza Valentina, Catania Alberto

Computer Engineering and Networks Laboratory – Kore University of Enna - Italy

Email: {valentina.costanza;alberto.catania}@unikorestudent.it

Abstract

This paper proposes an integration of the ZigBee protocol in a home automation system. In detail, the chosen context is a generic apartment. The system manages the interaction with the different “parts” of the house (lights, air conditioners, thermostats, etc.), allowing the user to manage and monitor them.

INTRODUCTION

The electronic devices related to home automation are rapidly spreading recently, thanks to the lower costs of them and the relative ease of use. The standardization of protocols, suitable for this purpose, has led to the placing on the market of a large variety of products that allow each user to check the desired parameters within the home. In detail, this has led to a dissemination of sensors that enable the energy savings and other features that deal with the safety of the house.

Home Energy Management Systems (HEMS) aim to find a solution in order to save energy and to increase the comfort in the home area. The deployment of HEMS could permit every family to know the consumption comprehensively and to recognize how to get benefits from efficient energy management. HEMS is demanded to have functions for the monitoring and controlling of every appliance in the home. The deployment of HMES depends on the development of home area networks that enables such functions.

The ZigBee protocol is defined by the IEEE 802.15.4 standard, which describes all the standards for Personal Area Networks (PAN) [1]. ZigBee operates in the Industrial, Scientific, and Medical (ISM) radio bands: 2.4 GHz in most jurisdictions worldwide; 784 MHz in China, 868 MHz in Europe and 915 MHz in the USA and Australia. Data rates vary from 20 kbit/s (868 MHz band) to a maximum of 250 kbit/s (2.4 GHz band). ZigBee supports various network topologies, including star, tree, and mesh. ZigBee devices are of three kinds: ZED (ZigBee End Device), ZR (ZigBee Router) e ZC (ZigBee Coordinator). ZigBee products have low power consumption depending on the transmission rate; the batteries could work for a couple of years without recharging. Therefore, ZigBee products, compared to other technologies, have a low operation cost. However, ZigBee (at 2.4GHz) has the problem that it shares the same frequencies with other protocols, Wi-Fi for instance; therefore, the signal might be interfered leading to a degradation of performance of the network.

In this paper, a possible implementation of a home automation system, based on ZigBee, one of the most common standards for the IoT, is studied. The rest of this paper is organized as follows: Section II shows other examples, found by analyzing the state of the art, about possible implementations of PAN using the ZigBee protocol. Section III gives a list of the network devices and the steps that have preceded the network creation. Section IV describes in detail the test environment, while in Section V the performance metrics of the environment are analyzed. Finally, section VI gives concluding remarks and plans for future research.

RELATED WORKS

In the last few years, the number of literature works focused on the analysis of PAN networks has increased exponentially compared to previous years due to the progress and development of fields of use. The authors of [2] have proposed a possible implementation of a network with ZigBee devices. The main aim is to show how simple is the communication among devices of different manufacturers.

In [3] it is highlighted that the implementation of home networks often doesn’t allow the user an immediate change of the system status, therefore the authors introduced inside the network a device for voice recognition and a remote controller, increasing the user comfort. The latter, in fact, can have the ability to set up automatic mode that allows the system to operate independently and a manual mode that stops the activity of sensors and permits the user full control of the actuators through the use of voice command.

With the spread of PAN standards, external attacks for the acquisition of the data are increased. An example of a defense mechanism against these events is described in [4] through the use of machine-learning algorithms that allow the system to figure out when it is under attack and provide the necessary countermeasures acting on the physical and network levels. The authors analyze in detail several techniques and examples of attack that the system could sustain and, at the end, show the appropriate countermeasures.

THE PROPOSED SOLUTION

As mentioned previously, the main aim of this paper is to show an implementation of a WSN (Wireless Sensor Network) in a home automation scenario. The wireless sensors interact with each other forming a tree network topology. The network, divided into 4 rooms (bathroom, kitchen, and two generic rooms) consists of 20 sensors (5 per room), specifically:

- 5 temperature sensors, equipped with a 2000mA battery, as applicable specifications [5];
- 5 humidity sensors, the same type as those for the temperature;
- 5 light sensors, with the same capacity of the previous;
- 5 presence detectors, equipped with two batteries whose total capacity is approximated to the capacity indicated in the previous sensors;
- 5 sensors for the detection of CO_2, with the specifications entered with data similar to those of devices of the same type available in the market [6];
- 4 gateways [7], of which one in common for the two rooms, one for each of the remaining rooms and a central one;
- 2 controllers, one that deals with the data received from the humidity and temperature sensors, the other one of the other sensors;
- 1 actuator who will execute the commands received from a proper controller;
- 1 regulator that through the data received from the controller, mimics the operation of an air conditioning system.

The entire network communicates through the ZigBee standards. In fact, each sensor has its own parameters, such as the energy consumption and the capacity of the battery. Moreover, each sensor has its own sampling time.

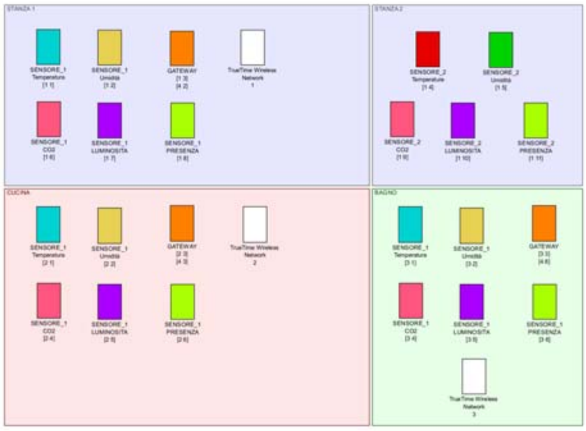

Figure 1: House Plan

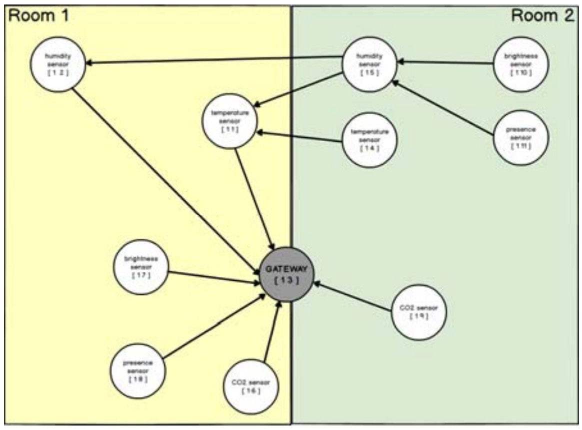

Figure 2: Network 1 model

TEST BACKGROUND

The chosen test environment, developed in Matlab/Simulink and TrueTime Simulator, is an apartment that consists of four rooms (Fig. 1). In each room, there are five sensors: each one of them refers to a gateway installed in the same room. Generic rooms, called Room 1 and Room 2 in the project, share the same gateway, in this way they belonged to the same network (network 1). In the two above-mentioned spaces, we distribute the nodes of the first network with a tree topology, as shown in Fig. 2. This arrangement was originally designed in order to create a mesh sub-network, which depending on traffic reported to the sensors would allow the redirection of packets to prevent network congestion. A clear policy has been applied to the priority management of the task, in order to allow the proper functioning of the services that require a response within a certain period. In particular, messages sent by CO_2 gas sensor have high priority as fundamental for the safety. The same priority has been applied to messages originating from presence sensors because they require a quick response for the switching on of the lights when a person enter in the room.

The gateways of the four spaces are connected to a central gateway that acts as the network coordinator, which redirects packets through the execution of five different tasks, each of them related to the type of message and the room of origin, to the controller. The humidity and temperature controller uses fuzzy logic in order to adjust the value of the power conditioner. The received values of temperature and humidity will be processed by the controller through *if-then* rules, in order to obtain an output in accordance with the established logic.

The received power value will be read by the controller, which, using a specific function will be able to set the values of temperature and humidity for the room. Similarly, the controller of presence sensors, brightness, and CO_2, uses the fuzzy logic: light and presence values are passed as input, while the output is the percentage of brightness suited to that environment for a greater energy efficiency. It has been necessary to insert a flow chart controller that:

- verify the effective presence of an individuals into the room, in order to ensure the switching off of light, regardless of the percentage of brightness;
- mimic the external inputs from the user, handled by a switch simulated by the following values:

0. the user sets the automatic mode of the fuzzy controller;
1. the user sets the brightness level indicated by the fuzzy, regardless of the received presence value;
2. the user turns off the light of a particular room;
3. the user sets the maximum brightness.

The updated value of the brightness percentage is transferred to the actuator with the CO_2 parameter. The latter will ensure the status of the home environment safety: in case the allowable CO_2 levels are exceeded (over 100ppm), it will raise an alarm level and will activate a buzzer according to the value of the criticality.

PERFORMANCE METRICS EVALUATION

Two simulations have been carried out in order to evaluate the performance metrics. The first in "normal" conditions, i.e. each sensor transmits at a realistic frequency; in the second, all the sensors transmit every second, in order to simulate the network overload. In both scenarios, the reaction time, the response time and the throughput have been measured. Finally, by comparing the obtained results, the stretch factor has been calculated.

The reaction time, i.e. the amount of time between the submission of a request and the start of its execution, has been calculated for each sensor in the system. In this case, it represents the time that elapses between the sending of the message and the receipt by the next node. The response time, i.e. the amount of time between the user request and the response of the system, has been calculated for temperature and the CO_2 sensors of the kitchen. The time that elapses between the sending of the message of the sensor until the sensor receipt by the actuator/controller has been measured.

The throughput has been obtained by calculating the number of bits per unit of time (second); the total number of packets sent by the sensors have been counted during the simulation, multiplied by the minimum size (272 bits) of each packet divided by the simulation time. The stretch factor has been calculated through the ratio of response time to a certain load and the response time in standard conditions.

Simulation 1: 3600 seconds (normal conditions)

Reaction Time: using the data obtained from the simulation, an average has been done of the reaction time values of the individual sensors. The reaction time has been calculated by saving the detection time of the data along with the identification data of the sensor, in a structure sent to the next node which, once read these values, carries out a subtraction between the current time and the one sent to him, returning the time value used for transfer. Table 1 shows the average values of reaction time for each sensor, from which the average time of a generic package has been obtained, which is approximately equal to 0.2774 seconds. This value is influenced by the execution time and by the priority assigned to the task. In detail, the data that weighs more on the calculation of the average is the time value of the light, presence, temperature and humidity sensors that belongs to the network 1, since the sensors are not directly connected to the gateway, but, through a Peer-To-Peer connection. The temperature and the humidity sensors serve as means for forwarding the messages, so the received messages will suffer a delay equal to the execution period of the task (1 sec).

Table 1

Sensors Reaction Time

					Average
CO2	0.189	0.1892	0.1411	0.1411	0.1651
Brightness	0.002	0.0018	1	0.0018	0.2516
Presence	0.073	0.0723	1	0.0723	0.3045
Temperature	0.003	0.1412	1	0.1412	0.3215
Humidity	0.095	0.1413	1	0.1413	0.3444

Response Time: with the same initial procedure of the reaction time, the transmitted values are sent with a related field that allows the sensor identification (room, type and detection time). The submitted data structure allows the packet to be redirected correctly through the network up to the proper actuator/controller. As mentioned previously, the response time has been calculated for the temperature and CO_2 sensors of the network 2 (kitchen). From the studied samples, it is possible to derive the average time needed for all the response times. The average response time of the temperature sensor is approximately equal to 0.8490 seconds, while the average response time of the CO_2 sensor is around 0.5181 seconds. This difference, as previously mentioned, is due to the priorities assigned to the tasks of the related nodes of the network; tasks related to temperature, humidity, and light have a lower priority than the task that handles the messages from the presence and CO_2 sensors.

Throughput: during a test of one hour, the number of packets sent by the various sensors has been 243. This value has been multiplied by the minimum frame size relative to amount to 272 bit network and divided by the duration of the simulation, in seconds:

$$\frac{243 \cdot 272}{3600} = 18.36 \left[\frac{\text{bit}}{\text{s}}\right] = 2.295 \left[\frac{\text{Byte}}{\text{s}}\right]$$

Simulation 2 - 3600 sec - Network overload conditions

The simulation has been executed by changing the execution period of the tasks. In this way, all sensor functions are called every second, without any distinction. The results are almost equal to what is found in normal conditions. This is due to the internal control of the tasks of the sensors that provide for the dispatch of data only if the difference of this with the previous one is greater of a certain index. Therefore, the network has not suffered any particular delays due to the load and indeed has shown marked improvements regarding the throughput, increased due to the number of packets transmitted per unit of time.

CONCLUSIONS

The purpose of this paper was to show one of the possible deployment scenarios of a home automation through the use of the ZigBee protocol. Given current costs and ease of use, the automated home provides a significant support for users.

Regarding future developments, in addition to effective implementation, it would be possible to add additional nodes and typologies of sensors. It might be interesting to add an intermediate router that enables communication with the Wi-Fi standard for remote control of the system via smartphones. Moreover, it could be managed through appropriate algorithms, the routing packets with the creation of a dynamic mesh network.

REFERENCES

[5] Zhen Zhao, Kodjo Agbossou, Alben Cardenas, “Connectivity for Home Energy Management applications”, Year: 2016, Pages: 2175-2180, 2016 IEEE PES Asia-Pacific Power and Energy Engineering Conference (APPEEC).

[6] Vladimir Moravcevic, Milan Tucic, Roman Pavlovic, Aleksandar Majdak, “An Approach for Uniform Representation and Control of ZigBee Devices in Home Automation Software”, Year: 2015, Pages: 237 – 239, IEEE 5th International Conference on Consumer Electronics Berlin (ICCE-Berlin).

[7] Ishan Krishna, K. Lavanya, “Intelligent Home Automation System using BitVoicer”, Year:2017, Pages 237-239, 2017 11th International Conference on Intelligent Systems and Control (ISCO).

[8] Paria Jokar, Victor Leung, “Intrusion Detection and Prevention for ZigBee-Based Home Area Networks in Smart Grids”, Year: 2016, IEEE Transactions on Smart Grid.

[9] ZED-THL-M: ZigBee sensor of temperature, humidity and brightness.

[10] TPZRCO2T/L: Titan Products Wireless Room CO2 & Temperature Sensor with LED.

[11] Gateway Modbus Ethernet.

MAGNETIC CORE MEMORIES: HOW TO CONSTRUCT ONE AND HOW TO SURVIVE AN OLD IBM DJB 373330 SMS CARD

Del Popolo Salvatore, Didomenico Nicola

Department of Electrical, Electronics and Computer Science (DIEEI)
University of Catania - Prof. Orazio Mirabella

E-mail: popolo@tin.it, nicola.didomenico@gmail.com

Abstract

Writing about magnetic core memories means coming back more than 50 years ago in the digital era and making an effort to survive a technology that represented in a concrete way, the possibility to store data in a nonvolatile manner. In the past century, around forties and fifties, scientists, technicians and engineers all over the world began to project and realize first examples of computers for military aims.

One of the fundamental elements of a computer is the possibility to store, either for the functioning of the system itself, or for future elaborations and uses. Magnetic, ferrite core memories made this fundamental function and were the dominant technology among fifties and seventies, before being substituted by transistors first and integrated circuits after.

Figure 0: IBM 1440 DATA PROCESSING SYSTEM

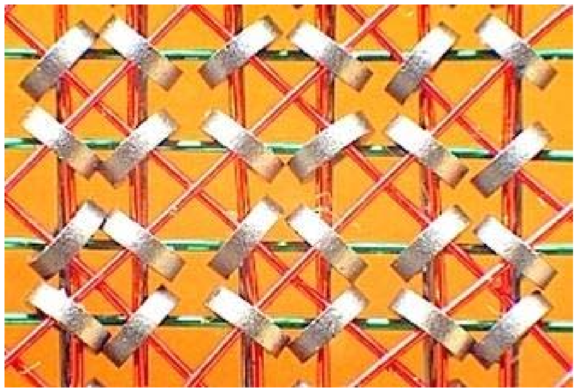

Figure 1: Magnetic Core Ferrite Memory (1940)

INTRODUCTION

In this short paper, pointing out functioning principles of magnetic core memories, starting from the work of two American researchers Ben North and Oliver Nash and only using open source software, we very briefly summarize how we built our 32 memory array and how succeeded in controlling it by an STMicroelectronics microcontroller.

At the end, we demonstrate that, a DJB 373330 SMS Card, owned by one of our professors and coming from an IBM mainframe of the past century, is still functioning.

MAGNETIC MEMORIES: FUNCTIONING PRINCIPLES

Far from being extremely reliable, magnetic core memory was an attractive techonology, as based on a very simple idea.

A core is a magnetic ring able to store just a bit, depending on the direction of its magnetization, how we can see from the graph in Figure 2.

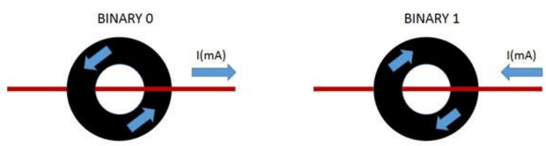

Figure 2: Logic States of Magnetic Core Memories

A magnetic core is a ferrite ring that can be permanently magnetized, either clockwise or anticlockwise, along its own axis. Hereby, a core can represent a bit of digital memory, imposing that the two states of magnetization are interpreted as 0 or 1, respectively, how we can see from the graph in Figure 3.

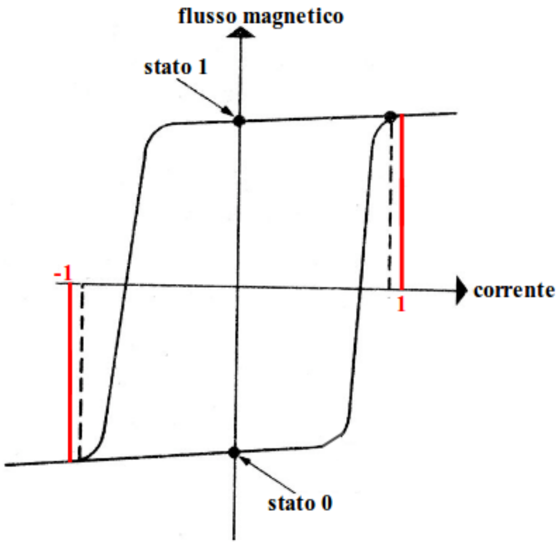

Figure 3: Direct and Opposite Current

The core need not to be powered to maintain its own value, realizing in this manner, a kind of nonvolatile memory as modern hard discs, but with an incomparably lower writing/reading speed.

As the technology evolved, core dimensions' decreased, passing from 2 mm in '50 to 0.4 mm in first years of '70 of past century. At the same time, access speed increased from 200 kHz to 1 MHz and assembling together hundreds of cores, built memories with more than 500.000 bits, how we can see from the graph in Figure 4.

Figure 4: Evolution of memories

The functioning principle of magnetic memories is based on a characteristic affecting all ferromagnetic elements. These can have two permanently states of magnetization. In the case of the ferrite ring, the two states of magnetization are identified by the two directions, clockwise and anticlockwise, around its circumference.

To set the magnetization core state's two conductive wires have to pass through it. A conductive wire generates a magnetic field and varying the intensity and the direction of the current that passes through it, it is possible to induce a change in the magnetization state of the core, creating what is defined as hysteresis cycle, illustrated in Figure 5.

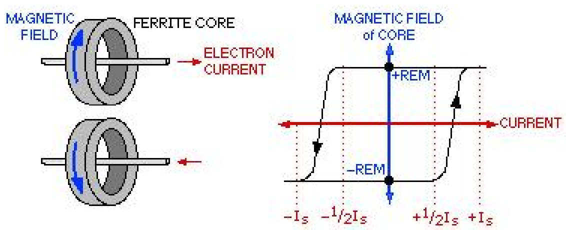

Figure 5: Ferrite Core Magnetization

Hysteresis cycle describes how changes the core magnetic field, as current varies in the wire. Points identified by ± REM represent the remaining magnetic field as no more current flows across the wire, they are the two magnetization states' that indicate the value 0 and one of the memory. Points identified by ± Is represent the required, current values to saturate the magnetic state of the core.

Organizing the cores, forming a two-dimension array, as in Figure 6, the only core affected by a change in the state is the one in which the two wires across each other and the two 1/2 currents sum themselves. Once the state changed, although removing the two 1/2 currents, magnetization core state does not change, storing a possible value. Remaining cores are not affected, as the 1/2 current that they receive, is not enough to induce a change in the direction of magnetization.

The orientation of cores versus currents is fundamental, as the two 1/2 currents must sum to each other to reach the necessary value to obtain the changing in the state. In fact, in this situation currents are defined coincident. To optimize driving lines in the control unit of the memory, it is also applied the mechanism of non-coincident currents, summarized in Figure 6. Finally, associating state of magnetization and logical value zero or one, is absolutely arbitrary.

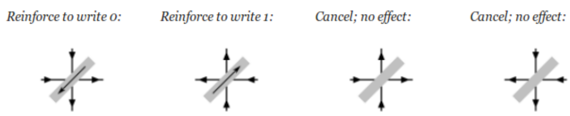

Figure 6: Coincident and Non-Coincident Currents

WRITING TO A MAGNETIC CORE MEMORY

We arbitrary impose that the two states of magnetization clockwise and anticlockwise represent values zero and one, respectively. With reference to Figure 7, let the two 1/2 currents flow, in the direct direction, in the two wires that identify the core we desire to write, until the direction of magnetization switches to clockwise. When that happens, the core will contain and maintain he value zero, even if no more current flows.

To change the value of the core from 0 to 1, it is necessary to reverse the direction of magnetization. The two 1/2 currents have to flow in the opposite direction, until the state of magnetization reverses to anticlockwise. As explained before, the core will retain the value even if no more current flows, Figure 8 summarizes the entire process. Values of currents and time of impulse to obtain reversal of magnetization state are material and thickness dependent and can be found experimentally.

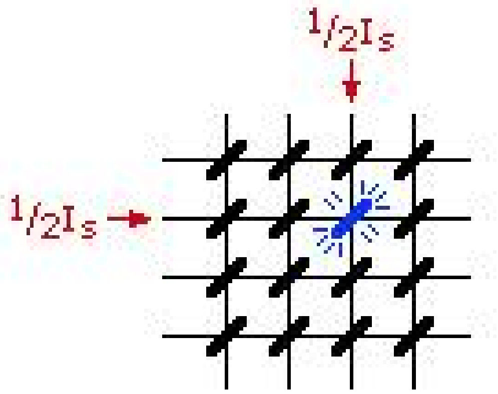

Figure 7: Driving Coincident Currents

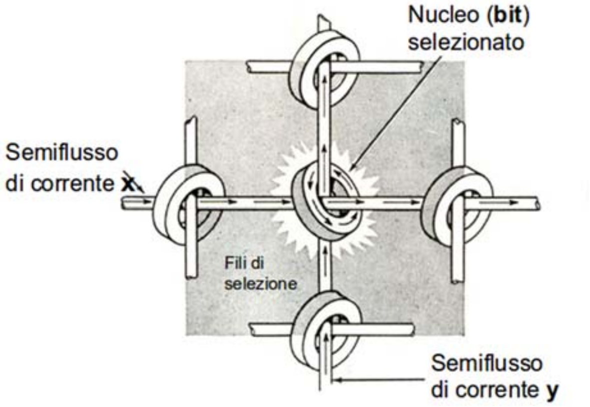

Figure 8: Writing 0 or 1 to a Magnetic Core Memory

READING FROM A MAGNETIC CORE MEMORY

Reading from a magnetic core memory is a bit more difficult and it is necessary to introduce a new concept: a change in a magnetic field creates a current.

So, every time we reverse the magnetic field from clockwise to anticlockwise or vice versa using the two wires to identify the desired core, a little current is produced and can be revealed by a third wire, called the sensing, spread along the memory. See Figure 9.

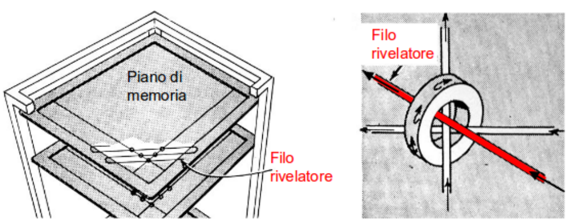

Figure 9: Sensing Wire

Keeping in mind the role of the sensing wire, to read a bit from a magnetic memory, we proceed as follows:

1. We write a 0. Whether the sensing reveals no current, no change in the magnetic field has happened, so, the core contained and will maintain 0.
2. Whether the sensing reveals a current, a change in the magnetic field has happened. So, the core contained 0, but now, that the magnetic field has reversed, it contains 1. Consequently, we lose the correct value 0 contained in the core and substituted it with 1, a wrong value. Now, it is necessary to write a 0 on the core, by reversing the magnetic field again.

This process is defined "destructive reading": in reading process, each time we write a value and the sensing reveals a change in state, we must regenerate the value contained in the core.

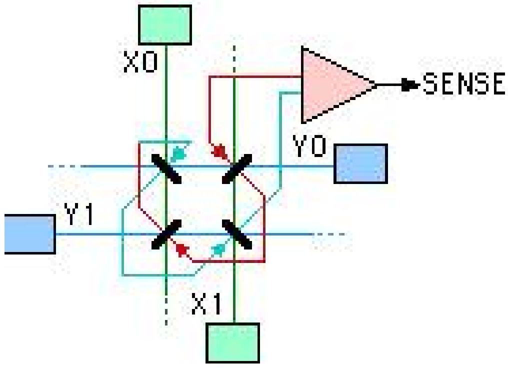

*Figure 10: Sensing Wire in a 2*2 Memory Array*

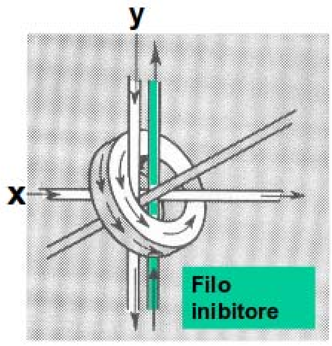

Figure 11: Inhibit Wire

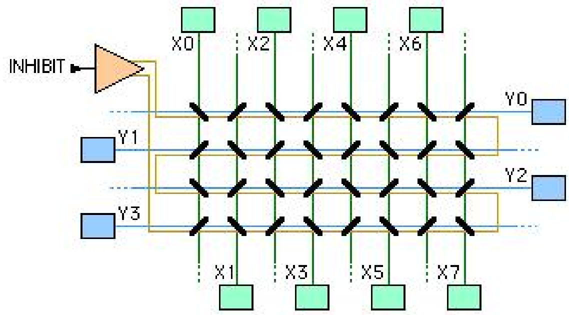

Figure 12: Inhibit Wire in a Bit Array

This simple schema can be further complicated, whether, instead of considering two-dimensional memories, we are interested in working with memories organized in core planes, one on top of each other, in order not to write a bit at a time, but a byte or a word at a time. In that case a fourth wire, a for each plane, the "inhibit" is inserted. At reading time, it is necessary to activate the inhibit pertaining to the plane containing the core we do not want to modify. Figures 11 and 12 summarize this concept.

HARDWARE AND SOFTWARE TO CONTROL OUR MAGNETIC CORE MEMORY

Figure 13 summarizes the theoretical background we exposed so far and the required hardware to concretely build a functional magnetic core memory.

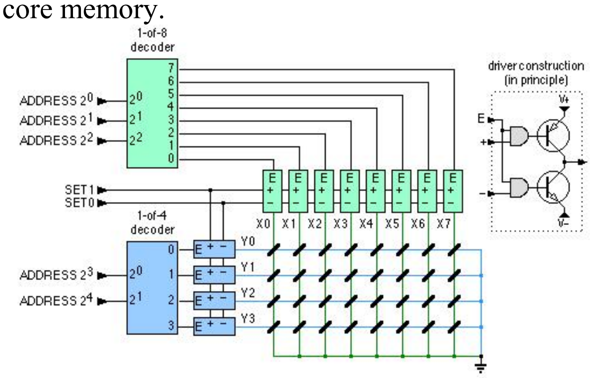

*Figure 13: Driving in a 4*4 Bit Array*

The circuitry receives X and Y coordinates of the selected core, together with the direction of the two currents and performs either reading or writing task.

As memories grew the simple, driving schema shown above began inappropriate because the required, increasing number of driving lines. To afford the problem, as shown in Figure 14, decoders were inserted. One decoder identifies the slice of the memory, while the other one determines the direction in which the currents have to flow. The theoretically, necessary 64 driving lines have been reduced to 16.

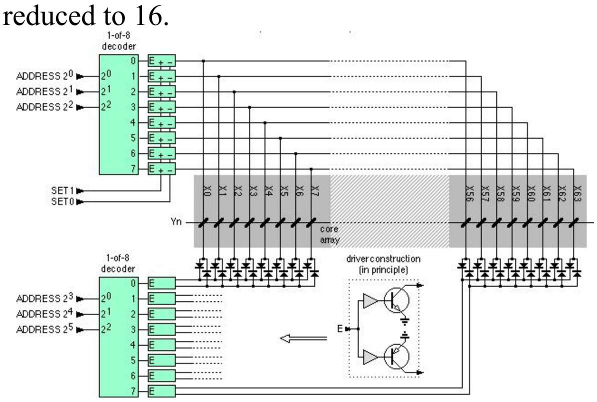

Figure 14: Reducing Driving Lines from 64 to 16

The method of non-coincident currents is used to further halve the number of driving lines. Considering a core identified by its two driving lines; of the four, possible combinations of the two currents, only two of them produce a change in the state of magnetization, those in which the two currents sum. They are defined coincident currents. The other two produce no effect, as being opposite currents, they delete each other.

They are defined non-coincident currents. Figure 6 summarizes these concepts. Considering now the two cores of Figure 15. We have still two driving lines, but one of them, describing two right angles, goes through one of the two cores in the opposite direction.

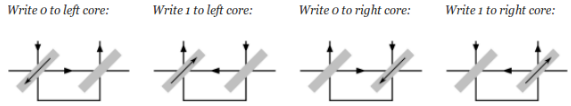

Figure 15: 4 Possible states of currents' Magnetization

Considering again all the four, possible combinations. We notice that all four states become valid, two for each core. It is like whether the array was divided in two slices and each core of the left side driven by coincident currents, has an homologous in the right slice driven by non-coincident currents, utilizing though the same two driving lines.

Starting from the project of Ben North and Oliver Nash, we built our magnetic core memory. After soldering components, one by one and many tests on

Arduino, uploading the firmware written by the two American researchers, we obtained the shields shown in Figure 16 and 17.

Then, we went a step further. We ported the firmware from Arduino Uno to STMicroelectronics' STM32 and connected our shields to a Nucleo F411RE. Figures 18 and 19 below, show the assembled hardware: Nucleo, Core Shield and Drive Shield.

The software we wrote is similar to that written by North and Nash, apart from tracing, logging and current calibrating functions that we did not implement. Our development work was entirely done under the Linux operating system, using only open source software. We also wrote some, little templates to automate compiling, uploading and debugging the code for Nucleo F411RE.

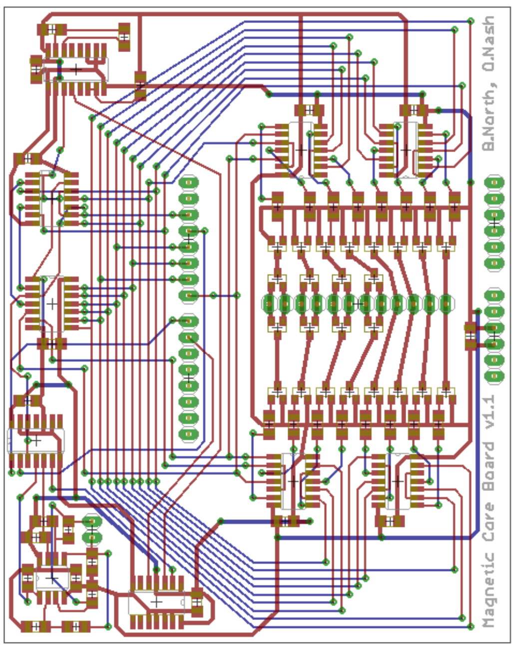

Figure 16: Eagle Drive Shield Layout

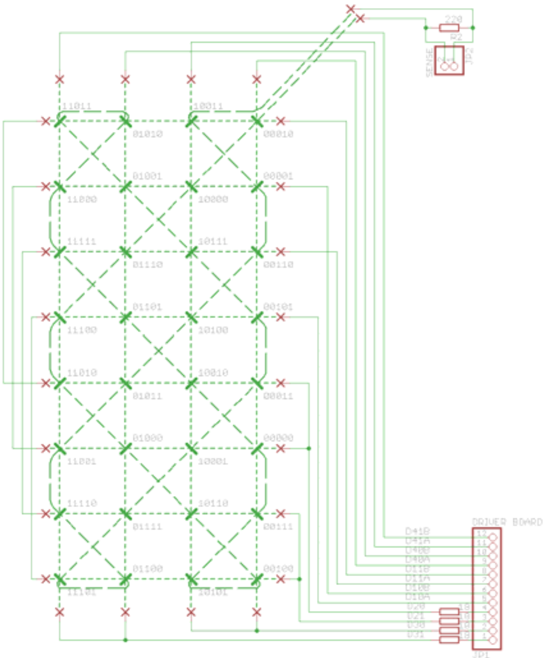

Figure 17: Eagle Core Shield Layout

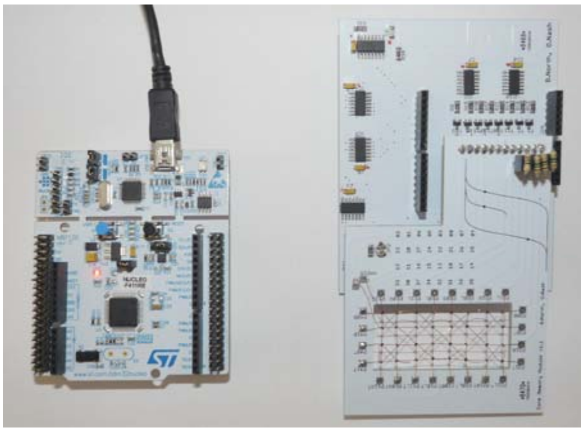

Figure 18: Nucleo F411RE, Drive and Core Shield (View From Above)

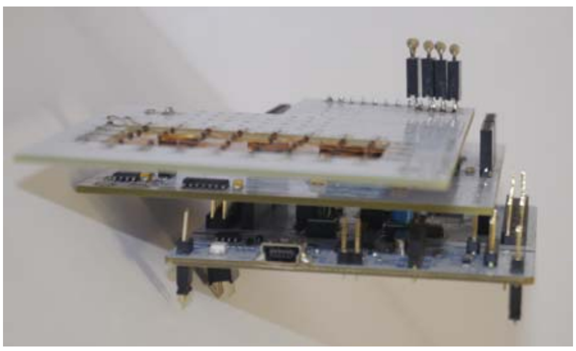

Figure 19: Nucleo F411RE, Drive and Core Shield (Front View)

In Figure 20 you can see a screenshot of the interactive menu, in which: t stands for 'testing all bits' array', r for 'reading a specific bit', R for 'reading the entire array', w for 'writing a specific bit' and W for 'writing the entire array'.

Single bits are specified by binary addresses from 0 to 31.

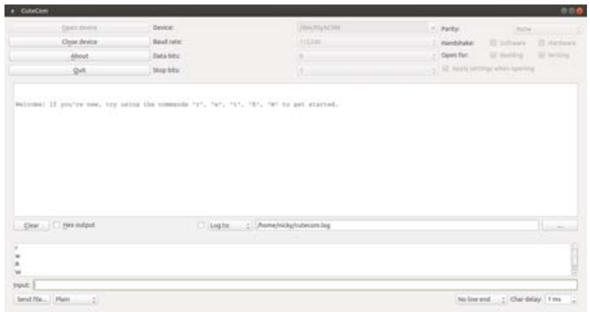

Figure 20: Screenshot of the Interactive Menu of the Firmware

We finally substituted the Core Shield with an IBM DJB 373330 SMS card, shown in Figure 21, owned by our professor.

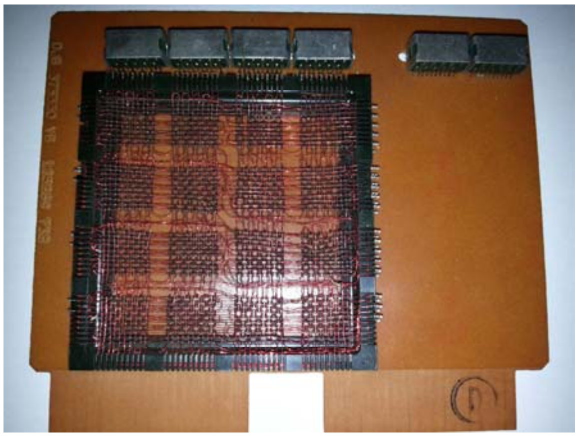

Figure 21: DJB 373330 Card

Unfortunately, although we contacted people all over the world, we did not find any documentation about electric schemes and circuitry of IBM DJB. So, using an oscilloscope and an electronic microscope, we drew the CAD representation shown in Figures 22, 23 and 24.

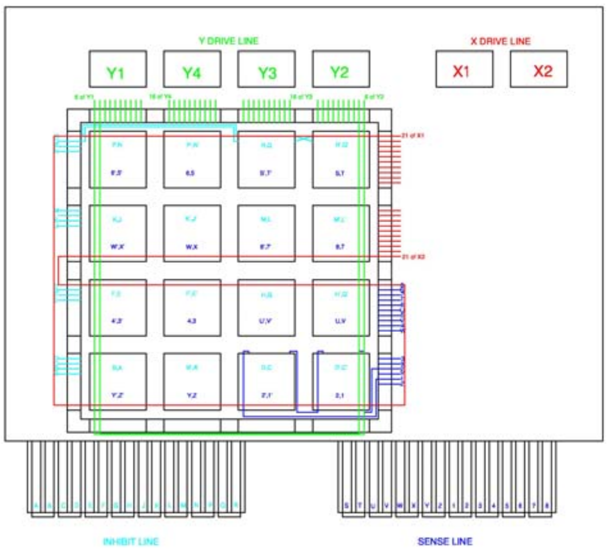

Figure 22: CAD DJB 373330 Schema 1 of 3

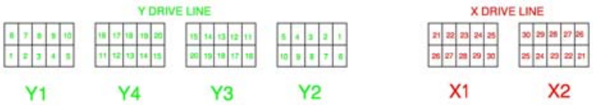

Figure 23: CAD DJB 373330 Schema 2 of 3

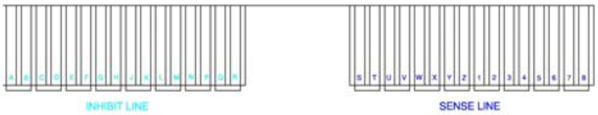

Figure 24: CAD DJB 373330 Schema 3 of 3

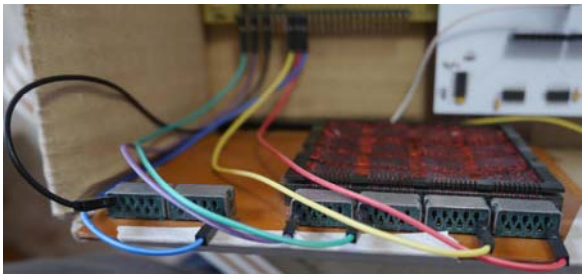
Figure 25: Connections for addresses 4 and 14 on the DJB Card

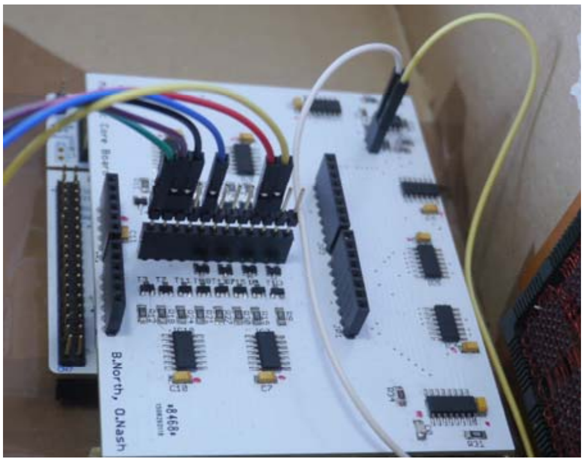

Figure 26: Connections for addresses 4 and 14 on the Drive Shield

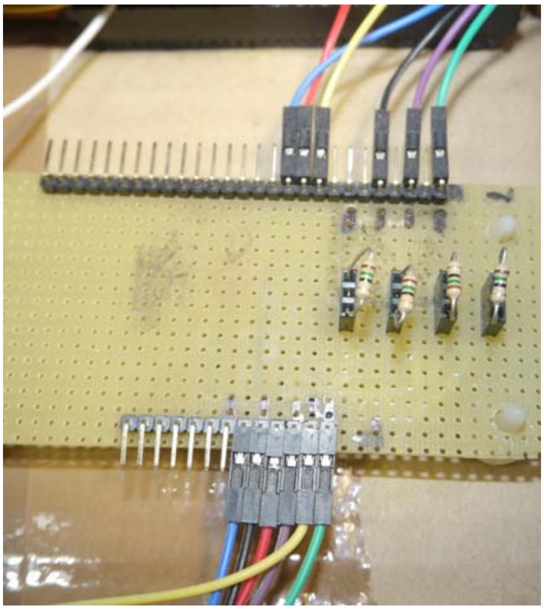
Figure 27: Connecting Board between DJB and Drive Shield

After a hard testing work, we succeeded in identifying the pins that addressed two of the DJB's 1600 cores, that could be driven by our Drive Shield. Figures 25, 26 and 27 show these connections together with a connecting board.

We could write and read two cores, demonstrating that, at least partially, the DJB card was still functioning. In Figure 28 you can see our final, assembled project, whereas, a screenshot of the firmware uploaded on the Nucleo is shown in Figure 29. It specifically refers to the two addresses, 4 and 14, identified on the DJB.

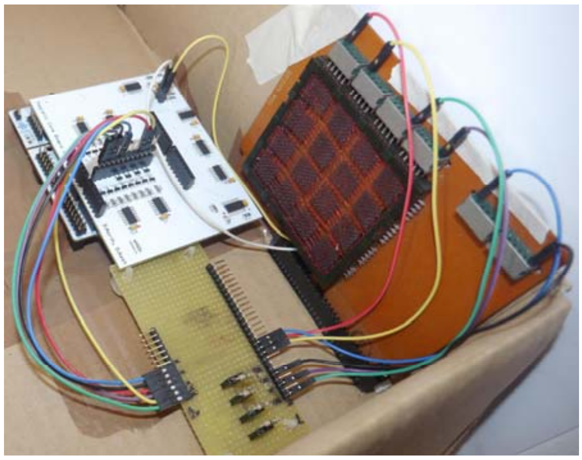
Figure 28: DJB Card's Entire, Driving System

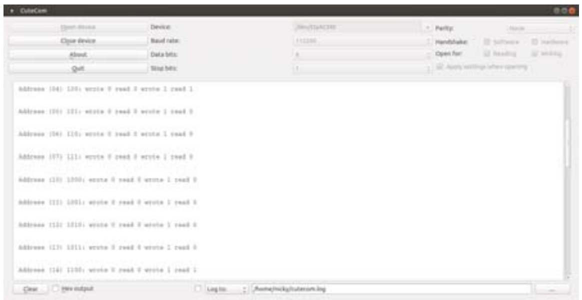
Figure 29: Screenshot of the Software controlling DJB Card

CONCLUSION

Working with Magnetic Core Memories was an exciting experience. It is not easy to tackle with this sort of problems, especially nowadays, that this technology is no more used and find technical references is almost impossible. Moreover, owning an original IBM DJB 373330 SMS Array built more than 50 years ago is really a pleasure for future engineers. So, although the difficulties we encountered to develop our project and although we started from a very well done work of North and Nash, we very much thank our Professor Orazio Mirabella and our Tutor Engineer Antonio Raucea, who gave us the possibility to concretely experiment with a piece of technology that represented an important step in modern computer science.

We very much desire to thank all people from many countries who helped us to end our work and being coherent with our idea of knowledge sharing, at the addresses GitHub or Corememory Shield is freely available all the documentation and software we produced for our project. A video is available at Magnetic Core Memory, as well.

REFERENCES

[1] Geoffrey Brown "Discovering the STM32 Microcontroller", 10 Aprile 2015.

[2] Joseph Yiu "The Definitive Guide to ARM Cortex M3 and Cortex M4 Processors", Newnes, 2013.

[3] ARM Limited "Cortex-M4 technical reference manual", 2010.

[4] Trevor Martin "The Insider's Guide To The STM32 ARM Based Microcontroller", Hitex, 2009.

[5] STMicroelectronics "Datasheet STM32F303xB STM32F303xC", rev. 7, 2013.

[6] STMicroelectronics "STM32F3DISCOVERY peripheral firmware examples AN4157", rev. 1, 2012.

[7] STMicroelectronics "Datasheet STM32F405xx STM32F407xx", rev. 4, 2015.

[8] STMicroelectronics "STM32F4DISCOVERY peripheral firmware examples AN3983", rev. 2, 2011.

[9] STMicroelectronics "Datasheet STM32F401xD STM32F401xE", rev. 3, 2015.

[10] STMicroelectronics "STM32 Nucleo boards UM1724", rev. 7, 2015.

[11] STMicroelectronics "Description of TM32F30xx/31xx Standard Peripheral Library UM1581", rev. 1, 2012.

[12] STMicroelectronics "Description of STM32F4xx HAL drivers UM1725", rev. 1, 2014.

[13] Free Software Foundation "Using the GNU Compiler Collection", for gcc version 4.8.4 (GNU Tools for ARM Embedded Processors).

[14] Free Software Foundation "Debugging with GDB", Tenth Edition, for GDB version 7.9.

[15] Free Software Foundation "GDB Quick Reference", version 5.

[16] Free Software Foundation "GNU MAKE", Version 4.1 September 2014.

[17] ARM Limited "ARM and Thumb-2 Instruction Set Quick Reference Card", 2008.

[18] Free Software Foundation "OpenOCD User's Guide", for release 0.10.0-dev 5 October 2015.

[19] STLINK development team "Using STM32 discovery kits with open source tools"

[20] Brian W. Kernighan, Dennis M. Ritchie "Il linguaggio C. Principi di programmazione e manuale di riferimento", Pearson 2004.

[21] Texas Instruments "The Integrated Circuits Catalog for Design Engineers", First Edition January 1970

[22] DEC Equipment "PDP-8 Maintenance Manual", 1966

[23] "Byte Magazine - Core Memories", James R. Jones Number 11 July 1976

[S1] www.st.com/web/en/catalog/tools/FM116/SC959/SS1532/PF254044

[S2] http://www.st.com/web/catalog/tools/FM116/SC959/SS1532/PF252419

[S3] http://www.st.com/web/catalog/tools/FM116/SC959/SS1532/LN1847/PF260000

[S4] http://www.arm.com/products/processors/cortex-m/cortex-m4-processor.php

[S5] http://www-micrel.deis.unibo.it/LABARCH/2015/materiale. html

[S6] http://homepage.cem.itesm.mx/carbajal/MR2010/slides.htm

[S7] http://www.openstm32.org

[S8] https://github.com/gnunicky

[S9] http://jeremyherbert.net/get/stm32f4_getting_started

[S10] https://launchpad.net/gcc-arm-embedded

[S11] https://gcc.gnu.org/

[S12] https://sourceware.org/gdb/download/onlinedocs/

[S13] http://www.gnu.org/software/binutils/

[S14] http://www.gnu.org/software/make/manual/

[S15] http://www.doc.ironwoodlabs.com/gnuarm/gnuarm-distribution/web/www.gnuarm.com/

[S16] http://beej.us/guide/bggdb/

[S17] www.wolinlabs.com/blog/linux.stm32.discovery.gcc.html

[S18] www.openocd.org

[S19] https://github.com/texane/stlink.git

[S20] http://www.emcu.it/STM32.html

[S21] http://www.carminenoviello.com/category/elettronica-it-it/

[S22] https://github.com/RIOT-OS/RIOT/wiki/RIOT-Platforms
[S23] http://mdda.net/oss-blog/
[S24] http://web.stanford.edu/class/cs107/resources.html
[S25] http://www.pixelbeat.org
[S26] http://www.corememoryshield.com/report.html
[S27] http://www.cs.ubc.ca/~hilpert/e/coremem/index.html
[S28] http://ed-thelen.org/comp-hist/Byte/76jul.html
[S29] http://nid.dimi.uniud.it/history/history.html
[S30] http://www.retrocomputing.net/eventi/toscana/pi/pisa/20090518/corsobonfanti/corso.htm
[S31] https://sites.google.com/site/wayneholder/one-bit-ferrite-core-memory
[S32] http://www.ffellico.com
[S33] http://members.iinet.net.au/~daveb/
[S34] http://tinyurl.com/pdp8core
[S35] http://www.qrp.gr/microwave/
[S36] http://www.aholme.co.uk/
[S37] http://other-1.webs.com/
[S38] http://www.righto.com/2015_03_01_archive.html
[S39] https://www.flickr.com/photos/132738729@N05/sets/72157653027710200

MODELING THE ALGORITHM FOR INTEGRATING THE RESULTS OF INDEPENDENT MEASUREMENTS

Grigoriev Evgeniy

Saint-Petersburg State University of Aerospace Instrumentation,
Saint-Petersburg, Russia

E-mail: ev.grig95@gmail.com

Abstract

This article discusses 3 algorithms for determining the range to an object in radiolocation: impulse, frequency and phase methods. Made the analysis of the increasing accuracy of the measurements for each method, when increasing the number of sources of measurements. Special attention is paid to the task of finding the optimal number of observers to achieve the best accuracy characteristics of each method.

INTRODUCTION

The task of increasing the accuracy of radar measurements was relevant from the beginning of radiolocation. The accuracy of measurements can be increased by two methods - hardware and software, in the article discusses algorithm for increasing the accuracy of the range determination by combining the measurements obtained from independent (separated) observers.

This method can be used in the tasks of searching for and rescuing people using unmanned aerial vehicles (UAVs), which can be launched into the sky in large numbers, and they do not require a large investment of financial resources.

FORMULATION OF THE OBJECTIVE

The task should be formulated in the following way. There are several spaced observation stations – radars(R), each of which monitors the object, calculating the range to the target (T).

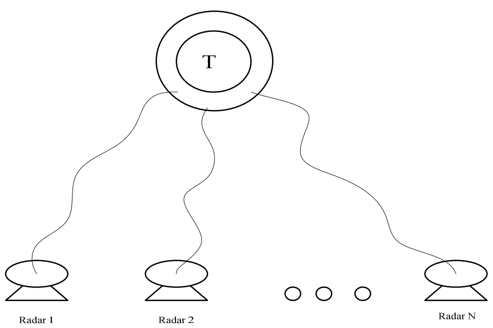

Fig 1. Determine the range to the object, using N radars

All radar stations has its own measurement errors due to both the imperfection of the measuring equipment - systematic, and external factors, which we can't influence - random. Systematic measurement errors, by calibrating the equipment, can be compensated, and in the case of random errors, statistics methods are usually used. We must determine the optimum number of radars in order to minimize the measurement error. To assess the accuracy are root mean square error σ(α), which corresponds to a probability equal to 0.68, i.e. the error for 68% of all measurements will have absolute values less than σ(α)[5]. The error of each measurement of α (in our case, distance to the target)

$$\Delta\alpha = \alpha_0 - \alpha_k \tag{1}$$

where α_0 is the true value, and α_k - value in k-th dimension. If produced sufficiently large number n of measurements, the root mean square error value was found in the unbiased error variance

$$\sigma(\alpha) = \sqrt{\sum_{k=1}^{n} (\Delta\alpha_k)^2 / (n-1)} \tag{2}$$

In the first part we will describe the methods of measuring the range to the target, and in the second part - the effect of the method of data fusion on the accuracy of measurements of each method.

ANALYSIS OF ALGORITHMS FOR DETERMINING THE RANGE TO THE TARGET

After analyzing the literature about three methods of measuring the range in radiolocation, obtain the table 1:

Table 1

Frequency distance measurement method **Pluses:** 1) Allows you to measure very small ranges. 2) A low-power transmitter is used. **Disadvantages:** 1) Need to use two antennas. 2) The radiating antenna induces noise on the receiver. 3) High requirements for linearity of frequency measurement.
Impulse distance measurement method **Pluses:** 1) The possibility of constructing a radar with a single antenna 2) Simplicity of the indicator device. 3) Convenience of measuring the range of several targets 4) The simplicity of the emitted pulses that last a short time T_{imp} and the received signals. **Disadvantages:** 1) The need to use large transmitter power pulses 2) It is impossible to measure small ranges 3) A large dead zone. 4) It is necessary to measure the time very accurately.
Phase distance measurement method **Pluses:** 1) Low-power radiation because Undamped oscillations are generated. 2) The accuracy does not depend on the Doppler shift of the reflection frequency. 3) The simplicity of the range finder. **Disadvantages:** 1) No permission for range. 2) The radiating antenna induces noise on the receiver

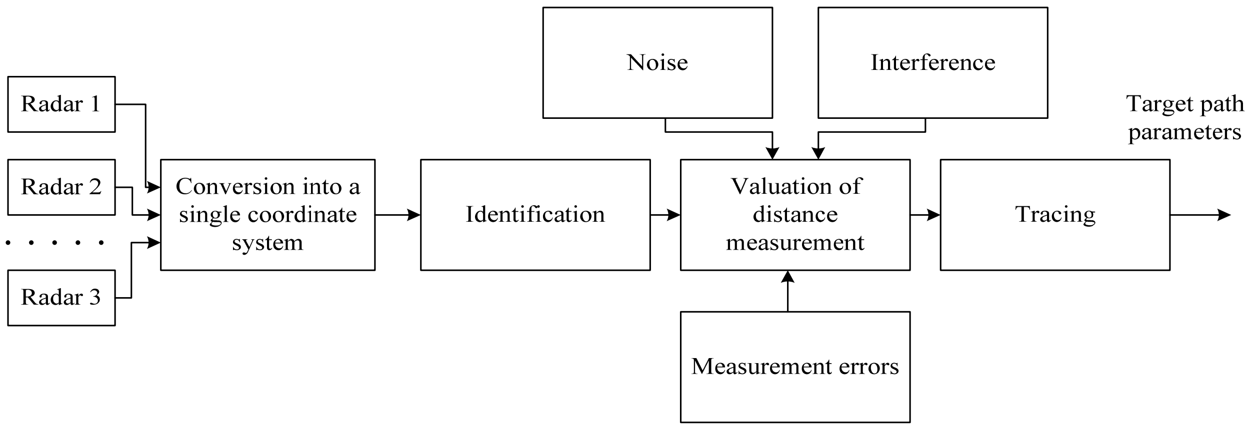

Fig. 2. Method of data fusion flowchart

The following table explains the advantages and disadvantages of techniques in terms of their implementation in specific electronic devices, further into the article, we will analyze each of the methods in terms of improving the efficiency of the measurement range with an increase in the number of observers.

THE METHOD OF DATA FUSION FOR STATIONARY MULTI-POSITION SYSTEMS

The final result of radar surveillance is the construction of the trajectory of targets. In multi-station radar stations, information is processed together in the construction of trajectories. Such processing should be carried out in several stages[1].

This flowchart needs clarification. At the first stage, the data coming from the separated positions must be transformed into a single central coordinate system (for example, into Cartesian), the beginning of which must be linked to the center of the receiving-transmitting position in order to simplify the algorithm of processing. About the positive sides of the transformation precisely in the Cartesian coordinate system is written in [1,2,3]. Mutually uncorrelated measurement errors of different "primary coordinates" in each position become generally correlated after the data transformation into a Cartesian coordinate system.

The task before the information gathering point (block - identification) is the following - to correctly group the messages belonging to the targets, and correctly link them to the corresponding combined trajectories. This problem reduces to the problem of checking statistical hypotheses. Let's imagine all possible combinations of grouping and binding of messages. In doing so, we will be guided by the rule that two messages issued by one radar station and selected in group A belong to different purposes. Therefore, when solving the problems of grouping and linking two new unified paths, the following 4 incompatible hypotheses are possible:

Hypothesis I (H_I): messages mes_{11} and mes_{21} refer to the $traj_1$ trajectory, and mes_{12} and mes_{22} refer to the $traj_2$ trajectory.

Hypothesis II (H_{II}): messages mes_{12} and mes_{22} refer to the $traj_1$ trajectory, and mes_{11} and mes_{21} refer to the $traj_2$ trajectory.

Hypothesis III (H_{III}): messages mes_{21} and mes_{12} refer to the $traj_1$ trajectory, and mes_{11} and mes_{22} refer to the $traj_2$ trajectory.

Hypothesis IV (H_{IV}): messages mes_{11} and mes_{22} refer to the $traj_1$ trajectory, and mes_{21} and mes_{12} refer to the $traj_2$ trajectory.

In this problem, the losses associated with the erroneous acceptance of any of the above hypotheses can be considered the same. The loss function can be taken equal to some predetermined constant number when choosing any wrong hypothesis and equal to zero when choosing the correct hypothesis. As a result, the decision to select a hypothesis (from the possible four) can be taken using the maximum likelihood criterion, that is, the maximum value of the corresponding likelihood function of the hypotheses[4].

The following are graphs explaining results of this method, for all ways to measure the distance in radiolocation:

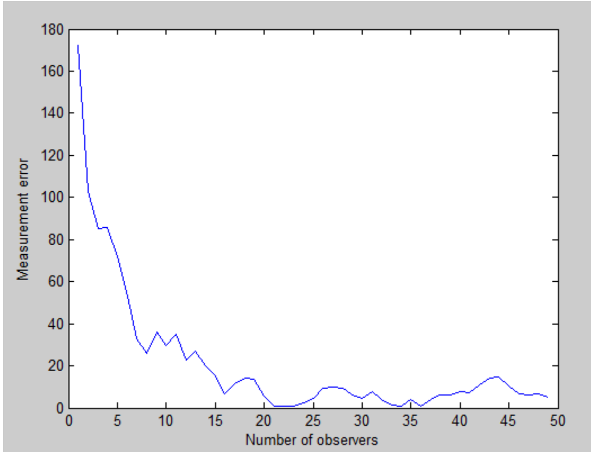

Fig. 3.Impulse distance measurement method

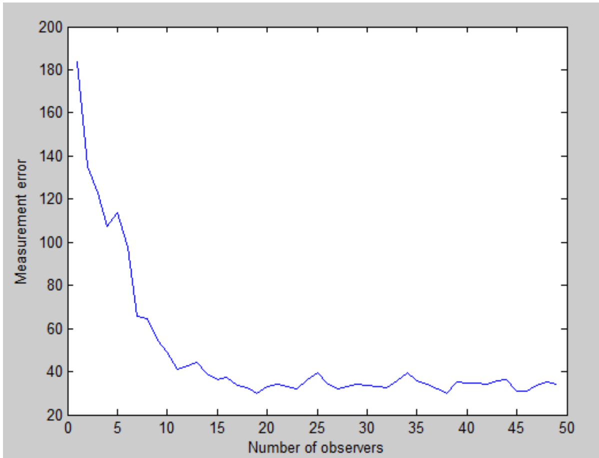

Fig. 4. Phase distance measurement method

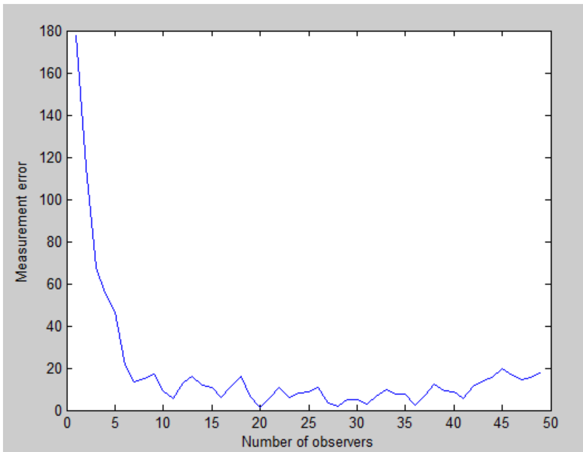

Fig. 5. Frequency distance measurement method

CONCLUSIONS

The proposed method can be applied in real-world conditions for timely search and rescue people in emergency zones. It can be used for example in squadron of the UAV's.

from the figures 3,4,5 we can see, that the optimal number of observers for the frequency method turned out to be the smallest. Technical characteristics, and accordingly the economy, as well as the accuracy of measurements can be selected, depending on the chosen measurement method.

REFERENCES

[1] *Зайцев Д.В.* Многопозиционные радиолокационные системы. Методы и алгоритмы обработки информации в условиях помех. М.: Радиотехника 2007.

[2] *Кузмин С.З.* Основы проектирования систем цифровой обработки радиолокационной информации. -М.: Радио и связь, 1986.

[3] *Farina, A.* Tracking function in bistatic and multistatic radar system // IEE Proc., 1986, vol. 133, no. 7.

[4] *Кузмин С.З.* Основы теории цифровой обработки радиолокационной информации. -М.: Советское радио, 1974.

[5] М.И. Финкельштейн. Основы радиолокации. – М.: Советское радио, 1973

EXPERIMENTAL INVESTIGATION OF THE OPTICAL FIBER INFLUENCE TO SPREAD FUNCTION OF THE GRATING SPECTRAL DEVICE

Kazakov Vasily, Paraskun Artur

Saint-Petersburg State University of Aerospace Instrumentation,
Saint-Petersburg.

vasilykazakov@mail.ru, arthur.paraskun@gmail.com

Abstract

Carried out the experimental research impact to transfer analyzed signals via optical fiber on diffraction grating spectral device power resolution. Assembled a laboratory model of the device and a system for signal transmission on single-mode and multimode fiber. Assembled device for reading the spectrometric information on the CCD ruler

.

INTRODUCTION

Development of spectral control devices for different physical processes makes it possibility use of remote control [1]. One of many possible solutions for achieving this intention of development fiber-optic transmission system for analyzing signals from a radiation source to spectral measurement systems [2]. It is known that for spectral analysis, diffraction spectroscopic instruments are necessary to provide a homogeneous plane wave front of the analyzed physical optical radiation. The transmission of analyzed optical radiation along the optical fiber deform wave front, that leads to change in spread function of spectral device.

LABORATORY MODEL.

In work [1] was obtained theoretical and experimental researches of influence on optical fiber of spread function of spectral device, basis on acousto-optical tunable filter. This paper presents the results of experimental studies of the influence of the fiber-optic transmission system of the analyzed signals on the spread function of diffraction grating optical spectral device. For these purposes was implemented, a laboratory model of a spectral device with fiber-optic transmission system.

Photos of the laboratory model and its individual components are shown in figures 1-3. The laboratory model is assembled on optical bench type ОСК-2 and includes the following blocks:

1. Optical bench ОСК-2;
2. He-Ne laser ЛГН-214 with a power of 1 mW and a central wavelength of 632 nm;
3. The collimator АКТ-15;
4. Fiber-optical system for transmission of analyzed signals, consisting of symmetric optical input-output devices with standard connectors for connection various types of optical fiber (Figure 2). The system has the ability to change the type of optical fiber from single-mode to multimode. In addition, the system is equipped with adjusting screws and the ability to move optical lens to achieve maximum efficiency input and output optical radiation (Figure 3).
5. Diffraction grate operating in transmitted light.
6. Lens with a focal length of 90 cm. The combination of the lens and two layers of free space provide the necessary spatial transformation optical signal formed on the output plane of diffraction grating [3].

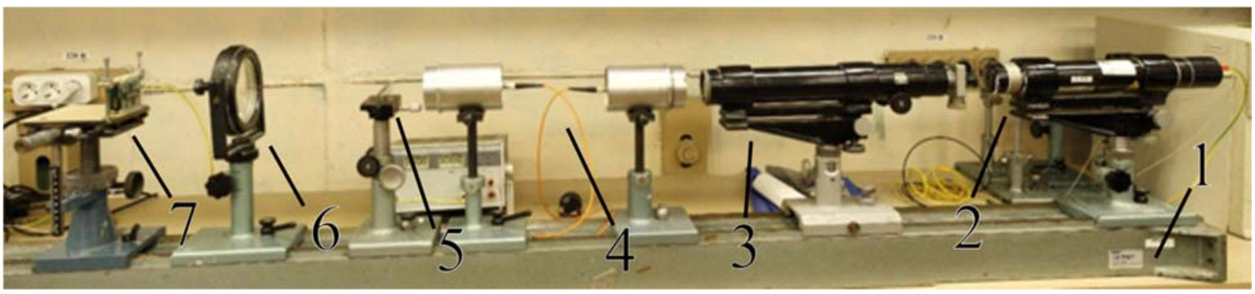

Figure. 1 – Laboratory model

Figure. 2 – Fiber-optic transmission system for analyzing signals

Figure. 3 – System for fixing the end of a fiber with a threaded tip of the "FC" type

7. A device for reading spectroscopic information basis on a CCD ruler.

RESULTS OF EXPERIMENTAL RESEARCHS

Carried out three experimental tests with optical fibers on the spread function of diffraction grating spectral:

a) under exposed collimated laser radiation on a diffraction grating (Fig. 4);

b) with systems for transmission analyzed signals via single-mode fiber OFNR 8/125 µm (Fig. 5);

c) with system transmission of analyzed signals via multimode fiber OFNR 50/125 µm (Fig. 6).

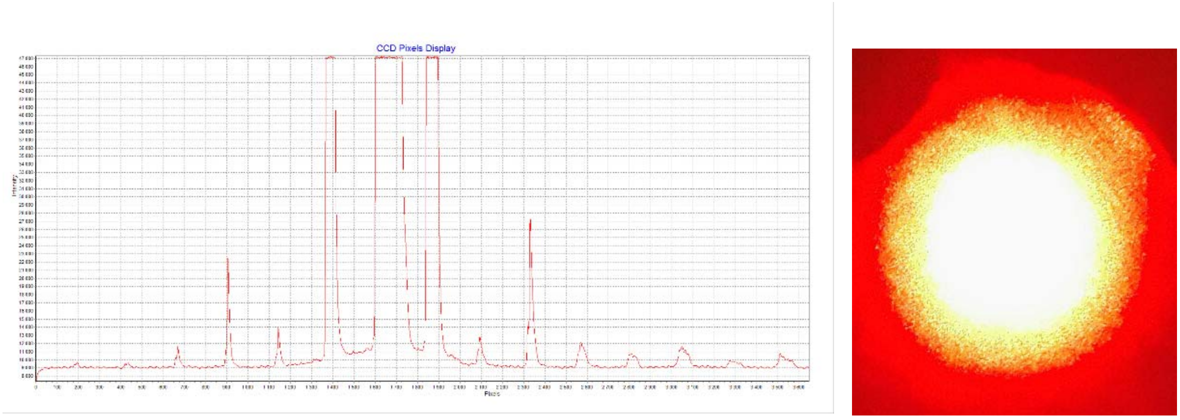

a) b)

a) the spread function of the diffraction spectral spectrometer without the use of a fiber-optic transmission system;
b) collimated laser radiation falling on the grate.

Figure. 4

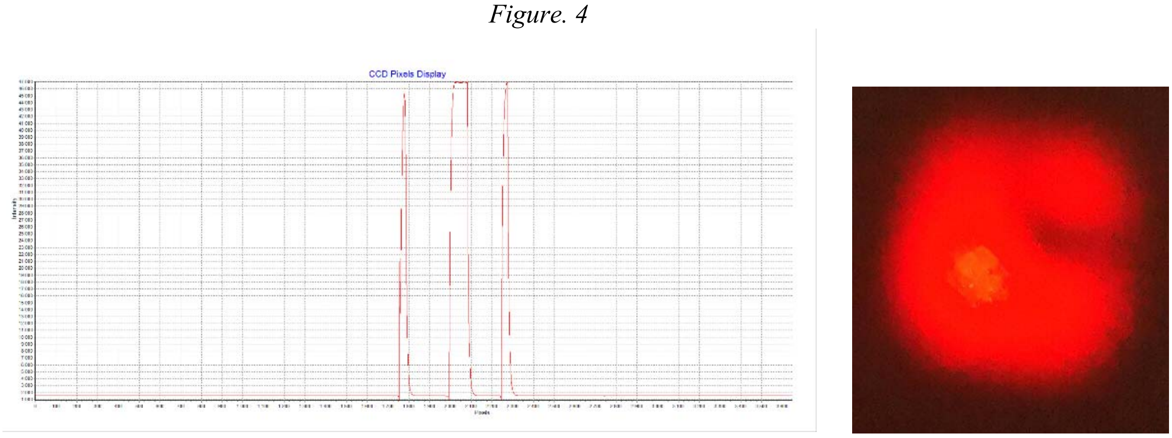

a) b)

a) the spread function of a diffraction grating spectral device with use a single-mode optical fiber;
b) laser radiation transmitted through a single-mode fiber transmission system.

Figure. 5

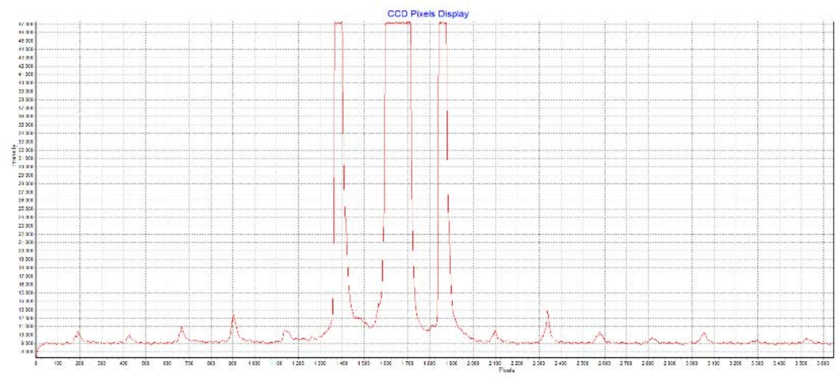

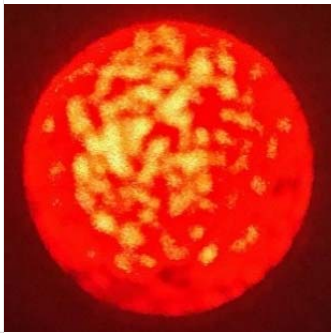

a) *b)*

a) the spread function of a diffraction grating spectral device with use a multimode optical fiber;
b) laser radiation through a transmission system with multimode fiber.
Figure. 6

For improvement mass-dimensional parameters of layout, as provide management of registration and processing received spectroscopic information based on the CCD ruler. At the last moment developed a preliminary version of the device and software, that allows processing and displaying spectroscopic information on a PC.

The device for reading spectroscopic information is realized basis on the programmable gate array Altera Cyclone EP1C3T100C8N. As a ruler of photodetectors use Toshiba TCD1304.

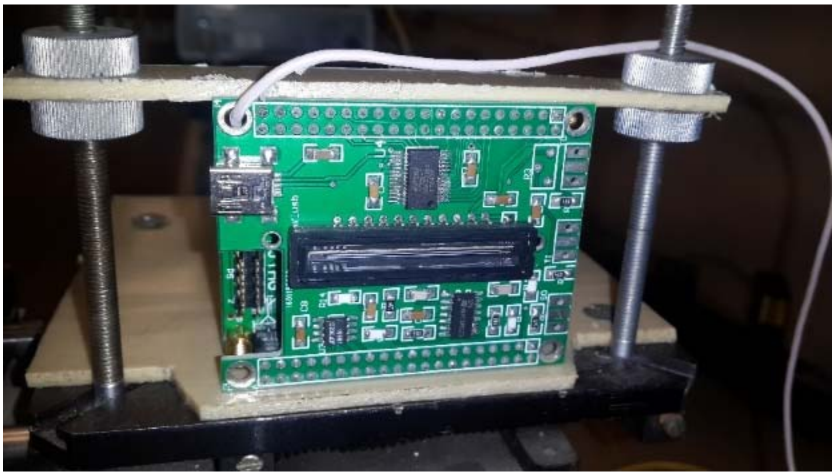

Figure. 7 – spectroscopic information reading device

Figure 7 shows a printed circuit board with a USB CCD ruler. Board size: 62 mm (length) * 50 mm (width). The device consists of two boards. On the top board are: linear CCD-matrix TCD1304, converter USB interface for parallel FIFO (FT245RL), LTC1865CS8 – analog to digital converter and LM32 – analog amplifier. On the back board is the Cyclone FPGA – printed circuit board, which provides signal processing from the CCD chip, provides control and signal for ADC and USB chips. At the bottom there are technological holes for the printed circuit boards. Can also use M3 screws to harden the entire board. All used from the available interfaces of the CCD board are located on the top board. The Mini-USB connector is employed for power supply, and the CCD intensity and control commands (for example, the integration time of the CCD) are transmitted via the USB interface.

CONCLUSION

According to the results of the experimental research can be concluded that the spatial modulation of optical radiation, which appears when the optical fiber is used as the transmission line of the analyzed signal, will broaden and distort the shape of the spread function of the diffraction spectral device and therefore worsens resolution.

When single-mode fiber is used – 1.5 times, and multimode fiber – 2 times. At the same time, the energy losses when single–mode fiber is used are significantly higher than when using multimode fiber.

From what has been said above, can be concluded that the use of a fiber-optic bundle as the transmission line of the analyzed signal will lead only to a multiple increase in the spatial modulation of the analyzed optical radiation and consequently to a significant deterioration in the resolving power of the device.

This work was supported by the Russian President's scholarship for young scientists and graduate students carrying out advanced research and development in priority areas of modernization of the Russian Economics (СП-536.2016.5).

This work was funded by the RFBR-The Russian Foundation for Basic Research: project No.16-07-00549.

REFERENCES

[1] *Ваганов, М. А.* Резонансный метод бесконтактного анализа оптических спектров и его техническая реализация для решения задач контроля процессов горения: дис. канд. тех. наук: Спец. 05.11.13: защищена 26.03.2014: утв. 05.10.2014 / Ваганов Михаил Александрович. СПб., 2014. 152 с.

[2] *Калинин, В. А.* Спектральные измерения в оптическом диапазоне с передачей анализируемых сигналов по оптическому волокну: дис. канд. тех. наук: Спец. 05.13.01: защищена 30.05.2006: утв. 13.10.2006 / Калинин Владимир Анатольевич. СПб., 2006. 133 с.

[3] *Папулис, А.* Теория систем и преобразований в оптике. – М.: Мир, 1971. – 495 с.

THEORETICAL AND EXPERIMENTAL PARAMETERS OPTICAL SPECTRAL DEVICES BASED ON THE ACOUSTO-OPTIC TUNABLE FILTER

Korol Georgy

Saint-Petersburg State University of Aerospace Instrumentation,
Saint-Petersburg, Russia

E-mail: G-King7@yandex.ru

Abstract

Consider method of analysis of the spectra dynamic signals optical range techniques acoustooptics at light diffraction on a traveling acoustic wave excited by a periodic sequence of radio pulses with a rectangular envelope and linear variation of the instantaneous frequency. As part of the research acousto-optic interaction is thought of as a bilinear transformation of the spectral components, which are radio and optical radiation. Analysis of the spectrum in the optical range is seen as the result of the optical signal at the determined diffraction screen, that is, the acousto-optic modulator, which is driven deterministic acoustic wave. The results of the research are the relation describing the electrical oscillations at the output of the photodetector, which in turn are the result of the spectral measurements at different rates of change of the instantaneous frequency of oscillation of the control, as well as mathematical simulation results describing the process

.

INTRODUCTION

The optical spectral instruments on the based of an acousto-optic tunable filter have the highest speed among systems with sequential reading spectrometric information. The restructuring of the acousto-optic tunable filter over a range of frequencies can be analyzed linear speed: how consistent and for a given program. Management acousto-optic tunable filter is easy to organize with the help of a computer.

The resolution of the optical spectral device based on acousto-optic tunable filter the of the same order of the, and spectral lattice devices and can reach units angstrom.

A very important advantage of optical spectral devices based on the acousto-optic tunable filter is the possibility of correction of the frequency characteristic preliminary acoustooptic interaction, and therefore, only the optical path of the measuring system by changing power supplied control signal. It should be added that such spectral instruments have a number of advantages, such as: reliability, small size and weight [2]. This is a decisive argument in favor of the use of equipment in the considered spectral optical spectral device based on an acousto-optic tunable filter.

COMPLEX HARDWARE FUNCTION

In this paper the analysis of the spectrum of optical radiation at its diffraction on elastic wave.

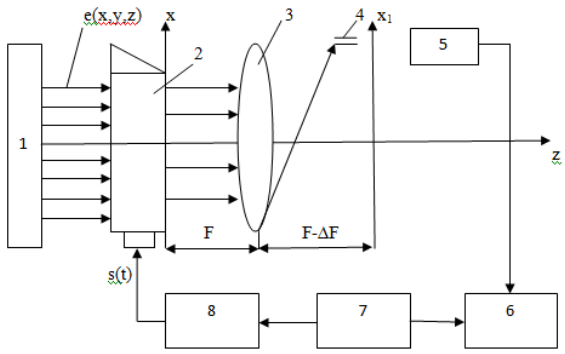

Figure 1
Figure 1 where 1 - forming optics, 2 - solid state acousto-optic modulator, 3 - lens with a focal length F, 4 – slot, 5 – photodetector, 6 – display, 7 – synchronizer, 8 - generator.

Distribution light in a plane z=F:

- Transparency transparency function is a linear map of the electric oscillations S (t), the exciting environment acousto-optical interaction acousto-optic modulator in a plane acoustic wave $U(x_1, t)$;

$$U(x,t)=\mathbf{V}s(t), \quad (1)$$

where t - current time; V - linear operator transition from fluctuations s (t) to a uniform plane acoustic wave.

- Plane light wave e (Z, t), is normally incident on an acoustic wave $U(x_1,t)$;

- Attenuation and dispersion of acoustic waves in the acousto-optic modulator acousto-optical interaction neglect;

- An optical Fourier transform processor comprising a cylindrical lens and two layers of space ideally performs either a spatial Fourier transform or spatial Fresnel transform[3];

- Signals S (t) and e (t), determined by acoustic and light waves are adequately defined and Fourier-Stieltjes integrals

$$S(t)=(\frac{1}{2\pi})\int_{-\infty}^{\infty} \exp\ i\omega'_s\ dt\dot{Z}_s(\omega'_s); \qquad (2)$$

$$e(t)=(\frac{1}{2\pi})\int_{-\infty}^{\infty} \exp\ i\omega'_1\ dt\dot{Z}_1(\omega'_1) \qquad (3)$$

It is assumed that the fluctuations of e (t) correspond to a uniform plane light wave. The function $A(\omega'_s, \omega'_1, x_2, t)$ is the kernel of the bilinear transform spectral

$$F(x_2,t)=\int_{-\infty}^{\infty}\int_{-\infty}^{\infty} A(\omega'_s, \omega'_1, x_2, t)$$

$$d\dot{Z}_S(\omega'_s) \qquad d\ \dot{Z}_1(\omega'_1) \qquad (4)$$

If $\omega'_1 = \omega_{1_0}const_1$,

$dZ_1(\omega'_1)=\delta(\omega'_1 - \omega_{1_0})d\omega'_1$ we get a comprehensive hardware function diffraction spectral instrument optical range in the fall of acousto-optic modulator homogeneous plane monochromatic light wave.

$$S(\omega_{1_0}, \omega'_s, x_2, t)=$$

$$=a\ exp i(\omega_{1_0} + \omega_S)tS_0(\omega_{1_0}, \omega'_s, x_2)=$$

$$=\dot{a}exp(\omega_{1_0}, \omega'_s)t\int_{-0.5L}^{0.5L} exp\ i[\omega_{1_0} x_2 \frac{1}{F}\frac{1}{C} -$$

$$-\dot{k}_s(\omega'_s)]x_1dx_1. \qquad (5)$$

At $\omega'_s = \omega_{s_0} = const_2$, $dZ_S(\omega'_s - \omega_{s_0})\ d\omega'_s$, $\dot{k}(\omega_{s_0}) = \omega_{s_0}\frac{1}{v_0}$, we get a comprehensive hardware function diffraction spectral instrument optical range in the fall of acousto-optic modulator homogeneous plane monochromatic light wave.

$$\dot{L}(\omega_{s_0}, \omega'_1, x_2, t)=$$

$$= a\ exp i(\omega_{s_0} + \omega'_1)tL_0(\omega_{s_0}, \omega'_1, x_2)=$$

$$= a\ exp i(\omega_{s_0} + \omega'_1)$$

$$t\int_{-0.5L}^{0.5L} exp\ i(\omega_{s_0}\frac{1}{v_0} - \omega'_1 x_2 \frac{1}{F}\frac{1}{C})x_1dx_1 \qquad (6)$$

wherein the acoustic wave acts as a diffraction grating, thereby forming a structure in the form latticed acousto-optic modulator.

Integrated hardware functions (5) and (6) define Moving (instant) spectra and light electric oscillations, provided movement analyzed by fluctuations fixed window, and the ratio (4) makes sense superposition integral for the corresponding spectral instrument, that is the acousto-optic analyzer radio spectrum or diffraction spectral instrument optical range in the diffraction optical radiation latticed structure in the form of acousto-optic modulator.

Since the information signals are adequately described in the theory of stochastic processes, in case the analysis of the spectrum of radio signals takes place deterministic diffraction light wave on a stochastic screen, and the analysis of the optical spectrum, diffraction occurs at a determinate wave stochastic screen.

For oscillations with finite spectrum frequency dependence can be approximated by entire functions on the basis of this and the Paley-Wiener $\dot{S}_0(\omega_{s_0}, \omega'_1, x_2)$ и $\dot{L}(\omega_{s_0}, \omega'_1, x_2)$ are entire functions of exponential type in both variables, their values at all points determined by two-dimensional sampling theorem in the spectral region.

Acousto-optic modulator in Figure 2 as a one-dimensional transparency, converts the complex amplitude of $E_1(x)$ is incident on a plane monochromatic wave uniform rule $E(x,t)=E_0T(x,t)$, where in E_2 (x) the complex amplitude distribution at the output face (the right along the axis z) of the acoustooptic modulator; T (x, t) - transparency function acousto-optic modulator as a banner.

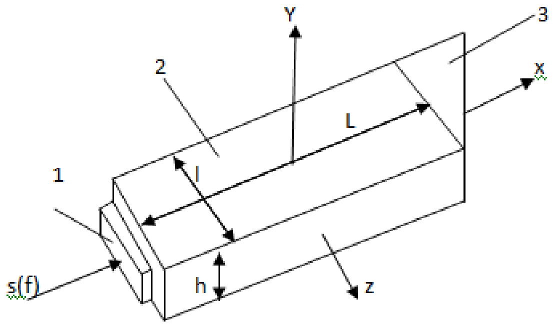

Figure 2

Figure 2 shows a diagram of the acousto-optic modulator, which includes a piezoelectric transducer 1, media 2, acoustic absorber 3.

HARDWARE FUNCTIONS OF OPTICAL SPECTRAL INSTRUMENTS BASED ACOUSTO-OPTIC TUNABLE FILTER

In this paper the analysis of the optical spectrum at its diffraction by elastic waves excited by a periodic sequence of rectangular radio pulses with a duration τ with linear variation of the instantaneous frequency [1] and a repetition period 2T. Next there is a view of an idealized model of observing the diffraction of light by elastic waves, assuming that the condition.

To determine the integrated hardware functions is sufficient to consider one cycle of operation, this corresponds to an electrical oscillation as a function of time t,

$$s(t)=S_m \exp[-i(\Omega_0 t+0{,}5Mt^2)],\ t\epsilon[-\tfrac{\tau}{2},\tfrac{\tau}{2}]\ , \qquad (7)$$

where

$$M = \frac{d\Omega(t)}{dt} = \text{const} \qquad (8)$$

- the rate of change of the instantaneous frequency control electric fluctuations; Ω_0 – average frequency electric fluctuations.

Within the radio-optical analogies connection input - output optical processor under consideration is given by

$$g(x_1)=\int_{-\infty}^{\infty}\int_{-\infty}^{\infty} f(\xi)\exp[i\gamma_1(\eta-\xi)^2]$$
$$\exp(i\gamma_1\eta^2)\cdot\exp[i\gamma_2(\eta-x_1)^2]\,d\xi\,d\eta \qquad (9)$$

Integration over η leads to the expression

$$g(x_1) = \frac{\pi^{\frac{1}{2}}}{i}\exp\left(-i\gamma_1^2\frac{1}{\gamma_0}x_1^2\right)$$
$$\int_{-\infty}^{\infty} f(\xi)\exp\left[i\gamma_0\left(\xi-\gamma_1\frac{1}{\gamma_0}x_1\right)^2\right]d\xi\ , \qquad (10)$$

where $\gamma_0 = \gamma_1(1-\gamma_1\frac{1}{\gamma_2}) = \omega'\frac{1}{2z_0F_0}(1-z_0\frac{1}{F_0})$

we obtain from the original formula for the complex hardware function optical spectral device based on acousto-optic tunable filter

$$K(M,t,\Delta\omega') =$$
$$=A_0\,\omega'\int_{-L_0}^{L_0}\exp\left\{i\left[Mt\frac{1}{v}+\Delta\omega'\frac{1}{\omega_0}\Omega_0\frac{1}{v}\right]\xi\right\}\cdot$$
$$\cdot\exp\left(\omega'\frac{1}{\omega_0}M2\frac{2}{v}\xi^2\right)d\xi\ .$$

Mathematical modeling was carried out on the basis of the following parameters:

$c := 3\cdot10^8$ $\qquad L := 0.01$

$\lambda := 565\cdot10^{-9}$ $\qquad v := 200($

$\Delta\omega := 10^9$ $\qquad t := -2, (-2+0.01)\,..\,2$

$\omega := \dfrac{2\cdot\pi\cdot c}{\lambda}$ $\qquad M := 1\cdot10^6$

$A := 6.672\times10^{13}$ $\qquad M1 := 1.5\cdot10^6$

$A := 6.672\times10^{13}$ $\qquad M2 := 2\cdot10^6$

$$K(t) := \left|\frac{1}{A}\cdot(\omega+\Delta\omega)\cdot\int_{-L}^{L} e^{i\cdot\left[\left(\frac{M\cdot t}{v}+\frac{\Delta\omega\cdot\Omega}{\omega\cdot v}\right)\cdot x+\left[\frac{(\omega+\Delta\omega)\cdot M}{2\cdot\omega\cdot v^2}\right]\cdot x^2\right]}dx\right|$$

(11)

$$K1(t) := \left|\frac{1}{A}\cdot(\omega+\Delta\omega)\cdot\int_{-L}^{L} e^{i\cdot\left[\left(\frac{M1\cdot t}{v}+\frac{\Delta\omega\cdot\Omega}{\omega\cdot v}\right)\cdot x+\left[\frac{(\omega+\Delta\omega)\cdot M1}{2\cdot\omega\cdot v^2}\right]\cdot x^2\right]}dx\right|$$

$$K2(t) := \left|\frac{1}{A}\cdot(\omega+\Delta\omega)\cdot\int_{-L}^{L} e^{i\cdot\left[\left(\frac{M2\cdot t}{v}+\frac{\Delta\omega\cdot\Omega}{\omega\cdot v}\right)\cdot x+\left[\frac{(\omega+\Delta\omega)\cdot M2}{2\cdot\omega\cdot v^2}\right]\cdot x^2\right]}dx\right|$$

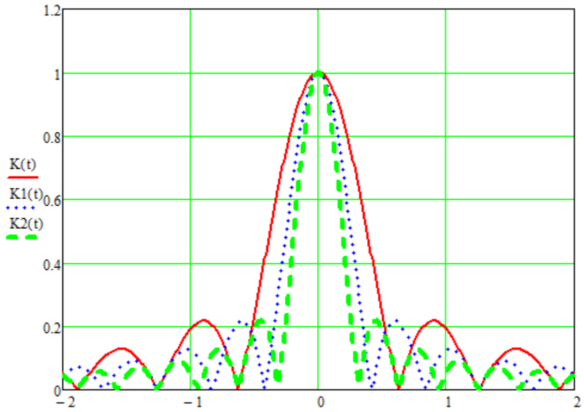

Figure 3

Figure 3 shows the results of mathematical modeling of complex hardware functions of the optical spectral device based on an acousto-optic tunable filter.

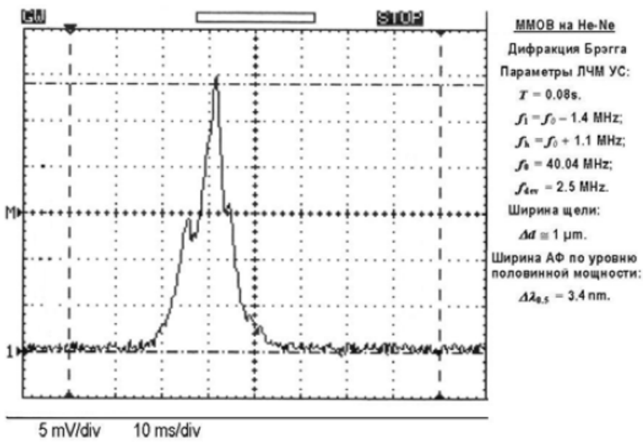

Figure 4

Energy transmission function of the optical spectrum device, measured at a width of the slit diaphragm photodetectors equal to 1 micron

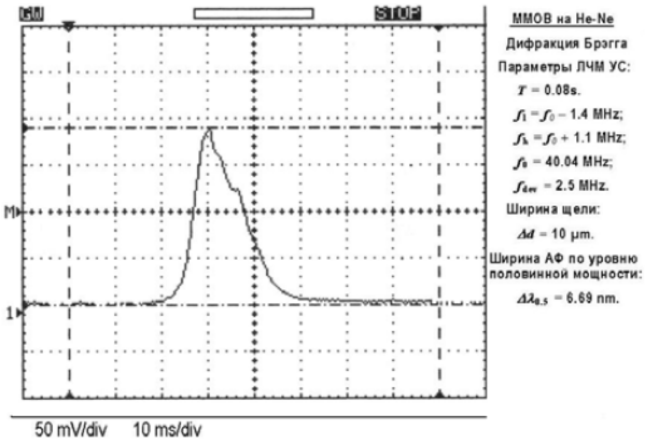

Figure 5

Energy transmission function of the optical spectrum device, measured at a width of the slit diaphragm photodetectors equal to 10 micron

CONCLUSION

The present work shows the role of spectral measurements in the optical range and marked dignity optical spectral device based on acousto-optic tunable filter.

A general expression of complex hardware functions of optical spectral device based on acousto-optic tunable filter and parameters are specified on which it depends.

As a result of the research, it was found that the acousto-optic interaction can be considered as a bilinear transformation on the spectral components that are physically: radio spectrum and the spectrum of the optical radiation. In the general form of linear transformations defined by the expansions of the nonlinear operator in a Taylor series and the establishment of the linear approximation. This technique is suitable to describe the linear approximation of any dynamic physical system.

As a result of this work, a formula for calculating the square of the modulus of the instrumental function of the optical spectral device based on acousto-optic tunable filter. This formula takes into account all the parameters and modes of operation of the optical spectral device based on acousto-optic tunable filter.

REFERENCES

[1] O.B. Gusev, V.V. Kludzin. Acousto-optical measurement. Leningrad: The Publishing House LSU, 1987.

[2] Kalinin V. A. Spectral measurements in the optical range with the transfer of the analyzed signals over optical fiber: dis. Candidate. those. Sciences: Spec. 05.13.01: protected 30.05.2006 / Kalinin Vladimir Anatolevich. SP., 2006. 133p.

[3] Moskaletz OD One type of diffraction of light by acoustic waves as a bilinear transformation. Materials XII All-Union Conference on acoustoelectronics and quantum acoustics. Part 1 Saratov 1983. P. 286-287.

[4] Moskaletz O.D. Dynamic signals and spectral measurements, 2013. P.152-158.

[5] Goldman Information theory. M.: Mir. 1957.

[6] Georgy Korol, Dmitry Moskaletz, Oleg Moskaletz «Effect of rate of change of frequency characteristics of the optical spectral device based on acousto-optic tunable filter» Proc. of SPIE Vol. 9216 92161F.

This work was supported by RFBR grant
№ 15-07-04720 A

STUDY OF AN ACOUSTIC LINK FOR WIRELESS COMMUNICATIONS

La Malfa Antonella, La Paglia Federico

University of Catania
Department of Electrical, Electronics and Computer Engineering

ABSTRACT – the main goal of this work is to develop a communication system which uses the acoustic medium in order to send commands from a control device (like a smartphone) to a receive device. The communication protocol realized uses five frequencies and a M.F.O.O.K modulation (Multiple-Frequency-On-Off-Keying).

INTRODUCTION

In the last few years many wireless communication technologies have been developed. In our home we can find a lot of devices which can use communication over the air. Most apartments have a Wi-Fi network and almost all mobile devices, like smartphones, are able to transmit information through several communication channels. There are many applications that allow to check emails, the bank account and many other information, using a smartphone and an internet connection. Nevertheless, the raising interest for sustainable technologies with minimum impact on human health drew the attention to technologies based on alternative means in order to not increase the electromagnetic pollution.

In some cases, the wireless data transfer based on radio frequencies may interfere with other electric devices; this is the case of hospitals, research and measurement labs.

We chose the acoustic waves which have several limitations such as the inability to pass through walls, short communication distances and low bit rate, but they have also several advantages. There are many scenarios where is acceptable to use a low bandwidth and a short transmission distance; actually, a limited distance allows to increase the communication security or to minimized the interference between different acoustic networks. Moreover, the acoustic waves do not electrically interfere with biological tissues.

The acoustic waves are used in undersea communications [1],[2] and there are autonomous under-water machines which are able to communicate using acoustic waves with frequencies between 12 KHz and 30 KHz.

In this paper we briefly illustrate the design, problems and technique used to develop the transmission physical medium which is based on sound and the development of it on hardware such as smartphone and embedded circuits, in order to allow the interaction between them.

This work continues the one started by Dr. Salvatore Tarda[3].

The system consists of two parts: the Android application and the *STM32F4* microcontroller of STMicroelectronics as embedded device. The Android application allows to interact with the embedded device, converting the commands in sounds.

The embedded device decodes the audio signals and executes the corresponding commands.

STM32F4[4] is provided with an ARM Cortex-M4 processor with a Flash memory of 1 MB and 192 KB of RAM; in this Discovery-Kit there is the ST-LINK device which allows to program the microcontroller via USB port. This board includes a lot of peripherals such as: MEMS sensors (MP45DT02 -Microphone), an audio DAC (CS43L22), eight colored led, etc.

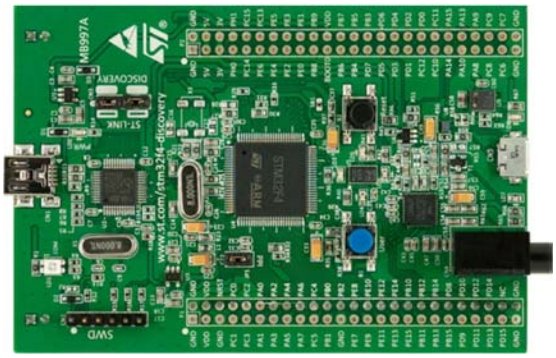

Fig. 1: STM32F4 board

The firmware has been developed using the C programming language and the software libraries provided by STMicroelectronics.

ACOUSTIC LINK

The commands are codified by the Android application and sent as acoustic waves, in order to be acquired and executed by the *STM32F4* board; the acquisition is performed by the integrated MEMS microphone (MP45DT02).

Data are transmitted using a sinusoidal waveform with a M.F.O.O.K. modulation (Multiple-Frequency-On-Off-Keying)[5]; this modulation allows to perform a parallel transmission over more carrier frequencies, representing the binary values 0 and 1 through the variation of the amplitude of the frequency transmitted.

In order to reduce the transmission time, a couple of bit is assigned to each frequency; thereby, using only four frequency is possible to send four couples of bit (00 – 01 – 10 – 11).

The frequencies chose by Dr. Tarda[3] for the data transmission were:

- 16250 Hz
- 17000 Hz;
- 17750 Hz;
- 19250 Hz;
- 20000 Hz.

As we can see there is a guard band of 750 Hz; the frequency of 16250 Hz represents the synchronization signal between sender and receiver; this frequency is sent at the beginning of transmission and before the transmission of each byte of data.

The original version of this project had several problems, and sometime did not properly work; the SMT32F4 board not always decoded data correctly, even with the smartphone placed at short distance from the board.

In order to find the origin of this problem, we analyzed the code of the Android application, in particular the MainActivity class; this class gets as input the string related to the command and converts it in a binary code using the “str2bin” function; the result is passed to “sendData” function, which generates the synchronization frequency, assigns the correct frequencies to each couple of bit, creates the audio track in PCM format and finally sends it.

We verified that the binary encoding and the related frequencies were correct, using the AUDACITY software; we recorded the sound emitted by the smartphone and then we inspected the frequencies spectrum.

Once we verified that the encoding of the smartphone was correct and that the audio signal did not present important distortions by the smartphone speaker, we inspected the firmware.

The board documentation reports that the bandwidth of microphone is between 20 Hz and 20 KHz[5], as is shown in the image below:

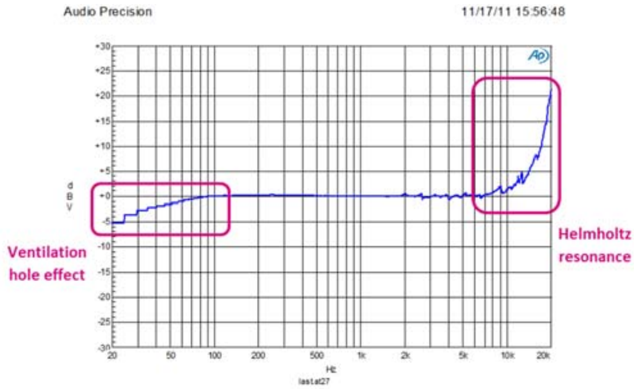

Fig. 2 : Microphone Bandwidth

The MEMS microphone, starting at about 17KHz, shows some distortions. We chose different frequencies inside the flat bandwidth of MEMS microphone (100Hz-2KHz). For this reasons, we chose this transmission frequencies:

- 1150 Hz
- 2150 Hz
- 3150 Hz
- 4150 Hz
- 5150 Hz

in this way, the MEMS microphone does not generate distortions into the received signal. Moreover the use of a greater guard band allows us to have less distortions. The synchronization frequency is 1150 Hz. Initially we had chosen a lower synchronization frequency, but in order to avoid the environmental noise we opted for a greater frequency.

Even though we had changed the frequencies range, the board was not able to decode the commands sent by smartphone. So, we continued our work by analyzing the decoding algorithm and understanding received signals. This brought us to change the code.

We modified the libraries:

- Firmware:
- ucom.h
- mems_acq.h
- App Android:
- MainActivity.java

ucom.h

It is the main part of the project; this library allows to decode signal from the acquired samples. It consists of three functions: record_init, DataFlowDec and DataExec.

- record_init

The record_init function allows to take audio samples from the buffer. It has an infinite loop which controls the presence of information inside 20 ms of sound (20 ms is the duration of one frequency which corresponds to one couple of bit).

Then the Fast Fourier Transformation is computed using a window of 512 samples;

then the power spectrum is computed, scaled and filtered, deleting too low frequencies. The index that contained the highest value, corresponding to the sent frequency, is selected from the buffer; in particular the frequency will be inside one of these intervals and the values will compose the array that contains data, which must be decoded:

- Synchronization Frequency: index between 12 and 19; the value "5" is inserted in the data array.
- The couple of bit 00: index between 20 and 30; the value "0" is inserted in the data array.
- The couple of bit 01: index between 31 and 42; the value "1" is inserted in the data array.
- The couple of bit 10: index between 43 and 53; the value "2" is inserted in the data array.
- The couple of bit 11: index between 54 and 63; the value "4" is inserted in the data array.

If the index is not inside one of these intervals, the value of "4" is inserted the data array; that means an error is occurred, a situation in which the information is not recognized. In this case there is a consecutive error counter in order to check if there are several consecutive information not encoded, which means that there are not other new data and is possible to start the decode.

The intervals allow to recognize a certain frequency even if it has some distortions, because the central value of the interval represents the index of the frequency inside the buffer containing the power spectrum. The indexes obtained with the new frequencies are:

- 14
- 26
- 36
- 48
- 59

To compute them, just use the equation below:

$$\text{index} = \frac{(\text{frequency} * \text{N})}{\text{Sample Frequency}}$$

Where "frequency" represents the one associated to the index (e.g. 1150 Hz); "N" is the window used for the Fourier Transformation (in our case 512); finally the "Sample Frequency" is 44100 Hz.

Finally, the empty part of the array is filled with "4" e the function DataFlowDec is called.

- DataFlowDec

The function DataFlowDec take as input the array containing data collected from the audio samples by function record_init. We modified this function, adding a synchronization system, enhancing the system performance. The main problem of the algorithm is the following: the microphone is not able to get the sounds perfectly; sometime a frequency is not detected or is not correctly decoded because of some environmental noise. When a command is sent, firstly the synchronization frequency is sent, and then the command itself. The latter corresponds to one byte, composed by 20 values subdivided into 4 parts of 5 element; each element corresponds to a frequency, which identifies a couple of bit to decode. An ideal command to decode had the following format:

55555   11111   00000   11111   22222

We have five values for the synchronization, followed by the command consisting in four parts.

Because of the imperfection of the microphone, the command can be received in a distorted format and the system should not be able to understand where is the beginning of the command, represented by the synchronization.

The new algorithm looks for the synchronization values and increment a counter. The latter counts the consecutive synchronization values; if there are at least three consecutive values, it's possible to go on and start the decoding. Then, since the synchronization is formed by five elements, the deviation is computed in order to know where the command begins.

When the beginning of the command is found, it is checked if in a window of 20 elements (the command) there are enough data in order to start the decoding: if there are more of 10 values different from "4" (this value means that the system does not recognized any frequency), it's possible to start the decoding.

The 20 elements are divided into five parts; for each part are counted the number of 0, 1, 2 and 3, which filling four counters.

The highest counter identifies the frequency (the couple of bit) sent; this result is stored in a data array with the following codify:

- 0 (for the couple of bit 00)
- 1 (for the couple of bit 01)
- 2 (for the couple of bit 10)
- 3 (for the couple of bit 11)

Finally a binary string is created with the values found. When the decoding is completed, the decoded command is passed to the function DataExec, which executes the command.

MEASUREMENT

The measurements made in order to test the system performance take into account the presence of different sources noise: voice, music, television and an object that falls near the microphone.

We made 40 measurements for each of these types, and in order to offer a better valuation, we tested the original code with the old frequencies, the new algorithm with the old frequencies, and finally the new algorithm with the new frequencies.

MEASUREMENTS WITHOUT NOISE

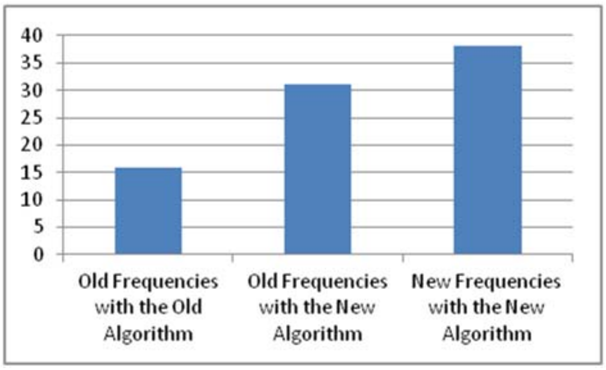

Fig. 3: Histogram without noise

As it is shown above, with the use of the new algorithm we reach a better system performance.

MEASUREMENTS WITH NOISE: VOICE

These measurements are made talking at a distance of 30 cm from microphone. The results obtained are:

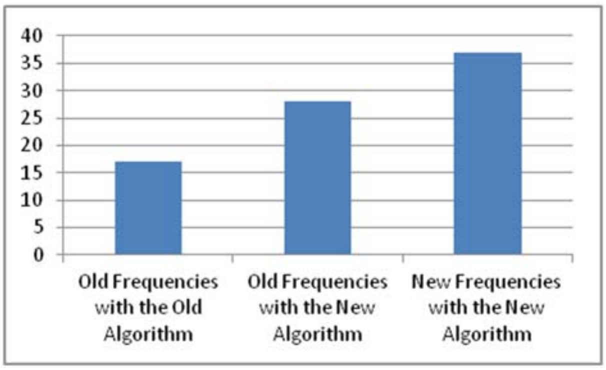

Fig. 4: Histogram with noise (voice)

Watching the results, we can assert that the voice does not affect the system performance.

MEASUREMENTS WITH NOISE: MUSIC

These measurements are made playing music at a distance of 30 cm from the microphone and we obtained the following results:

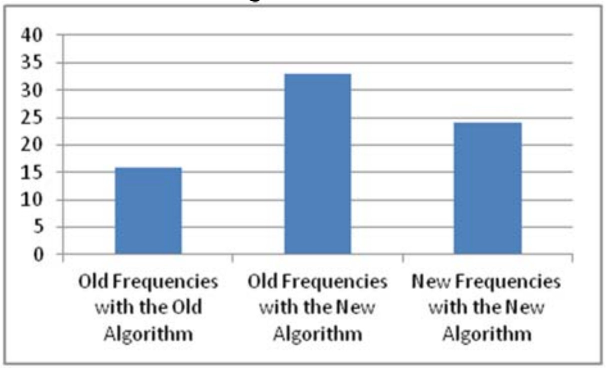

Fig. 5: Histogram with noise (music)

The performance reached with the use of old frequencies and the new algorithm is better than the one reached with the new frequencies and the new algorithm because the new frequencies are in a lower band which is affected by the musical noise; the old frequencies which are in a greater band are not affected.

MEASUREMENTS WITH NOISE: TELEVISION

This measurements are made using a television at a distance of 2 m from microphone. The results obtained are:

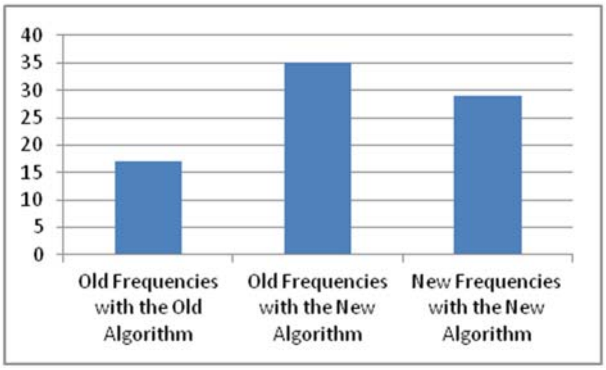

Fig. 6: Histogram with noise (television)

Also in this case, using the old frequencies, is possible to observe a small influence of television disturbances.

MEASUREMENTS WITH NOISE: OBJECT

These measurements are made by letting a small object fall (a chewing gum packet) at a distance of 5 cm from microphone. We obtained the following results:

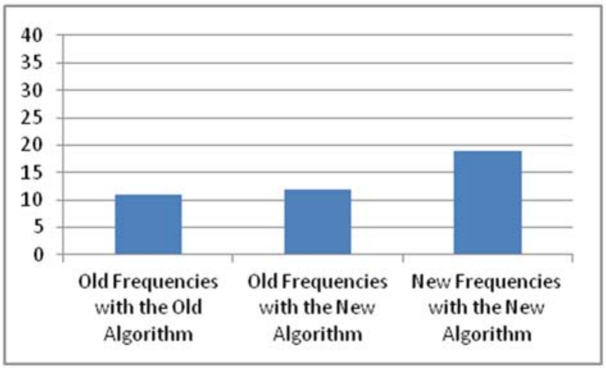

Fig. 7: Histogram with noise (falling object)

Observing the graph, it is clear that the falling of an object has a bad influence on microphone behavior.

CONCLUSION

The implementation of the new algorithm leads to a better synchronization between smartphone and board, increasing performance and the efficiency of system.

The new frequencies present less distortions than the old ones because they are in the flat band of STM32F4's microphone; however they suffer for disturbs present in urban environment.

In order to reach a better result, it might be useful to use a microphone which works over 20kHz, avoiding interference from outside noise. Moreover using the ultrasound, the commands are not audible from the human ear, so we have a lower environmental noise pollution.

This technology can be used in different scenarios, e.g. in the control of environmental variables, in the opening of doors and gates; in particular in the medical and childhood field it avoids to radiate the environment with the Wi-Fi signals.

BIBLIOGRAPHY

[1] Chitre, Mandar; Shahabudeen, Shiraz; Stojanovic, Milica : Underwater Acoustic Communications and Networking: Recent Advances and Future Challenges. Marine Technology Society Journal, Volume 42, Number 1, Spring 2008, pp. 103-116(14)

[2] IF Akyildiz, D Pompili, T Melodia : Challenges for efficient communication in underwater acoustic sensor networks- ACM Sigbed Review, 2004 - dl.acm.org

[3] Tarda Salvatore – Thesis: Open Issues in Acoustic Communication Networks

[4] STM32F4DISCOVERY Schematic

[5] PDM audio software decoding on STM32 microcontrollers

[6] Discovery kit for STM32F407/417

CONTROL SYSTEMS IN ROBOTICS

Mikheev Leonid, Perfiliev Alexey

Saint-Petersburg State University of Aerospace Instrumentation,
Saint-Petersburg, Russia

E-mail: ssv555ssv@yandex.ru

When creating control systems for robotic objects, a wide range of sensors, different configurations and designs are often used. To date, in 80% of cases, robotic systems are equipped with the following types of sensors: distances (optical and infrared); Vibration (mechanical); Video processing (cameras); Color recognition (optical), positions (gyroscopes and accelerometers), etc. Bluetooth, Wi-Fi, GSM and other technologies are used as information transfer channels.

However, there are anthropomorphic robotic systems for control, which need to read or repeat the movements of the human body. Often this applies to parts of the human body such as arms, legs and especially the fingers as the most subtle tool created by nature.

To build such control systems, a variety of approaches are used, but the most common is the way the information is read from a resistive bending sensor or a Flex sensor (Figure 1). Such sensors have a number of mechanical and electrical faults: a limited cycle of bends; Rigidity and impossibility of repetition, and following and interpreting small bends; Step change in the external characteristic [1].

The article presents a way to create and integrate optical bending sensors that are designed to control fingers with a mechanical hand.

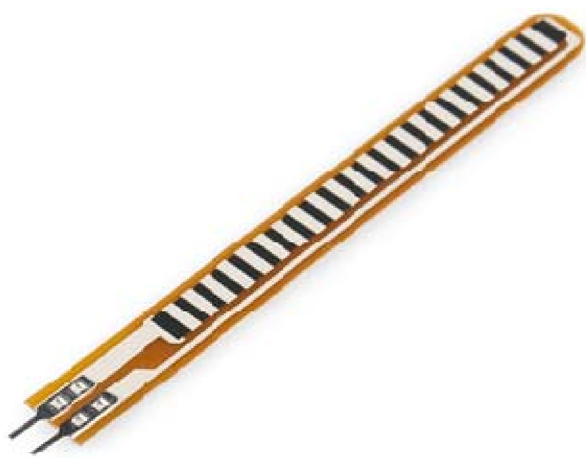

Fig. 1. Resistive Flex Bending Sensor

The basic electrical diagram of the optical bending sensor is shown in Fig. 2.

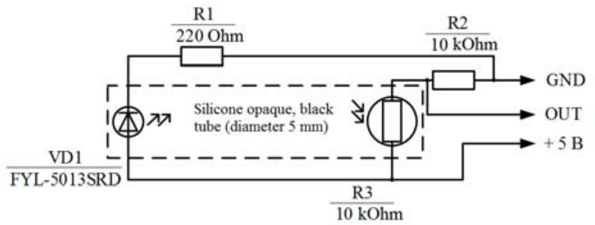

Fig. 2. Schematic diagram of an optical bending sensor

Structurally, the optical bending sensor is a silicone tube with a diameter of 5 mm and a length of 100-120 mm, it depends on which of the fingers of the human hand is the sensor. On one side of the tube, a VD1 LED (red, 5 mm in diameter) is welded, and on the other a photoresistor R3 (5 mm in diameter). After carrying out all electrical connections, according to the basic electrical circuit (Figure 2), the entire structure is inserted into a black heat-shrinkable tube with a diameter of 10 mm (Figure 3).

Fig. 3. Stages of manufacturing an optical bending sensor

To remove the characteristic of the output voltage of the optical bending sensor from the angle of its bending, a basic electrical circuit was used based on the Arduino UNO microcontroller [2] and an algorithm written in the Arduino IDE software [3] (Fig. 4).

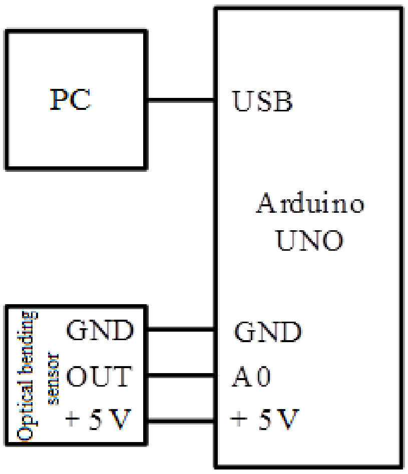


```
void setup() {
pinMode(A0, INPUT);
Serial.begin(9600);
}
void loop() {
int bb = analogRead(A0);
Serial.println(bb);
}
```

Fig. 4. Basic electrical circuit based on the Arduino UNO microcontroller and the algorithm in the Arduino IDE for removing the output voltage characteristic of the optical bending sensor from the angle of its bending

To build the dependence of the output voltage of the optical bending sensor on the angle of its bending, the "Port Monitor" (Ctrl + Shift + M) and "Plotter by serial connection" (Ctrl + Shift + L) were used in the Arduino IDE software, the dependencies are shown in Fig. 5).

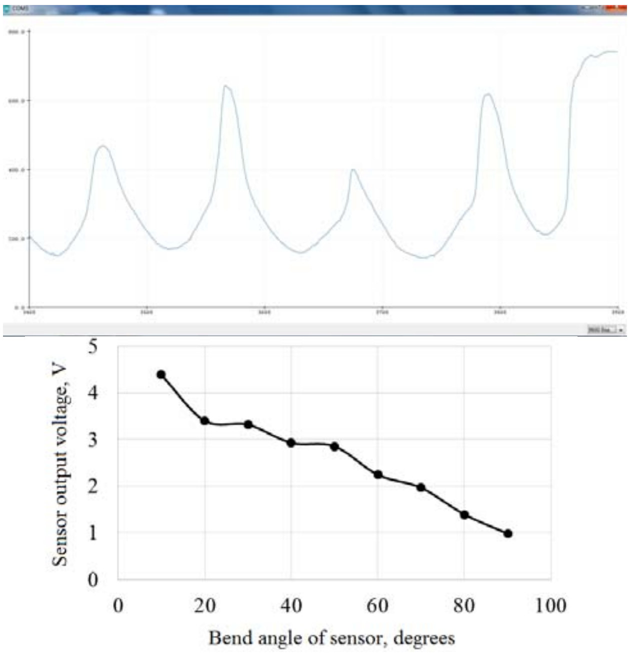

Fig. 5. Dependence of the output voltage of the optical bending sensor on the angle of its bending

Analysis of the dependencies (Fig. 5) showed a sufficient, and most importantly smooth, range of the output voltage of the optical bending sensor from the angle of its bending in the range of 0.98-4.38 V, The resulting optical bending sensor, after attaching it to one of the five fingers of the glove, can be used to control the Futaba S3003 servo, which will drive the fingers of the mechanical arm through metal cables (Figure 6).

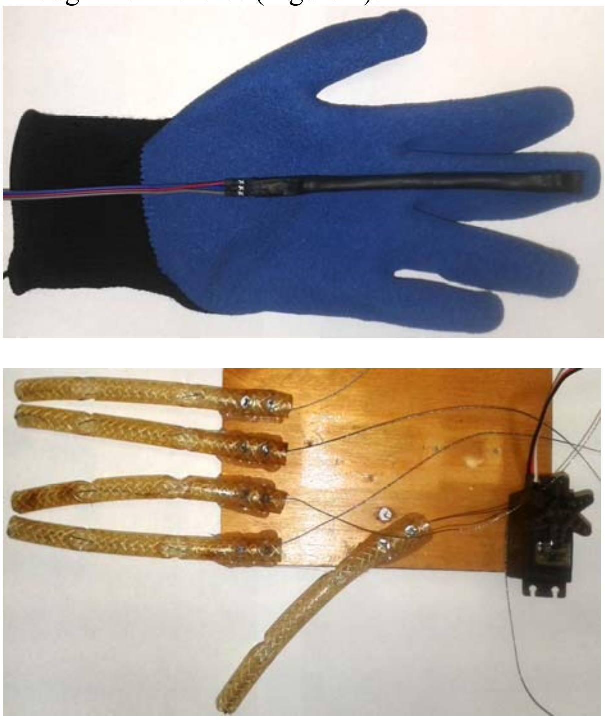

Fig. 6. Scheme fixing the optical bending sensor on one of the five fingers gloves and a mechanical arm with a servo and metal cables

To control the servo drive Futaba S3003 [4] using an optical bending sensor, a basic electrical circuit was used based on the Arduino UNO microcontroller and an algorithm written in the Arduino IDE software (Fig.7).

```
#include <Servo.h>
#define MAX_ANGLE 90.0
Servo myServo;
void setup() {
Serial.begin(9600);
myServo.attach(9);
pinMode(A0, INPUT);
}
void loop() {
int lightness = analogRead(A0);
int val = analogRead(A0);
int angle = int(val / 1024.0 * MAX_ANGLE);
angle = constrain(angle, 0, 180);
myServo.write(angle);
Serial.println(angle);
}
```

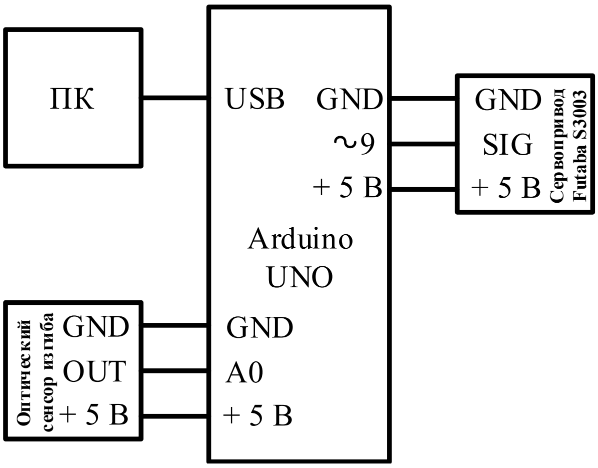

Fig. 7. Schematic circuitry based on Arduino UNO microcontroller and algorithm in Arduino IDE for servo control Futaba S3003

Tests of the basic electrical circuit and algorithm (Figure 7) showed sufficient sensitivity, smoothness and efficiency of the manufactured optical bending sensor when controlling the servo drive Futaba S3003. In the course of the experiments, it was found necessary to refine the Futaba S3003 servo control algorithm, since The optical bend sensor can bend in the range of 0-90 degrees, it is necessary to adequately project this range to the angle of rotation of the servo, which varies in the range of 0-180 degrees, further work will be aimed at improving the control algorithm.

REFERENCES

1. Official website of Sparkfun Start Something: https://www.sparkfun.com. [Electronic resource] / Flex Sensor, the mode of access to the link: https://cdn.sparkfun.com/datasheets/Sensors/ForceFlex/FLEXSENSORREVA1.pdf.
2. Sommer U. Programming of microcontroller boards Arduino / Freeduino. - St. Petersburg .: BHV-Petersburg, 2012. - 256 p .: ill.
3. Petin V.A. Projects using the Arduino controller. - St. Petersburg: BHV-Petersburg, 2014. - 400 p .: ill.
4. Methodological manual for performing laboratory work on the discipline "Software of mechatronic and robotic systems" (for students of the full-time course of training 15.03.06 "Mechatronics and Robotics"). Solenyi S.V., Solenaya O.Ya. St. Petersburg: GUAP, 2016. – 81

MODELS OF FORECAST OF TIME SERIES

Nikishina Maria, Reshetilova Svetlana

Saint-Petersburg State University of Aerospace Instrumentation,
Saint-Petersburg, Russia

E-mail: diadinwn@gmail.com, : sveticsspb@gmail.com

Abstract

Models and algorithms of programming are based on the forecast of time series. It allows to display correctly forming and development mechanisms of the process and stipulated by those or others trends of different ways of action. To date great number of prediction models have been developed among them such as exponential smoothing models, regression and autoregressive models, models based on Markov chains, neural network models, classification models.

The most often used models are regression and autoregressive models because of the analysis capabilities they provide[2]. One of the serious disadvantages of the class of autoregressive forecast models you can call the large number of parameters to identify each one required significant count of resources most of it ambiguous.

KEY words: time series, forecast, prediction, models.

OVERVIEW OF PREDICTION MODELS

Forecast is a prediction of the possible values in some process in future, based on already known characteristics in past and present time. Researched process most often presented in form of some time series. Time series is selective implementation generated consistently in time by a stochastic process which is influenced by many factors.

The essence of forecast of a time series is reduced to search functional dependence, which describes time series, otherwise(different) - prediction(forecast) model. These forecast models are divided into two big classes: statistical models and structural models.

The statistical models are include models such as:

- exponential smoothing models,
- regression,
- autoregressive.

In these models functional dependence is determined analytically.

The structural models are include models such as:

- models based on Markov chains,
- neural network models,
- on the basis of classification and regression trees.

In these models functional dependence is determined structurally.

AUTOEGRESSIVE MODELS

The autoregressive models are based on offer, that the value of some element of the time series Z(t) depends linearly from (depends linearly on) past values of the same time series Z(t-1),.....,Z(t-p)

The most popular of the simple models used is moving average autoregressive model[1]. This model of the autoregression (AR) is quite useful in formalizing time series encountered in applications. In it, the current value of the process Z(t) is determined by linear dependence of the previous values of the time series and "white noise"- the error of the model, implied as a random process with values evenly distributes over a certain range.

AR model of order p, usually denoted as AR(p), looks like this:

$$Z(t) = \mathrm{C} + \beta_1 Z(t-1) + \beta_2 Z(t-1) + \beta_p Z(t-1) + \varepsilon_t \quad (1)$$

where β_1,....., β_p - model parameters (autoregressive coefficient)

C-constant(usually means zero)

ε_t-model error(white noise)

Example, autoregressive process of the first order AR(1):

$$Z(t) = C + rZ(t-1) + \varepsilon_r \quad (2)$$

In considered example above autoregression coefficient converges with the coefficient of autocorrelation of the first order r .

Other quite common type of the model, used in conjunction with autoregression is moving average model of order q.

$$Z(t) = 1/q(Z(t-1) + Z(t-2) + \cdots$$
$$+Z(t-q)) + \varepsilon_t \qquad (3)$$

Here q is the order of the moving average.

Also there are other models of the moving average: simple, weighted, cumulative, exponential. There is an opinion[1] to get model more clear expediently to unite autoregressive and moving average into one model called ARMA(p,q). It combine the filter in the form of the moving average q-th order and autoregression of the filtered values of the p-th order series.

If the source data are not actually the values of the time series and the difference is *d-th* order (typically on practice ≤ 2) then that model is called the autoregressive model of the integrated moving average (ARIMA(*p,q,d*).

MODELS OF THE EXPONENTIAL SMOOTHING

The models of the exponential smoothing(ES) widely used at present. It is still simple, effective, visual considering that they were developed in the middle of the XX century.

The main idea of the ES is the continuous correction of the predicted values at the moment of the receive of new actual data. Therefore, the latest received data has a greater impact on the forecast of the value then previous observations.

The model of the ES looks like this:

$$Z(t) = S(t) + \varepsilon_t \qquad (4)$$

$$S(t) = \alpha\big(Z(t-1) + (1-\alpha)S(t-1)\big) \qquad (5)$$

Where α – coefficient of smoothing, $0 < \alpha < 1$;

The initial condition: $S(1) = Z(0)$

The Holt model or in the other words double exponential smoothing. These model effectively used for work with the processes which has trend. In the considered model it is necessary to analyze two conditions : the level and the trend.

Regardless of each other, the level and trend are smoothed out.

$$Z(t) = S(t) + \varepsilon_t$$
$$S(t) = \alpha \cdot (Z(t-1) + (1-\alpha) \cdot (S(t-1) -$$
$$- B(t-1)) \qquad (6)$$

$$B(t) = \gamma\big(S(t-1) - S(t-2)\big) + (1+\gamma)$$
$$\cdot B(t-1)$$

α — coefficient of smoothing, $0 < \alpha < 1$, (like in (5)); γ —smoothing trend coefficient

The Holt-Venters model, otherwise, triple exponential smoothing, is used to forecast processes which has trend and seasonality.

$$Z(t) = \big(R(t) + G(t)\big) \cdot S(t) \qquad (7)$$

$R(t)$ — smoothed level without seasonal component.

$$R(t) = \frac{\alpha \cdot Z(t-1)}{S(t-1)} + (1+\alpha) \cdot (R(t-1) +$$
$$+G(t-1)) \qquad (8)$$

$G(t)$ — smoothed trend.

$$G(t) = \beta \cdot \big(S(t-1) - S(t-2)\big) +$$
$$+(1-\beta) \cdot G(t-1) \qquad (9)$$

$S(t)$ — seasonal component.

$$S(t) = \frac{\gamma Z(t-1)}{S(t-L)} + (1+\gamma)(S(t-L) \qquad (10)$$

Quantity L -lengths of the season of the researching process.

The exponential smoothing models mostly effective to longtime predicted.

NEURAL NETWORK MODEL

Today, models which based on the artificial neural network(ANN) are among the maximum extensively used of the structural models. Due to the opportunities of working with noisy and controversial data.

Neural networks makes up the group of the models, that are analogues to the biological neural networks of the central neural system of animals (in particular, the brain), used for forecast and estimate, given a large number of initial parameters, mostly unknown.

Artificial neural network, as a rule, represented as a system of interconnected "neurons", which exchange messages with each other.

Neural networks are adaptive to inputs and able to learn due to connections that have numerical weights set up on basis of experience.

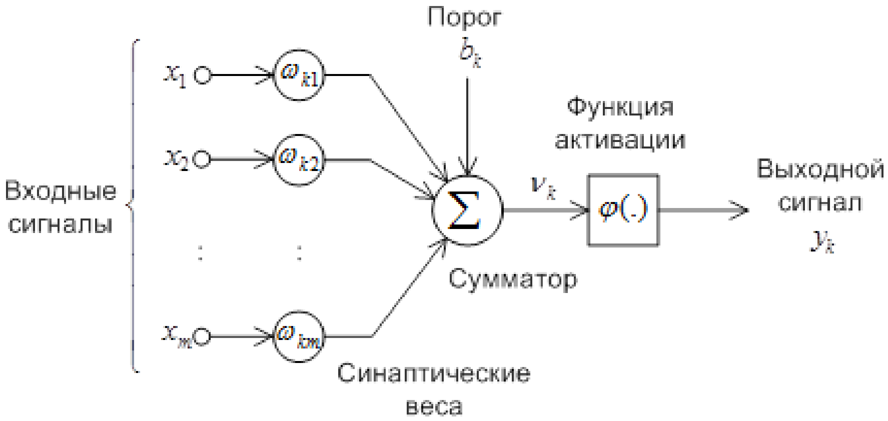

Figure 1 - Nonlinear model of neuron.

The neuron consists of 3 logical blocks: inputs, conversion function, output. (fig.1)

To describe models of neuron used two equations:

$$U(t)=\sum_{i=1}^{m} w_i Z(t-i)+b, \tag{11}$$

$$Z(t) = \varphi(U(t)),$$

where, $Z(t-1)$, … , $Z(t-m)$ – input signals; w_1, ... , w_m - synaptic weights of the neuron; b – limit; $\varphi(U(t)$ – activation function.

Architecture of the neural network depends on the connection of neurons. Features of the neural connection is define the three types of network:

- recurrence networks
- single-layer networks of direct distribution
- multilayered networks of direct distribution

The main meaning of the neural network predictive model is to generate some output sequence in response to some input sequence, the so-called time link. This task includes two aspects:

- sequence recognition
- sequence reproduction.

For forecast of the time series neural network certainly should have recurrence.

One of the several possible architecture of neural networks is multilayered one by one(priority one). By using additional of the direct or indirect loops of connection this network meets the requirements of recurrence and this is why this model is suitable for predicting the time series. As only little number of connections has inverse connection this networks is named partially recurrence. It uses context units. The context of the storage unit of the hidden layer of output from one or more previous steps in time use as additional input devices. Thus, they pass information from past to the state of the network now.

Therefore, neural networks models are effective in predicting of the nonlinear dependence of the future values of the time series from actually values and of the value of the external factors. Nonlinear dependence setup by the structure of the network and activation function.

Neural networks capable to learn based on input and output date. That is way, they can solve complex management tasks [2,3,4].

MODELS BASED ON MARKOV CHAINS

The model based on the Markov chain is applied when the future values of the process parameters are determined by its current state and independent the previous[5]. So, processes with short memory are modeled by Markov chains. The remark that the intensity of the probability flow entering the given state is equal to the intensity of the probability flow coming from this state is applicable to any Markov chain.

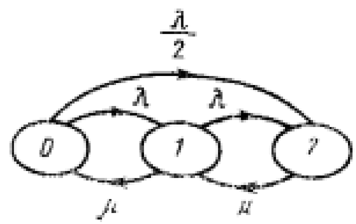

Figure 2

In the system, the transition from E0 to E1 is allowed.

$$\frac{3}{2}\lambda p_0 = \mu p_1 ;$$

$$(\lambda+\mu)p_1 = \lambda p_0 + \lambda p_2 ;$$

$$\mu p_2 = \frac{\lambda}{2} p_0 + \lambda p_1;$$

These equations correspond to the conditions of the flow conservation in the states E0, E1, E2, respectively. We note that the third equation is exactly the sum of the first two; for finite Markov chains, we always obtain exactly one excess equation. An additional equation is P0 + P1 + P2 = 1.

The solution of this system is:

$$p_0 = \left[1 \ \left|2\frac{\lambda}{\mu}\right| - \frac{3}{2}\left(\frac{\lambda}{\mu}\right)^2\right]^{-1}$$

$$p_1 = \frac{3}{2}\frac{\lambda}{\mu} p_0$$

$$p_0 = \left[\frac{1}{2}\frac{\lambda}{\mu}| \quad \frac{3}{2}\left(\frac{\lambda}{\mu}\right)^2\right] \quad p_0$$

The advantages of the enumeration method are used here to determine the stationary distributions of a number of Markov chains. Consequently, the structure of the Markov chain and the probability of state transition determine the relationship between the value of the process that will be and the one that is at the moment.

SUMMARY

The purpose of time series prediction methods is very relevant for a variety of applications and is considered an integral part of the health of many companies.

At the moment, a large number of models have been created, with the help of which it is possible to find a solution to the problem of predicting the time series, autoregressive and neural network models are more effective among these tasks.

An important defect of autoregressive models is considered to be a large number of independent characteristics that require recognition; Defects of neural network models are considered to be the opacity of the simulation and not easy to study the network.

A more promising course of model forecasting, whose goal is to increase the infallibility, is the emergence of combined models that perform clustering on the 1st line, and then the prediction of the time series from within the established cluster.

REFERENCES

1. Бокс Дж., Дженкинс Г.М. Анализ временных рядов, прогноз и управление. М.: Мир, 1974. 406 с.
2. Gheyas I.A., Smith L.S. A Neural Network Approach to Time Series Forecasting // Proceedings of the World Congress on Engineering, London, 2009, Vol 2 [электронный ресурс]. P. 1292 – 1296. URL: www.iaeng.org /publication/WCE2009/WCE2009_pp1292-1296.pdf
3. Morariu N., Iancu E., Vlad S. A neural network model for time series forecasting // Romanian Journal of Economic Forecasting. 2009, No. 4. P. 213 – 223.
4. Parzen E. Long memory of statistical time series modeling // NBER-NSF Time Series Conference, USA, Davis, 2004 [электронный ресурс]. 10 p. URL: http://www.stat.tamu.edu/~eparzen/Long Memory of Stat.. %20Time%20Series%20Modeling.pdf
5.http://www.bi-grouplabs.ru/Rech/electricity/ BI_EnergoPrice.html

STATISTICAL METHODS OF QUALITY CONTROL IN ADDITIVE MANUFACTURING

Petrashkevich Evgeniia

Saint-Petersburg State University of Aerospace Instrumentation
Saint-Petersburg, Russia

E-mail: Dgonya.94@mail.ru

Abstract

The article addresses the problem of quality control in additive manufacturing based on the lack of standardized indicators of the production process and technical regulations, which describe the defects arising in a production process of models. The analysis and the decision with use of Shewhart control charts is provided.

Keywords: additive technology, statistical methods of quality, defects of the production process.

INTRODUCTION

Increasingly in recent years we may be faced with the theme of additive technologies not only within use in research works or research and development, but also successful use of technologies in serial productions in various spheres around the world.

Russia doesn't lag behind – the market of materials, special composite thermoplastics and metal powders develops, and there are domestic equipment manufacturers with a quality which isn't inferior to foreign analogs [1].

Naturally there are difficulties and problems faced by producers and regular users of 3D printers. One of important issues concerns implementation and certification of the details made by an advanced method, but the main priority issue affects the feasibility and efficiency of such process innovations. However, many practices prove the viability and therefore the competitiveness of additive technologies [2].

Special demand 3D printing has in the space industry, aviation and automotive industries, where the high quality of the products has great importance [3]. Therefore, the main problem which face directly during production is appearance of defects for various reasons. In this connection, appropriate attention should be paid to researches of possible defects and the causes, and also to methods of minimization of losses through the timely application of appropriate tools of quality management.

RESEARCH PART

The basis of additive production is a thermal process with all its inherent disadvantages. Often found type of defect is called warping, which is characterized by compression and the shrinkage of plastic through temperature reduction and model distortion [4]. Not less common so-called "elephant foot" - detail at the base becomes larger than it was intended. In this case setting the printer table temperature plays a role. The most common, basic defect – friability, also called sagging when in areas where support is necessary, it is absent and the printing is performed by air or when badly chosen temperature causes formation of droplets, clusters of plastic. The material overheat may also lead to decomposition of the plastic, that is pyrolysis, which is not only contributes for changing the properties of the material, but frequent failures of the equipment [5].

It is easy to note that compliance with certain operating temperature has a significant impact on the quality of the models, so it is necessary to control the printing temperature and keep it within the range, depending on the type of material and equipment class. n order to be able to analyze information about the current state of manufacturing process model on a 3D printer with control bounds representing limits of their own variability (dispersion) of process, and determination whether process needs regulation at the time of production, it is advisable to consider the applicability of the quality and management control tool - Shewhart control charts.

Shewhart control charts – the tool intended for determination of the moment of an exit from a condition of statistical controllability of process which allows to minimize costs for elimination the cost of removal of non-compliance of the requirements.

The tool has significant advantages:

1. Usability;
2. Process visualization;
3. The availability of standardized criteria for the transition process in an unstable condition, considering which, it is possible to manage process

automatically.

In determining the state of statistical control of the printing process of model, as reference value which will be the central line (CL) we use intended target value of the characteristic of process (fig. 1). In the following experiment for this value was adopted nozzle temperature of 230 degrees Celsius when forming the task for the 3D printer based on the type of material. The upper (U (CL)) and (L (CL)) lower control limits were taken at a distance of $\pm 3\sigma$ from the center line [6].

In case of additive production it is necessary to know the working temperature to which the material should be heated in the print head, depending on the material characteristics and values based on information from the previous process.

There was used widespread ABS plastic that has an operating temperature of 220-248 degrees Celsius.

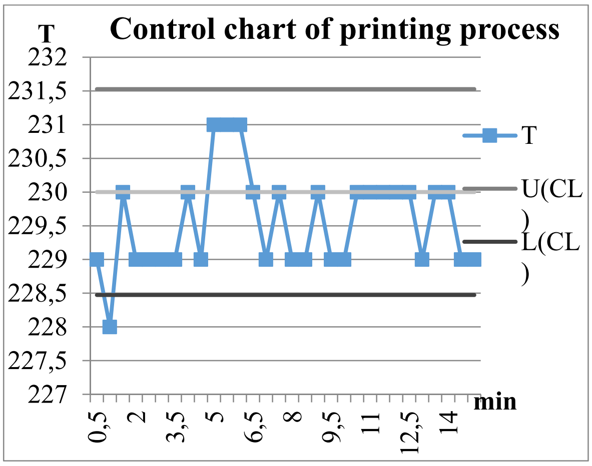

Fig.1.
Control chart of printing process on a 3D printer

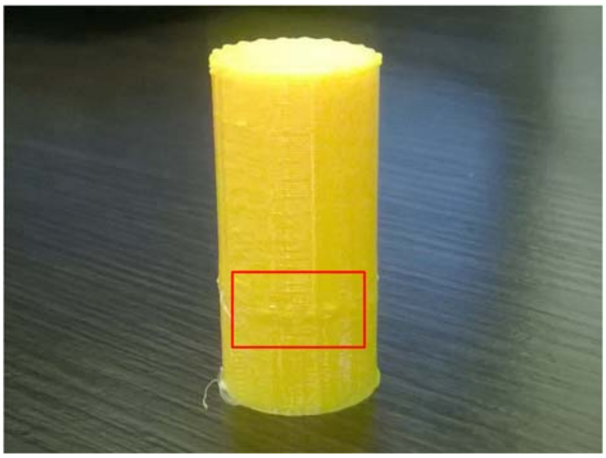

Fig. 2.
Defect "friability" on the model

Control charts graphically represent the dynamics of the process, i.e. change of indicators over time. On the map is marked the inevitable scattering range, which lies within the upper and lower limits [7]. Using this method it is possible to identify the cause of the defect, making sure at what point the process has shown an unstable condition. The map shows that in the interval between 4.5 and 6.5 minutes when there was a defect (Fig. 2), the temperature was at maximum values.

To obtain reliable reasons of emerging defects, it is necessary to explore additional data about external factors influencing the process. Such main factors include desktop (platform) temperature of the printer, the speed of cooling and printing speed. For each type of material and type of printer must be assigned its own parameters, often chosen experimentally. At the moment there are no standards governing the quality indicators of the process of additive manufacturing, which undoubtedly causes a lot of problems to manufacturers.

CONCLUSION

In any case, as a result of the conducted researches it can be concluded that the use of Shewhart control charts, in accordance with GOST R ISO 7870-2-2015 Statistical methods. Control cards. Part 2: Shewhart Control cards can positively affect the quality of production with the use of additive technologies. Subsequently will be analysed technical regulations in the sphere of quality management and the standards and standards of additive technologies for writing clear recommendations to improve the quality of the printing process on the 3D printers.

REFERENCES

[1] Совершенствование процессов управления наукоемким производством и оценки его потенциала Семенова Е.Г., Чабаненко А.В. Радиопромышленность. 2016. № 4. С. 38-43.

[2] Чабаненко, А.В. Стандартизация наукоемкой продукции/ А. В. Чабаненко // Стандарты и качество. 2015. № 1. С. 42-49.

[3] Комбинированная технология производства в авиастроительной промышленности России Чабаненко А.В., Петрашкевич Е.Э. Новая наука: Стратегии и векторы развития. 2016. № 2-1 (64). С. 32-37.

THE SYSTEM WHICH CAN HELP PEOPLE TRACK THEIR LIFE ACTIVITY

Pozharova Ksenia

Saint-Petersburg State University of Aerospace Instrumentation,
Saint-Petersburg, Russia

E-mail: orlovaksusha@mail.ru

Abstract

Discipline and understanding what a person do – is crucial. If a person understands, where and how he spends his time, he can manage it more successfully.

This article is about the system which is called “LiveHelper”. This system helps people track their sports activity, consumed food, sleep hours, consumed vitamins and so on. I’ve been working on this system for six months.

INTRODUCTION

These days more and more people start thinking of their life activity and sports activity. They want their body to be healthy and vigorous. There are a lot of fitness bands with their systems of sports control on the market. For example, Garmin has its sports system, but the main minus of this system is limited functional. Garmin’s system can track consumed calories, count of steps made a day, the distance that a person went, hours of sleep and what activity a person did in a gym, cardio or exercises with trainers. The sports system from Microsoft consists of the same functional, except the function of tracking food.

The “LiveHelper” has all features that were present in plus many others. For example, my system has a function which tracks consumed vitamins a day, tracks changing of analyses, fixes the quality of sleep, can track not only two activities in the gym but many others.

People interested in sport, health, healthy food. They want a simple system, which can help them track their life activity. My system can give them one.

MAIN FUNCTIONAL

The main page of my system consists of the main photo of a page’s owner, brief information, calendar, pressing on its date you can go to a form where you can add and analyse your data. The main page also consists of comment section (only for trainers) and action menu.

A person can add information like these: what kind of training had he done, what food had he consumed. Food has vitamins, so these vitamins are counted in a system as well. A person can add information of exercises, sets, reps, pulse, time which person spend in a gym, information of his analyses, check its progress.

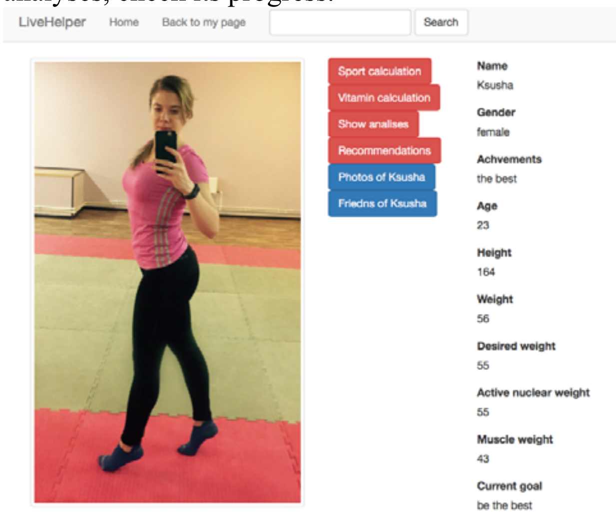

Fig. 1. The main page

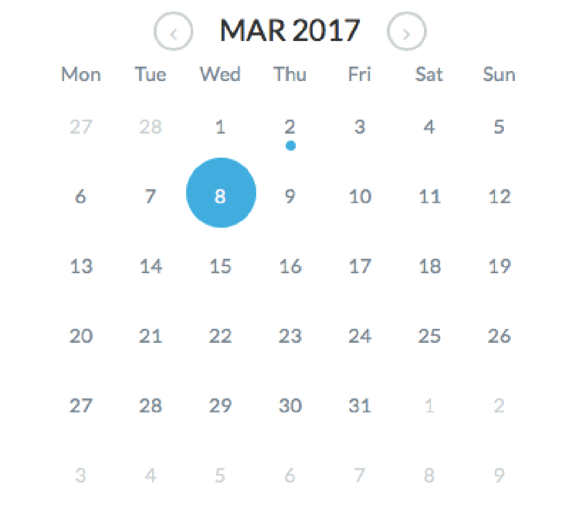

Fig. 2. The calendar

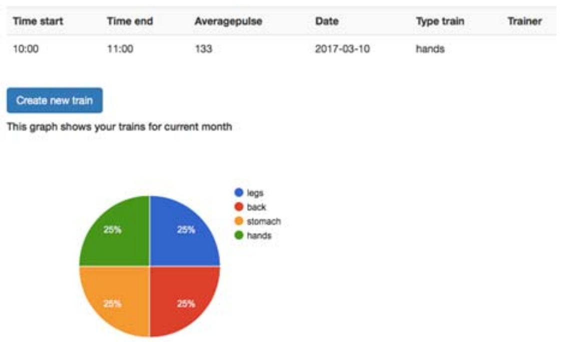

Fig. 3. The day menu

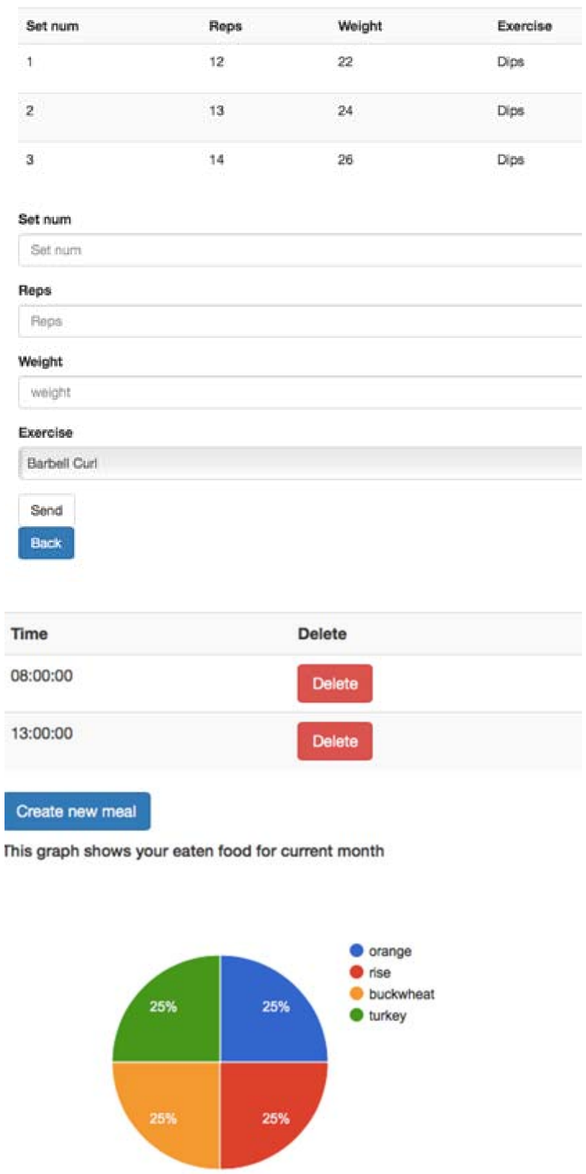

Fig. 4. The exercise menu

Consuming vitamins – is very important for people's health [1]. The "Live Helper" has a function which counts consumed vitamins a day. When the person add eaten food, my system analyses the food and count consumed vitamins. If the count of vitamins lower than normal consumption a day, the system gives a notification of this problem.

Name vitamin	Consumed vitamin
A	0
B	450
C	0
D	0
E	0

Fig. 6. The vitamin menu

The system can give recommendations for training. For example, a person wants to get the recommendation for his training, to get this recommendation, he must type required information about his weight, height, age, lifestyle and so on. When the system gets this data, it gives specific recommendations for trains.

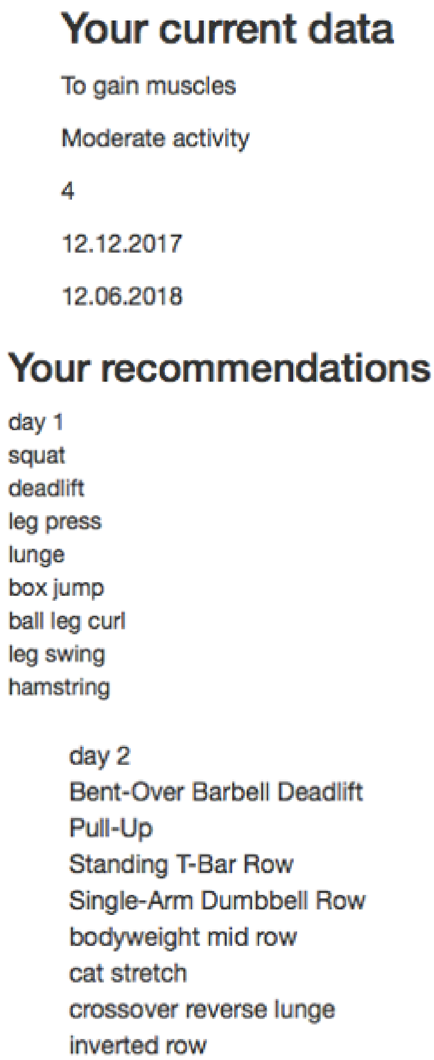

Fig. 7. Recommendations

A person can track his weight. For example, he has a goal to get 5 kilos in a month. He is working out and type his weight into the system every day. The graph helps him see the progress of his work.

Fig. 8. The weight menu

Sleeping is important for a person too [2]. The system has a function which shows to a person how many hours he slept. If the count of sleep hours isn't normal the system gives a notification to a person that he needs some sleep.

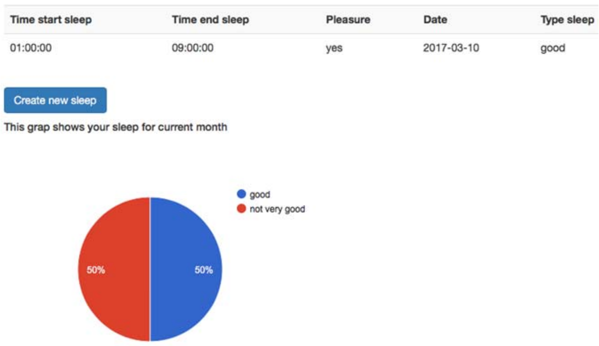

Fig. 9. The sleep menu

A person can add his analyses. He can check the progress every time he adds information into the system.

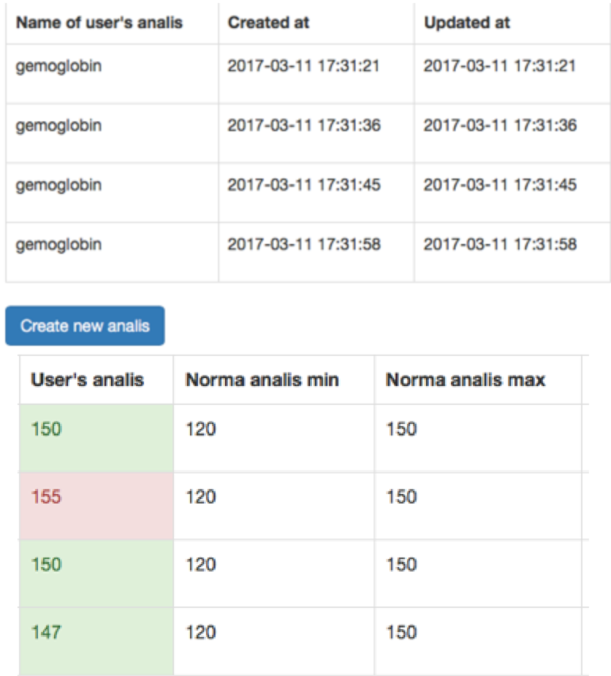

Fig. 10. The analyses menu

WHO IS THIS SYSTEM FOR

This system has created for the people who wants to track their life activity. For individuals who care about their health, people who can add data very carefully. For people, who interested in longevity and health body.

Regular people and trainers can use this system. There are a few functions for coaches, which help them to care of their wards. Coaches can add trains for clients, edit and delete them. Built trains carefully, analysing clients sleep, eaten food, consumed vitamins, analyses and so on. Regular people can do it by themselves.

WHAT METHODS I USED

To create this system the developer used in PHP. The system based on client-server architecture and uses Laravel Framework on the server side and JS on the client side. Ajax - for quick update the page. Web server Apache, the workbench application as a data base.

CONCLUSION

To create this system the developer used in PHP [3]. The system based on client-server architecture and uses Laravel Framework [4] on the server side and JS on the client side. Ajax - for quick update the page. Web server Apache, the workbench application as a data base.

This system had been tested for 2 months by regular people and trainers before I received a feedback. They found that the “LiveHelper” woks stability, does its job and helps people track their life activity.

I think that healthy life is important. I want to improve this system by adding a function which will able to analyse mental activity of the person, function which will able to count optimal amount of calories to lose weight.

REFERENCES

[1]HealthyEating
http://healthyeating.sfgate.com/importance-vitamins-body-5846.html

[2] Natioal Institute of Health
https://www.nhlbi.nih.gov/health/health-topics/topics/sdd/why

[3]PHP.net
https://secure.php.net/manual/ru/

[4] Laravel
https://laravel.com/docs/5.4/installation

A SIMULATED SCENARIO OF A SMART KITCHEN

Rizzo Salvatore, Esposito Giuseppe

Computer Engineering and Networks Laboratory – Kore University of Enna - Italy

Email: {salvatore.rizzo;giuseppe.esposito20}@unikorestudent.it

Abstract

Considering the development of the “Smart Home” (SH) technological concept, new technologies are born every day, making life experience smarter and depriving man duties that can result boring or in certain cases difficult or not immediate. In this paper, we propose a new approach for SH management, with particular attention to the “Smart Kitchen” world and its home appliance behaviors that compose it, using a collection of samples provided by a sensors network which picks data like temperature, humidity or CO level. The results, obtained from a daily life simulation, will be analyzed according to the variation of sensors samples.

INTRODUCTION

The continuous man’s evolution has allowed, during last years, to make its life and surrounding environment “smarter”. Thanks to the latest scientific discoveries, we’re entering a new era, where everything is controlled intelligently by electronic devices or, generally, by intelligent machines, which replace the man in simple things, such as light management, temperature etc. The technological development is focusing on the Home Automation [1], according to with the rising of Internet of Things (IoT), in which everything acquires intelligence thanks to the possibility to communicate data and use information from other devices [2].

In these home automation scenarios of IoT, we propose a new model of Smart Kitchen [3], in which the main home appliances, like fridge, air conditioner, light, anti-fire, and anti-thief are fully automated and independent. The home appliances are managed by a Central Controller, that receives data/samples from a sensors’ network [4], implemented on the IEEE 802.15.4/ZigBee protocol. These data/samples are transmitted through a Wi-Fi network to the smart home appliances, which process them and produce a specific output depending on the device that received the data.

The working function of the Central Controller will be described in the next paragraphs, as well as the function of the home appliances and sensors. Matlab/Simulink has been chosen as simulation environment, with the use of the TrueTime tool in order to simulate the scheduling algorithms and the network protocols.

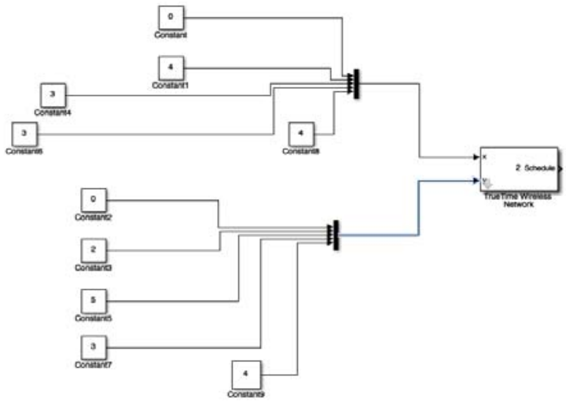

Figure 1: blocks scheme for Wi-Fi Network

THE PROPOSED APPROACH

For the model implementation, a center star network topology has been chosen, in which the center is the Central Controller. The two networks, Wi-Fi and ZigBee, have been implemented by two TrueTime Wireless Network blocs, as shown in Figures 1 and 2.

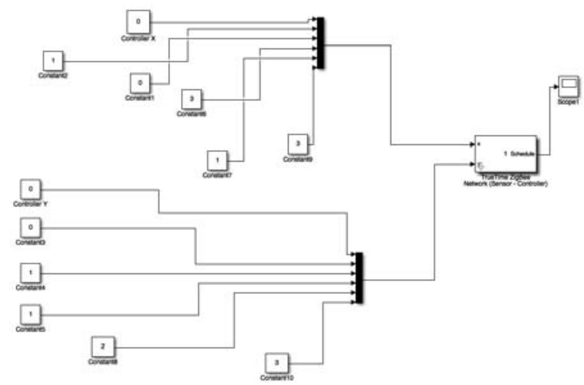

Figure 2: blocks scheme for ZigBee Network

Regarding ZigBee Network, the nodes are:

- Central Controller;
- Internal Temperature Sensor;
- External Temperature Sensor;
- Carbon Monoxide Sensor;
- Humidity Sensor;
- Anti-thief Sensor.

For Wi-Fi Network, the nodes are:
- Central Controller;
- Wi-Fi Light;
- Wi-Fi Fridge;
- Wi-Fi Dehumidifier;
- Anti-fire System.

CENTRAL CONTROLLER: it is the most important network's node. It receives the samples collected by the sensors and represents the start point of the data towards the Smart Kitchen domestic appliances. Furthermore, it's the first node of both the ZigBee network and the Wi-Fi one. The Central Controller is implemented in Simulink by a TrueTime Kernel, as shown in Figure 3:

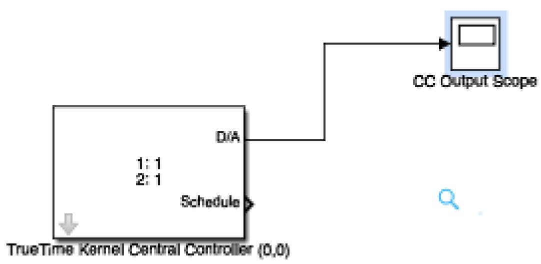

Figure 3: Central Controller

Our Central Controller is composed of several tasks: 'Ping Request Task' performs a ping to network devices of the two networks; 'Alarm from Anti-thief' is a high priority task that is activated only when movement is detected (only if the anti-thief system is active); 'Controller Date Sender Task' is a sporadic task used for sending time and season to the Wi-Fi Light; 'Power Control Controller Task' is a task used in setup phase to calibrate the transmission power depending on the distance between Central Controller and the other nodes of the networks (with this task the right transmission power to every device is ensured).

The most important task is 'Sensor Sample Task': this task is activated each time a sample is received by the Central Controller from the ZigBee network; this sample, when received, is stored on Central Controller memory, precisely in a "samples vector" of length equal to sensors' number plus one (the first position is reserved to CC); every sample that arrives from sensor number i is stored in the $i+1$ position of the samples vector; when the CC receives a sample from every sensor of the ZigBee Network, these samples are disposed to the appropriate device (for instance, humidity level and internal temperature are sent to Smart Dehumidifier); thanks to this, Smart Kitchen domestic appliances can work properly to vary from the situation.

SENSORS: each sensor communicates with the CC through the ZigBee network. There are two types of sensors: sampling sensors (such as internal and external temperature, humidity, CO level and movement based ones (anti-thief system). Regarding the first sensors typology, each time a value is sampled, this is sent to the Central Controller that stores it in the samples vector for future processing. All these devices have similar functions: they provide the presence of a sampling task, a power control task and a network handler for the reception of messages from the ZigBee Network. For the second sensors typology, the functioning provides an activation first: for instance, if the anti-thief system is activated, a voltage drop is simulated on the anti-thief sensor when people/things passed nearby it, activating the alarm. Naturally, these sensors have the task for ping request, for power control and a network handler.

Generally, sensors are placed in kitchen's corners, except for the CO sensor, placed in the center of the roof, and for the external temperature sensor, placed in the garden (for instance). As mentioned previously, each sensor has a network handler, that is a network listener: it saves messages received from the CC, analyzes the message type ("ping_request" type for ping request, "power_control" type for power setting, etc.) and starts the appropriate task.

WI-FI DEVICES: they are linked devices like Wi-Fi Light, Dehumidifier, Wi-Fi Fridge and Anti-Fire System.

1) Wi-Fi Light receives current simulation time and actual season from the Central Controller. Light Logical management is delegated to a Simulink Chart, according to MBSD logic, with current simulation time and season input. This Chart carries out checks on the light intensity from 00:00 to 23:59. For a better computing accuracy, the current time value is converted in seconds: the new time range is 0-86340 seconds. The proper functioning of the Wi-Fi Light provides the internal setting of the sunrise time and sunset time, that change in function of the current season. In Table 1, these values have been identified.

Table 2

Wi-Fi Light internal settings

SEASON	SUNRISE	SUNSET
Spring	24600 s	71100 s
Summer	21600 s	73800 s
Autumn	27000 s	66600 s
Winter	28800 s	60600 s

According to the Chart logic, the light intensity is 100% up to 40 minutes before sunrise: in this 40 minutes, light intensity decreases linearly up to sunrise time, according to the following equation (2400 s = 40 min):

$$intensity = 10 * \frac{sunriseTime\text{-}currentTime}{2400}$$

Light intensity will rise to 100% 20 minutes before sunset, according to the following equation (1200 s = 20 min):

$$intensity = \frac{10 * (currentTime\text{-}(sunsetTime - 1200))}{1200}$$

Value calculated for intensity must be multiplied by 10 for a percentage variation of intensity.

2) Wi-Fi Fridge needs internal and external temperature values for the right functioning (sent by the CC). These values are transmitted to a particular subsystem, called 'Fridge Power Controller', that takes internal and external temperature and passes them to a Fuzzy Controller, that returns, as output, the fridge power percentage value. The fuzzy output is filed by the Fridge intelligence for a better accuracy of the result.

3) Wi-Fi Dehumidifier needs internal temperature and humidity level (calculated in percentage) for its functioning. These values are transmitted to a particular subsystem, called 'Dehumidifier Regulator': in this subsystem, there is a Fuzzy controller that, taken as input internal temperature and humidity, computes the right power value for the dehumidifier and puts it on the output. The output of the Fuzzy Controller, as the same case of Wi-Fi Fridge, is filed by internal dehumidifier intelligence for a better resulting power.

4) Anti-Fire System is the last Wi-Fi device to analyze. It receives CO level from the CC: this value is 0 if CO level is less than 60%, otherwise, the value is the level of CO. Zero value is necessary because if the level of CO is <= 60%, then the Anti-Fire System must be turned OFF. CO level is passed to a Matlab Function block, that simulates dispensing of water to extinguish the fire. Greater is the CO level, greater will be the water delivery.

SCENARIO

The scenario that we want to simulate is the behavior of our Smart Kitchen during a day. For a better graphics visualization, the simulation has been limited to 200 seconds. The 4 Zigbee sensors, that sample the system intensive variable, send the samples directly to the Central Controller. An example of the sampling is showed in Figure 4.

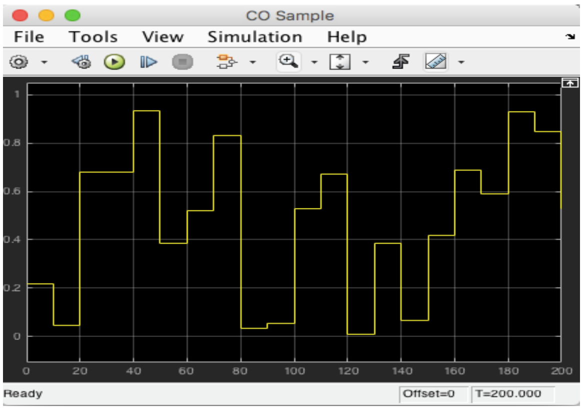

Figure 4: sampling of the CO level

The oscillations in the graphic represent the CO level variations. Same samples are produced by other sensors. When the samples are received by the Central Controller, these are transmitted to the appropriated device on the Wi-Fi Network. In Figure 5, the samples received by the CC are depicted.

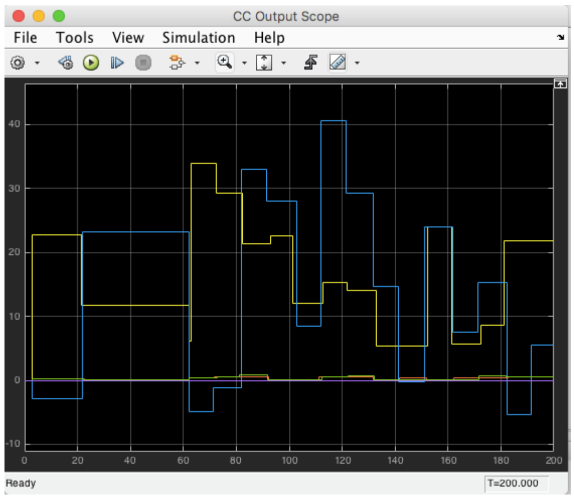

Figure 5: samples received by the CC

Different colors of graphics represent the different ZigBee sensors. Each sample has one color: for instance, internal temperature sample is yellow. Furthermore, Central Controller sends current simulation time and actual season to the Wi-Fi Light, using the Wi-Fi network: when these values arrive to the Wi-Fi light, it decides light intensity thanks to its algorithm aforementioned (Figure 6).

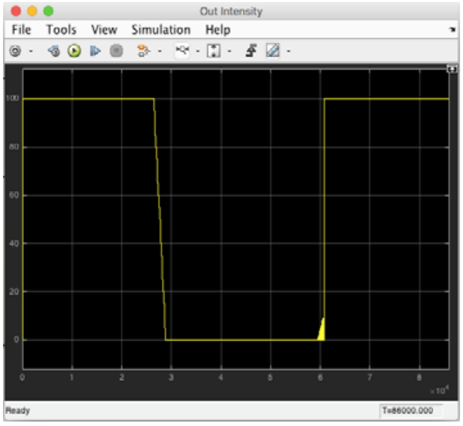

Figure 6: light intensity

As it is possible to note in Figure 6, during the night, the light intensity is 100%. Variations of the light intensity are registered 40 minutes before sunrise and 20 minutes before the sunset. Wi-Fi Dehumidifier, after receiving internal temperature and humidity samples, responds varying its power and adjusting temperature and humidity too, as it is possible to note in subfigures in Figure 7.

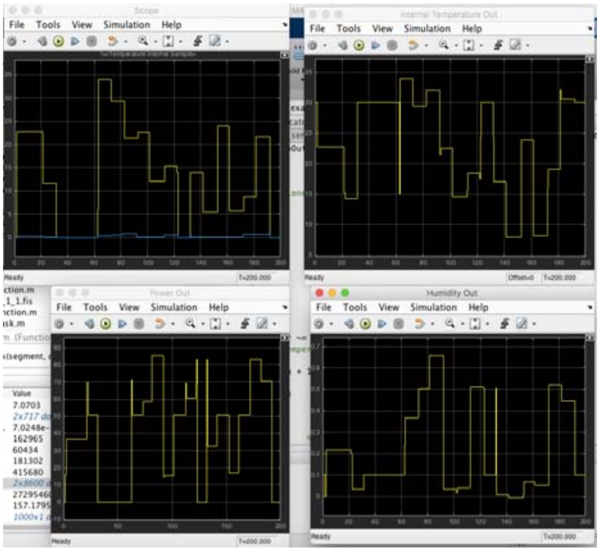

Figure 7: operation of the Wi-Fi Dehumidifier

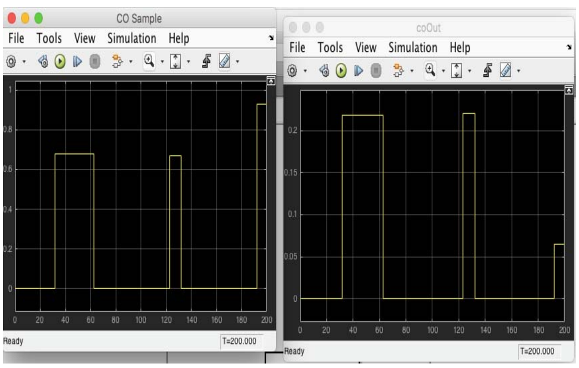

Figure 8: operation of the Anti-Fire System

In Figure 8, the operation of the Anti-Fire System is shown. The system receives zero from Wi-Fi Network until CO level is less to 60%. CO level is drastically reduced when Anti-Fire system is activated.

PERFORMANCE EVALUATION

The first performance to evaluate is the receiving time of a sensors' sample by the Central Controller. The internal temperature sensor has been chosen for this measurement. In Figure 9, the output obtained during a simulation of 50 seconds is shown.

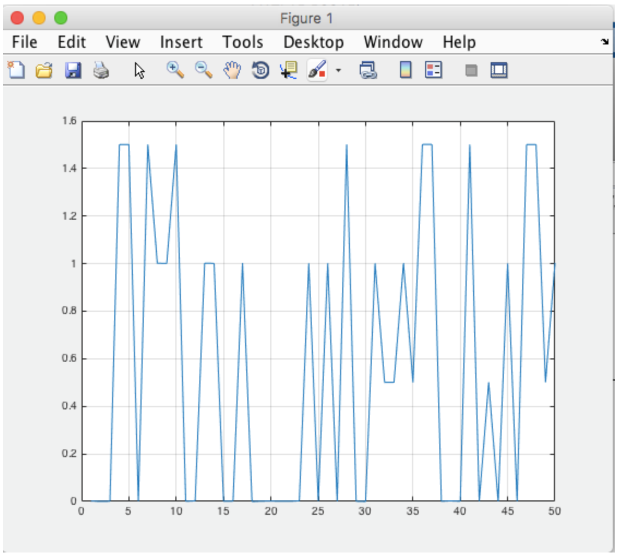

Figure 9: output of internal temperature sensor

The minimum receiving time is approximately of 0.5 seconds against the maximum receiving time of 1.5 seconds. Since the sample is produced every 10 seconds, receiving time is acceptable.

Table 3

Networks performance

Network Type	Sent packet	Received packet	Lost packet
WiFi	89958	80757	9201
ZigBee	206400	29986	176414

The packets loss during the simulation has been evaluated and the obtained results are shown in Table 2. During a day, several packets are transmitted in the two networks. Definitely, there 11% of packets are lost on Wi-Fi network and 85% on ZigBee network. Moreover, the throughput has been measured. During an all-day simulation, thus in 86000 seconds, 13517440 bytes are placed in the network, with an average throughput of 158 bytes/s.

CONCLUSIONS

From a general point of view, the proposed solution could be considered acceptable in some parts, such as in sample generation, communication to the Central Controller, illumination system, and anti-fire reliability. The model results less efficient in the anti-thief system and in the ZigBee packet loss. A future reimplementation could focus on the implementation of new domestic appliances in order to increase the automation of the kitchen, keeping unchanged part model's systems, like home appliances power control or illumination systems.

REFERENCES

[12] Guilherme Mussi Toschi, Leonardo Barreto Campos, Carlos Eduardo Cugnasca, Home automation networks: A survey, Computer Standards & Interfaces, Volume 50, February 2017, Pages 42-54.

[13] Terence K.L. Hui, R. Simon Sherratt, Daniel Díaz Sánchez, Major requirements for building Smart Homes in Smart Cities based on Internet of Things technologies, Future Generation Computer Systems, Available online 1 November 2016.

[14] Jacob Aron, Smart kitchens keep novice chefs on track, New Scientist, Volume 215, Issue 2877, 11 August 2012, Page 17.

[15] A. Mahmood, I. Khan, S. Razzaq, Z. Najam, N.A. Khan, M.A. Rehman, N. Javaid, Home Appliances Coordination Scheme for Energy Management (HACS4EM) Using Wireless Sensor Networks in Smart Grids, Procedia Computer Science, Volume 32, 2014, Pages 469-476.

IOT FOR FARMING: A SMART SOLUTION PROPOSAL

Savatteri Giuseppe

Computer Engineering and Networks Laboratory – Kore University of Enna - Italy

Email: giuseppe.savatteri@unikorestudent.it

Abstract

This paper shows a proposal for a scalable, simpler and smarter crop management to enable a company, independently of its size, to face new industry challenges. The introduction of Internet of Things (IoT) solutions could actually lead to an improvement of the quality, quantity, sustainability and cost effectiveness of agricultural production. The chosen scenario is a small company that produces legumes, asking for an automatic irrigation system, crop monitoring through a Wireless Sensor Network (WSN) and other smart features to simplify the routine operations.

INTRODUCTION

The rising phenomenon of the IoT is transforming the agriculture, allowing farmers to deal with the new requests from the industry. Since the consumption needs of the global population are increasing, a lot of companies are trying to find new solutions to face critical issues such as water shortages, limited availability of lands and the difficulty to manage crops during the entire process of production. Several case studies propose the introduction of WSNs to collect data and analyze critical parameters. This first approach is necessary but no more sufficient as the demand for smart irrigation systems and automated decision support has increased.

A WSN is a wireless network composed of distributed autonomous devices using sensors to monitor environmental conditions. It has been shown as a WSN could be a good starting point for a lot of IoT applications and this is especially true for the scenario addressed in this paper. Furthermore, the possibility to provide connectivity to the Internet through a gateway is even more convenient to enable remote management of the smart devices and remote analysis of the environment. The wireless protocols involved in a WSN may vary and strongly depend on the application requirements. In the scenario described in this paper, the IEEE 802.15.4 (ZigBee) and the IEEE 802.11b (Wi-Fi) standards are used, the first one to send data among the nodes of the network and the second one to establish a communication between a gateway of the WSN and an administration device.

ZigBee is a wireless networking standard that aims at remote control and sensor applications. It is suitable also for operation in harsh radio environments and in isolated locations. As mentioned before, ZigBee technology builds on IEEE standard 802.15.4 which defines the physical and MAC layers. Above this, ZigBee defines the application and security layer specifications enabling interoperability among products from different manufacturers. The distances that can be reached transmitting from one station to the next extend up to about 70 meters, although very much greater distances may be reached by sending data from one node to the next in a network. The main uses for IEEE 802.15.4 standard are aimed at control and monitoring applications where low levels of data throughput are needed. Furthermore, a low power consumption profile can be maintained, for battery powered devices such as sensors, setting a low data rate. ZigBee operates in unlicensed radio frequency bands, including 2.4 GHz, 900 MHz, and 868 MHz. For this reason, some interferences with Wi-Fi may generally occur but in this specific scenario, due to the long distances between the devices, this is not an issue.

The IEEE 802.11b is a Wi-Fi standard developed by the IEEE for transmitting data over a wireless network. It operates on a 2.4 GHz band and allows for wireless data transfers up to 11 Mbps. This version of the 802.11 standard has been chosen for simulation purposes but another version, such as 802.11g, could be used as well.

In the following sections, some related works will be described, showing the most interesting solutions they propose. Subsequently, a new approach, to comply with the requests of the company for this application scenario, will be presented. Subsequently, a performances evaluation of the system will be shown.

RELATED WORKS

Several years have passed since the automation in the agricultural industry has become necessary, but in these last ten years, new proposals and new approaches, following the evolution of mobile and embedded devices, have been presented. As described in [1], the introduction of a WSN, in scenarios where nodes are battery powered devices and where power consumption is a key element, has made necessary the development of optimized routing algorithms. Taking an energy efficient WSN as a base, several papers about different applications for smart agriculture, described how to improve and optimize single aspects involved in the production processes. The authors of [2] introduce a water management system to save water and maximize productivity. A very interesting detail of their implementation is the possibility to irrigate at a variable rate depending on a distributed in-field sensor network.

A more convenient option could be to activate electromechanical systems using sensors as triggers as simulated in [3]. The authors present preliminary ideas and the results obtained from the simulations of a WSN with event-based control applied to a greenhouse temperature control system are described. Even in an industrial farm scenario, similar methods are necessary to prevent some issues that a too high inner temperature of the fields can cause.

All these studies agree with the introduction of a WSN in this kind of applications and highlight the advantages that such a network could actually bring. What still seems to lack though is a decision support system to fully automate routine operations. Provide this kind of system in scenarios where the manual control is still present, become even more difficult because manual control is based on the operator's opinion and often have no quantitative basis, as described in [4]. The authors try to solve this problem collecting and organizing data from sensors distributed in the area of interest, to quantify the critical parameters and provide real-time decisions.

What described in the previous paragraphs can be achieved with the IoT by giving to distributed smart objects, all connected to each other, the capability to collect data, analyze it and choose what's the best practice to adopt in a precise state of the entire system. Since the IoT market is expected to grow quickly in the next years, solutions, such as those analyzed in [5], will be more frequently adopted to remotely monitor crops with the aid of an information management system.

THE PROPOSED APPROACH

The company involved in this case study owns 5 hectares of land where grows four types of legumes including 1 hectare used for beans, 1 for the green beans and peas, and other 2 hectares for asparagus. It's necessary to pay particular attention to the latter since their growth is influenced by two critical factors: the amount of nitrogen contained within the soil and the soil internal temperature.

The company, in order to obtain an adequate soil temperature for the growth of the asparagus, uses some thin metal foils that are double-sided: white and black. The first one is useful to reflect sunlight to decrease the inner temperature of the ground, the second one is used to absorb sunlight and heat the ground. One of the requests made by the company is to provide an automatic system able to detect the soil temperature, thus avoiding an operator to carry out the measurement several times a day, also capable to automatically decide which side of the metal foil is more appropriate to use. The system proposed in this paper, shown in Figure 1, is organized as follows:

- 10 automatic irrigation pumps, calibrated according to the type of legume, using algorithms that take into account the water needs of each crop. All the pumps are equipped with a controller that receives data from the temperature and soil moisture sensors, submit them to a fuzzy logic controller and thereafter sends them to a power controller which, by means of a specific algorithm for each individual crop, calculates how many cubic meters of water should be delivered and for how long, depending on the temperature and humidity of the soil;
- 10 temperature sensors, powered by a non-rechargeable 2000 mAh battery. Due to the low power consumption of this sensors, the batteries are replaced every two or three years;
- 10 soil moisture sensors, equipped with the same battery. They have a structure similar to the temperature sensors;
- 15 soil nitrogen sensors, powered by the same battery used in the other sensors. Inside of them there's a logic system which periodically gathers, 10g at a time, soil samples up to reach a total amount of 100g. These soil samples are then analyzed from the sensor;
- 1 switcher, constituted by a controller and a mechanical device. The controller receives the data from the temperature sensors and submits them to a fuzzy logic controller which determines whether to use the white or black face of the metal foil. According to the value returned from the controller, the foil is then switched to the desired side by the mechanical device;

- 1 gateway that allows to forward the messages exchanged between the nodes of the WSN and an administration client;
- 1 administration client, useful to show the collected data and the general status of the system to the operators and farmers.

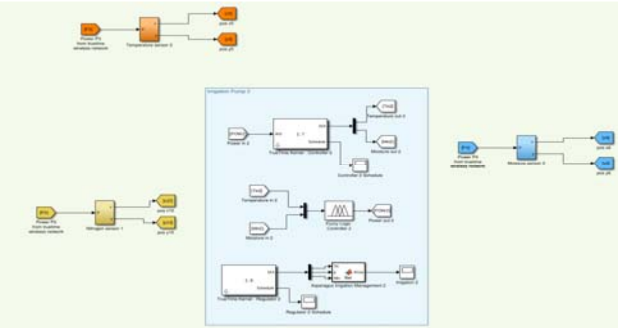

Figure 3: From left to right: a soil nitrogen sensor, a temperature sensor, an irrigation pump and a soil moisture sensor.
The pump receives data from the sensors and delivers the optimal amount of water.

The network has a mesh topology, useful to ensure proper communication and the reliability of transmission between nodes. Thus, if some messages are lost or it is impossible to deliver a given message, the system is able to work properly receiving the messages from another network node. For all the sensors and the irrigation pumps, the 802.15.4 ZigBee protocol is used and it is also useful to preserve the battery life of all devices. The transmission power is set to 6 dBm to reach as many nodes as possible by limiting energy consumption. The data rate was set to 30 kbits/s, sufficient to quickly transmit the packets. To allow the communication between the gateway and the administration client, a WLAN was implemented using the 802.11b protocol.

SCENARIO

This scenario has been simulated with Matlab / Simulink using TrueTime [6]. The simulation has been carried out immediately after the sowing period, in the spring, with a temperature that varies between 15 and 28 degrees centigrade and a soil moisture percentage between 50% and 90%. To effectively test if the projected system could assure reliable results during a long period, even a simulation of two years and a half has been executed.

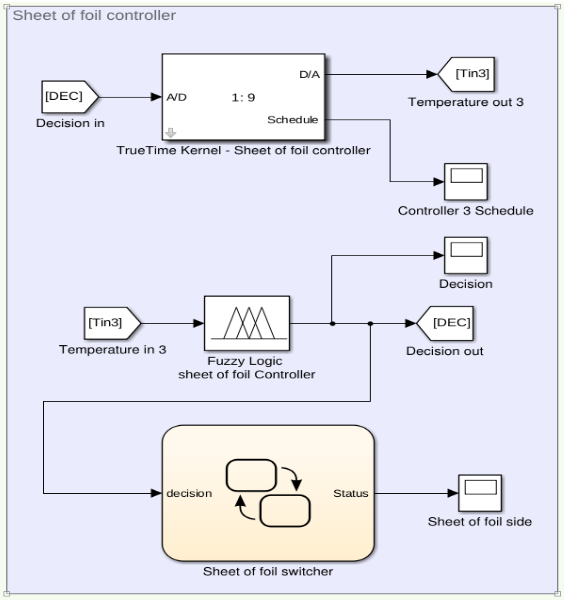

Figure 4: Internal components of a metal foils switcher. From up to bottom: the controller receives the data from the sensors and submit them to a fuzzy logic controller. Accordingly to the value returned by the fuzzy logic controller, a side of the metal foil is chosen.

As described in the previous section, the company owns 5 hectares of land and to provide the right amount of water accordingly to the needs, 2 irrigation pumps per hectare have been installed. The irrigation pumps are equipped with a controller to receive and analyze the data sent by the sensors and if a battery-powered sensor doesn't work anymore, the irrigation pump controller tries to fetch messages from other near sensors. Thanks to the mesh network topology this process can assure always new and reliable data to be processed by the devices that need them.

Another device required by the company is the metal foils (Figure 2) switcher for the cultivation of the asparagus. To simulate this device a flow chart controller has been used, in this way the side of the foils can be switched according to the value returned by a fuzzy logic controller.

Taking advantage of a mesh topology built upon a WSN, no pre-existing infrastructure is required to create a network in remote areas. In the system proposed, the nodes of the network can forward messages to other near nodes allowing an efficient routing even if the network changes or a node stops working. A gateway is then used to connect the mesh cloud to a WLAN containing the administration device which provides the data collected to the operators.

PERFORMANCE EVALUATION

For the presented scenario two main issues could be critical, the collapse of the mesh cloud due to an overload condition or to a change of the network morphology. To test the first potential issue a simulation of one hour has been carried out: to test the network at full load the simultaneous send of the packets to all the reachable network nodes has been set. Thanks to the mesh topology of the network and the implemented algorithms, the irrigation pumps and the switcher have successfully ignored the unnecessary data packets.

The second issue mentioned above is typically caused by battery-powered nodes, indeed when a battery runs out the node can't transmit its data neither forward the messages sent by other nodes of the network.

To test this issue and to provide a more realistic view of the entire working system, the duration of the simulation has been set to 788400000 seconds which are about two and a half years. With a data rate of 30 kbit/s, a transmission power set to 6 dBm, transmitting one message per minute the batteries run out after 2 years.

Another important parameter that has been tested in this simulation is the throughput. In the simulation period of 788400000 seconds 643860000 packet has been sent between the nodes of the network, multiplying this value by the minimum frame size, which is 272 bits related to the network, and dividing by the duration of the simulation it is obtained the value of 222.13 bit/s.

CONCLUSIONS

The intent of this paper is to illustrate one of the possible implementations of the "smart objects" concept, useful to support the agricultural labor management.

Future developments in this field of interest could be the introduction of advanced algorithms for the diagnosis of diseases affecting the crops and new machine learning techniques to bring the agricultural industry to a new level of automation.

REFERENCES

[16] K. Sohrabi, J. Gao, V. Ailawadhi, G.J. Pottie. “Protocols for self-organization of a wireless sensor network”, Year: 2002, IEEE Personal Communications.

[17] Yunseop Kim, Robert G. Evans, William M. Iversen. “Remote Sensing and Control of an Irrigation System Using a Distributed Wireless Sensor Network”, Year: 2008, IEEE Transactions on Instrumentation and Measurement.

[18] A. Pawlowski, J.L. Guzman, F. Rodriguez, M. Berenguel, J. Sanchez, S. Dormido. “Event-based control and wireless sensor network for greenhouse diurnal temperature control: A simulated case study”, Year: 2008, IEEE International Conference on Emerging Technologies and Factory Automation, 2008. ETFA 2008.

[19] Mauro Martinelli, Luca Ioriatti, Federico Viani, Manuel Benedetti, Andrea Massa. “A WSN-based solution for precision farm purposes”, Year: 2009, IEEE International Geoscience and Remote Sensing Symposium, 2009.

[20] Ji-chun Zhao, Jun-feng Zhang, Yu Feng, Jian-xin Guo. “The study and application of the IOT technology in agriculture”, Year: 2010, 3rd IEEE International Conference on Computer Science and Information Technology.

[21] Dan Henriksson, Anton Cervin, Karl-Erik Årzén. “TrueTime: Real-time Control System Simulation with MATLAB/Simulink”, Year: 2003 - http://www.lunduniversity.lu.se/lup/publication/17e2d2a4-09a9-4718-92c6-6a9780e20c08 - (accessed 03/17/2017)

ACCURACY IMPROVEMENT FOR AVERAGE DELAY ESTIMATON IN QUEUEING NETWORKS WITH RESOURCES RESERVATION

Shelest Maria

Saint-Peterburg State University of Aerospase Instrumentations,
Saint-Peterburg, Russia

mshshelest@mail.ru

Abstracts

In this work we describe the method of accuracy increasing for estimation of an average delay in queueing networks with resources reservation. The proposed method is based on parameters optimization of the lower bound earlie introdused in [1]. Also in this paper an accuracy of this bound is investigated using simulations.

INTRODUCTION

Nowadays it is almost impossible to imagine the modern society without using information systems (IS) in all spheres of life. It is important to provide a stable work for information system. Thus, it is necesary to determine parameters and characteristics of IS before it starts working [2]. As a rule, queueing networks (QN) are used as information system model for estimation its characteristics [3]. Also QN can be used when making business decisions about the resources needed to provide services. The main characteristic of information system is an average response time, which in queuing theory is equivalent to average delay in QN. It is not always possible to analytically calculate to average delay in most complex queueing networks. In such cases boundary value for estimating of average delay in QN are usually used.

In the next sections we give the algorithm for finding lower bound of average delay in QN with resources reservation. Also basic strategies for increasing an accuracy of this bound which were described in [1] are considered. Moreover the results of comparing proposed strategies are given with use of simulations.

SYSTEM MODEL

In work [1] a queueing network was considered as a model of transactions processing system. The following assumptions are used in this QN:

- It consists of a set of elementary queueing systems (EQS), each of which is a pair - a buffer and a serving device (SD).
- Service times in SDs are independent random variables.
- A job flow is Poisson.
- A set of possible routes is limited.
- Each route for each job is chosen independently with a given probability.
- Accepted for processing job blocks all the SDs on its route.

Calculation of an average transaction execution time in described system is an uncommon task. For it, as for many other non-Markovian QN, the corresponding closed-form expression is unavailable [4]. For solving this problem a procedure of average delay lower bound estimation was offered.

For finding lower bound estimation of average delay we will carry out some initial network transformations. We demonstrate these transformations using the network shown in Figure 1 as an example.

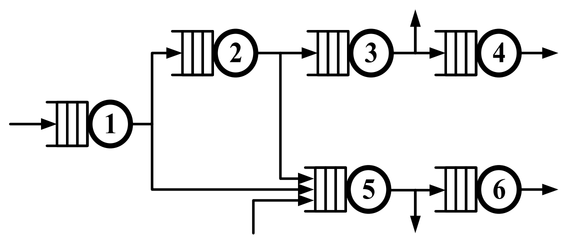

Fig. 1. An example of queueing network

The network was considered as set of 5 routes. Each of these routes can be selected with a given probability p_i, where i is the route number. The whole route can be considered as one compound EQS, because only one job can be execution on the route at a time. Thus, this network can be represented as a set of compound EQSs, not all from which can work in parallel. This set can be conveniently described as a graph of routes dependence $G(R,E)$ (see Fig.2). In this graph the i-th node (from set of R) corresponds to a i-th route, and the edge (from set of E) corresponds to a routes intersection.

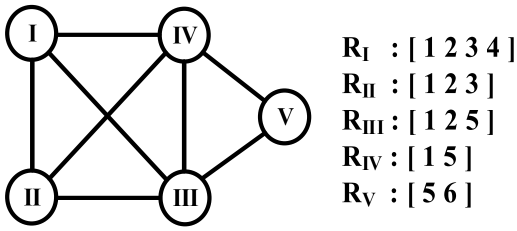

Fig. 2. The graph of routes dependence

Representation of the network in the proposed form is completely equivalent to the initial QN and allows to simplify a further analysis.

After then, the graph of routes dependence was split into detached complete subgraphs V_k ($V_k \subset G(R,E)$, k – number of subgraph), having removed some edges [5], [6] (see Fig.3).

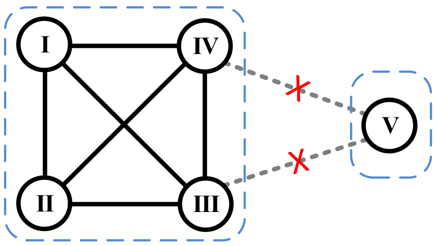

Fig. 3. An example of splitting of graph into detached complete subgraphs

Each from this complete subgraphs formed in such a way also can be considered to be compound EQS. The average delay for each such compound EQS is calculated via the following expression [1]:

$$\overline{T} = \sum_{k=1}^{K} \left[\frac{P_k L_k}{2} \int_0^{\infty} t^2 \varphi_k(t) dt \times \right.$$
$$\left. \times \int_0^{\infty} \frac{\varphi_k(t)dt}{\left(1 - L_k \int_0^t x\varphi_k(x)dx\right)^2} + \frac{P_k}{M_k} \right]$$

where P_k - probability that a job will be served in EQS which corresponds to a k-th complete subgraph; L_k - job arrival rate to a k-th subgraph; M_k - service rate in a k-th EQS; φ_k - service time PDF for a k-th EQS; K – quantity of complete subgraphs.

Splitting of a graph can be made in several ways. An accuracy of the bound can depend on how a graph of routes dependence is split into subgraphs. In the next section two basic strategies for splitting graph of routes dependence into detached complete subgraphs is given.

STRATEGIES FOR SELECTION OF COMPLETE SUBGRAPHS

In this work two of a possible strategies of splitting graph is considered. Also proposed strategies influence on an accuracy of estimating an average delay in QN is compared.

The following algorithm is used in the first and simpliest volume-based strategy (VBS) of splitting graph:

1. k = 1;
2. **while** $R \notin \varnothing$ **do:**
3. k = k + 1;
4. Find maximal subgraph V_k ;
5. $R = R \setminus V_k$;
6. **end**.

A subgraph with the maximum quantity of nodes is chosen at each iteration with VBS. This procedure will be repeated until the whole graph is not split into detached complete subgraphs.

The second strategy is load-based strategy (LBS) is a little more complicated than VBS. The algorithm for implementing this strategy is shown below:

1. k = 1;
2. **while** $R \notin \varnothing$ **do:**
3. k = k + 1;
4. Finding subgraph V_k with maximal value of network loading;
5. $R = R \setminus V_k$;
6. **end**.

In this strategy complete subgraph with a maximum average delay calculated by the Pollaczek–Khinchine formula is selected at each iteration [7].

In some cases LBS will be likely more accurately then VBS. This is due to the fact that we are trying to isolate routes with high loading from routes with low loading. In the next section the efficviency of cosidered strategies are compared.

SIMULATION RESULTS

We compare the above-considered strategies of splitting the graph of routes dependence into detached complete subgraphs for the QN, which shown in Figure 1.

Since routes selection probabilities can be influence to a split of routes dependence graph with using LBS, we maked a series of tests with just route selection probability changing. Parameters for tests are shown in Table 1.

Table 1

Parameters for tests

Test number	p_1	p_2	p_3	p_4	p_5
1	0.2	0.2	0.2	0.2	0.2
2	0.1	0.1	0.2	0.3	0.3
3	0.1	0.1	0.1	0.1	0.6

The results of splitting the routes dependence graph (see Fig.2) and results of average delay comparing for 1st test are shown in Figure 4.

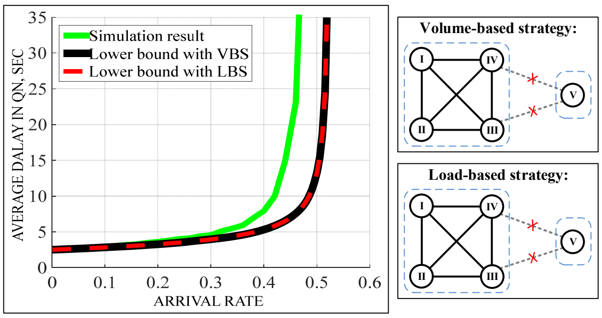

Fig. 4: Results for 1st test

The results of splitting the routes dependence graph (see Fig.2) and results of average delay comparing for 2nd test are shown in Figure 5.

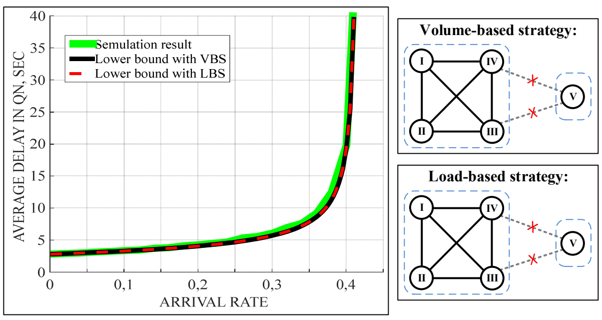

Fig. 5: Results for 2nd test

The results of splitting the routes dependence graph (see Fig.2) and results of average delay comparing for 3rd test are shown in Figure 6.

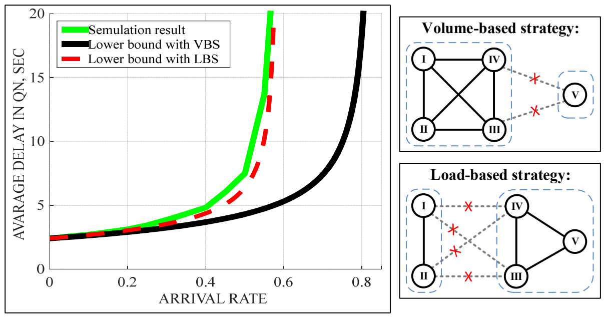

Fig. 6: Results for 3rd test

CONCLUSIONS

As a result of this reseach we can conclude that a choice of split the routes dependence graph strategy influence on the estimation of avarage delay in queueing network with resources reservation. Also test examples demonstrated that load-based strategy of split the graph of routes dependence into separate complete subgraphs is usually better than volume-based strategy. In some cases LBS provides an exact estimation for average delay in queueing network.

REFERNCES

[1]. M. Shelest "Lower Bound for Average Delay in Transactions Processing Systems", XV International Symposium Problems of Redundancy in Information and Control Systems, pp.142-145, 2016.

[2]. A. M. Langer, "Analysis and Design of Information Systems", Springer-Verlag London Limited, 2008.

[3]. R. Osman, I. Awan, M. Woodward, "Queuing networks for the performance evaluation of database Designs", UKPEW, pp. 172–183, 2008.

[4]. L. Kleinrock, "Queueing Systems: Vol. 2 – Computer Applications", New York: Wiley Interscience, 1976.

[5]. O. Ore, "Theory of Graphs", Providence, R.I.: American Mathematical Society, 1962.

[6]. Xiang-Ying Su, "An Algorithm for the Decomposition of Graphs into Cliques", Journal of Graph Theory, Vol. 20, No. 2, 1995.

[7]. L. Kleinrock, "Queueing Systems: Vol. 1 – Theory", New York: Wiley Interscience, 1975.

DEVELOPMENT AND ANALYSIS OF THE SUB-OPTIMAL ALGORITHM FOR PAIRWISE SEQUENCE ALIGNMENT

Tolubaeva Alyona

Saint-Petersburg State University of Aerospace Instrumentation,
Saint-Petersburg, Russia

E-mail: alena_tolubaeva@mail.ru

Abstract

The paper considers the heuristic algorithm for the global alignment of two nucleotide sequences with reduced complexity. We investigated an efficiency of proposed approach, comparing it with the optimal Needleman–Wunsch algorithm via simulations.

Keywords: bioinformatics, global sequence alignment, Needleman–Wunsch algorithm, dot-matrix comparison, dot plot, DNA.

INTRODUCTION

Practical significance of approximate matching and sequence comparison is based on a nature of the molecular data, namely the presence of active mutational processes in them. It is also widely used for such purposes as the search of databases containing biomolecular sequences, the tasks of making functional, structural, and evolutionary predictions on the basis of sequence alignments, as well as the problem of the presence of errors in molecular data [1]. The disadvantage of the existing classical optimal algorithms for sequence alignment is a large computational and space complexity.

The heuristic algorithm under consideration is based on the Needleman-Wunsch algorithm for global pairwise sequence alignment. Needleman-Wunsch algorithm uses an approach of dynamic programming and a scoring system including the similarity matrix and gap penalty to compare biological sequences and find the alignment. This alignment will include matched and mismatched characters and gaps in the two sequences that are positioned so that the number of matches between identical or related characters is the maximum possible.

The recurrence relation for this algorithm can be written as follows

$$F(i,j)=\max\begin{cases}F(i-1,j-1)+S(A_i,B_j),\\ F(i-1,j)+d,\\ F(i,j-1)+d.\end{cases}, \qquad (1)$$

$$i=\overline{0,n},\quad j=\overline{0,m}$$

where $F(i,j)$ – weighted edit distance, S – similarity matrix, d – gap penalty, n, m – length of the sequences A, B, A_i, B_j – current elements of the sequences A and B respectively.

This algorithm is referred to as the optimal matching algorithm and widely used when the quality of the global alignment is of the utmost importance. However, the computational and space complexity of the algorithm can be estimated as $O(nm)$ [1]. Such complexity of the algorithm often becomes critical for large n, m, which is typical for genetic data.

To solve this problem one can truncate the search area for the sequence alignment based on the statistical data and the specified parameters (size of k-words, the desired percentage of overlapping substrings within the boundaries).

THE SEARCH ALGORITHM OF THE ALIGNMENT BOUNDARY

A global alignment is more appropriately used to align sequences that are of approximately the same length and already known to be related [2]. Evaluation of the regions in which the sequences are similar before the alignment procedure begins will help to avoid unreasonable computational consumptions. To identify regions of close similarity between two biological sequences a dot matrix is constructed. Dot matrix element (i, j) has «a dot», if the word starting at position i in one sequence is identical to the word starting at position j in another sequence. To construct a dot matrix we used the Knuth–Morris–Pratt string searching algorithm (KMP) with computational complexity $O(n+m)$ [3].

The next step in solving the problem is to determine the boundaries of the alignment search area based on the obtained dot cloud.

One of the simplest approaches to determining the boundaries of the alignment search area can be the k-difference global alignment problem. It finds the best global alignment of S_1 and S_2 containing at most
k mismatches and spaces (if one exists), thus the complexity reduces from $O(nm)$ to $O(km)$. However, the approach uses symmetric intervals relative to the main diagonal, which causes an increase in the alignment search area in the case of large genome rearrangements (nonlocal inserts or deletions) in one of the sequences, or to the inability to find the optimal alignment in the specified boundaries (when $|n-m|>k$) [1].

In cases where the dot matrix is asymmetric, it is more appropriate to estimate which of the diagonals of the matrix contain the greatest number of coincidences of k-words. Finding diagonals in which the desired proportion of coincidences is achieved (algorithm parameter) allows to specify the boundaries of the alignment search area more precisely.

Let $G(h_1,h_2)$ be the alignment search area between the dot-matrix diagonals (h_1,h_2) containing greater than or equal to 0.9 proportion of the found substrings (k-words). Then the desired boundaries of the alignment search area can be written as follows

$$h_1^*,h_2^* = \\ = \arg\min_{h_1,h_2}\left\{\begin{array}{l}|h_1-h_2|: \\ \frac{1}{K}\sum I\{(i,j)\in G(h_1,h_2)\}\geq 0.9\end{array}\right\} \quad (2)$$

where (i,j) are coordinates of k-word, K – number of matches of substrings. Then the alignment search area S is defined as

$$S = G(h_1^*,h_2^*) \quad (3)$$

The search algorithm of the alignment boundary is written below:

Step 1. Splitting one of the strings into substrings of length k, k-word.

Step 2. Searching for unique k-words for an exact match in the second sequence using the KMP algorithm. Matches are marked with dots in the dot matrix. The distribution of dots in the matrix depends on the parameter k – the size of the desired substrings (algorithm parameter). If the sequences have a significant similarity, the cloud of dots is located in the vicinity of the main diagonal of the matrix, otherwise they are recognized as dissimilar.

Step 3. Splitting dot cloud along the diagonals to which they belong. Calculation the proportion of matching regions of two sequences that lie on each of the diagonals.

Step 4. Defining the boundaries of the search area alignment by finding two diagonals, the boundaries of which gets 90% (algorithm parameter) matches.

Step 5. Searching sub-optimal alignment within the diagonals using the Needleman-Wunsch algorithm.

SIMULATIONS

For the purpose of demonstrating the algorithm, a string over the alphabet {A, T, G, C} was generated. The second string was received by making mutations (insertions, deletions, replacements of segments of the original string).

Fig. 1 shows an example of a dot-matrix for strings of length 1000 for the different value of parameter k – the length of the substrings.

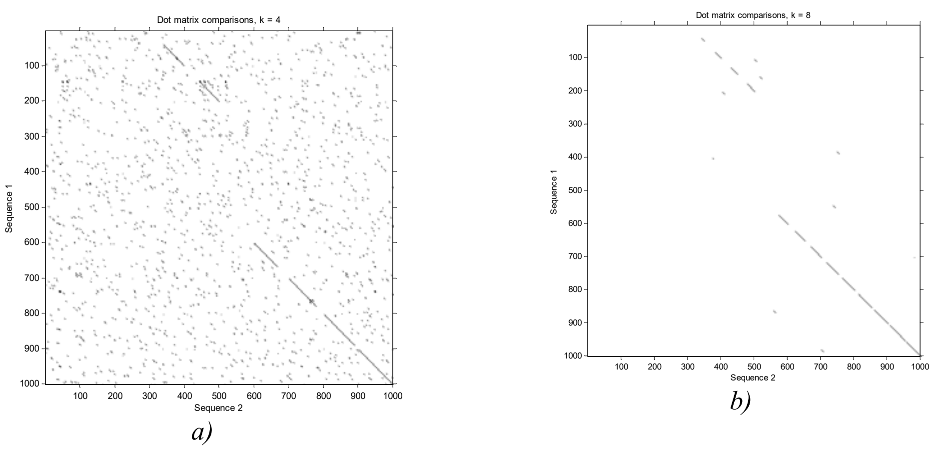

Fig. 1. The distribution of dots in the dot-matrix depends on the parameter k
a) k = 4; b) k = 8

Fig. 2 and fig. 3 reflect the result of the algorithm on strings of length 2000, k = 8, the desired proportion of string matches within the alignment search area – 90%.

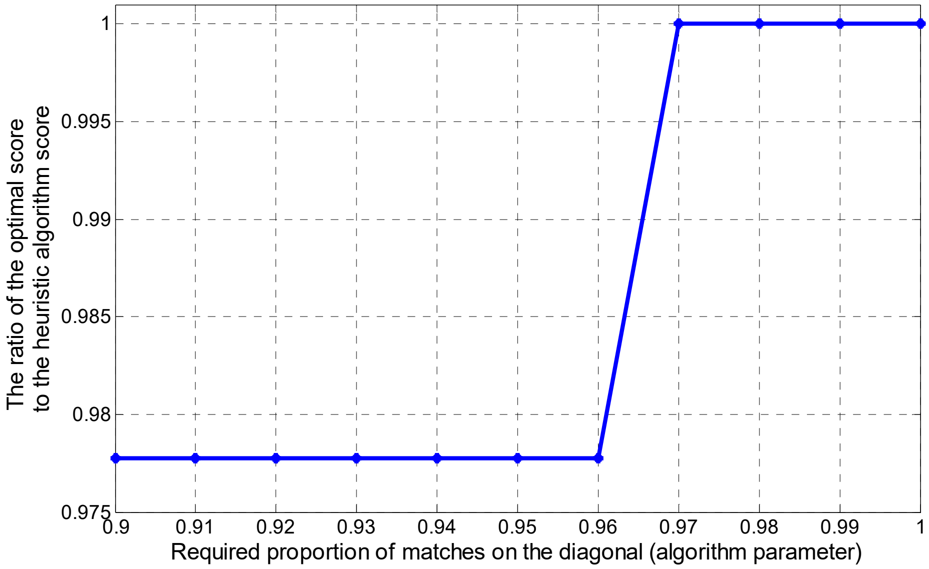

Fig. 2. The ratio of the optimal score to the heuristic algorithm score

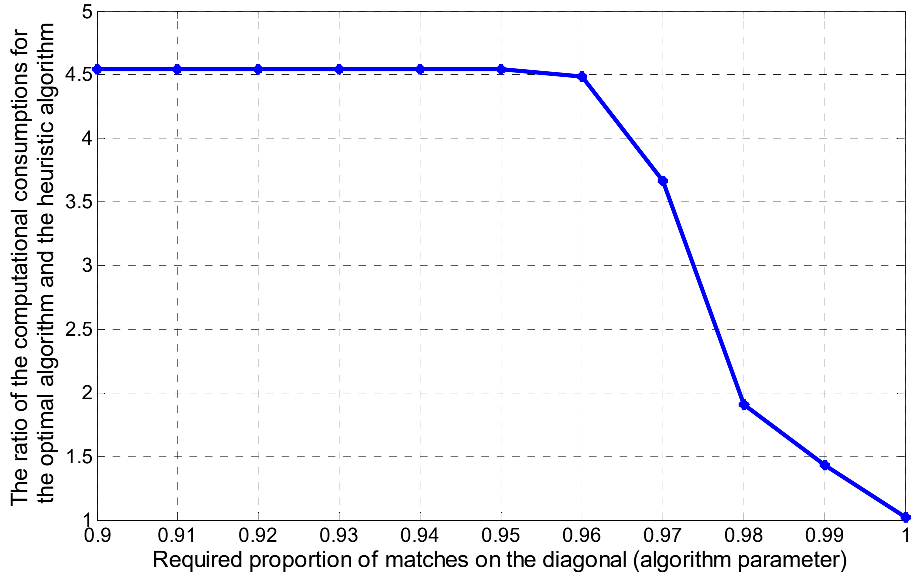

Fig. 3. The ratio of the comp. consumptions for the optimal and the heuristic algorithm

CONCLUSION

The considered heuristic algorithm allows reducing computational consumptions by defining the boundaries of the alignment search area. Prospects for further development of this approach are related to the choice of a tool that allows to specify nonlinear boundaries of the alignment search area.

REFERENCES

[1]. Gusfield D. Algorithms on Strings, Trees, and Sequences, 1 ed., University of California, Davis: Cambridge University Press, 1997, 530 p.

[2]. David W. Mount. Bioinformatics: Sequence and Genome Analysis, 2nd ed. Cold Spring Harbor, NY: Cold Spring Harbor Laboratory Press, 2004, 692 p.

[3]. Cormen, Thomas H.; Leiserson, Charles E.; Rivest, Ronald L.; Stein, Clifford. Introduction to Algorithms, 3rd. ed., MIT Press, 2009, 1312 p.

DEVELOPING UTILITY FOR SOLVING OPTIMIZATION PROBLEMS ALGEBRAIC OBJECTIVE FUNCTION

Ushakov Vitaly

Saint-Petersburg State University of Aerospace Instrumentation
Saint-Petersburg, Russia

E-mail: mr.vitaly.ushakov@yandex.ru

Abstract
This article considers the developing utility for solving the problem optimization of an algebraic objective function using the interactive Matlab/Simulink environment. The utility allows you to visualize the formation of an algebraic objective function and solve the nonlinear programming problem that arises in the synthesis nonlinear systems automatic control by the method orthogonal projections.

Keywords: Matlab, Simulink, automatic control system, nonlinear programming, extremum function, optimization, algebraic objective function, utility.

INTRODUCTION

The article shows the Matlab/Simulink for the use of an effective solution of problems of nonlinear programming with algebraic criterion function, which occurs, for example, in the synthesis nonlinear automatic control systems by the method of orthogonal projections [1, 2]. Using Matlab/Simulink allows you to avoid writing code algebraic objective function on some high-level languages, and reduces the problem to a more understandable language-block schemes. The problem of synthesizing of nonlinear automatic control system is often encountered in practice in various fields [3].

Develop a utility in Matlab/Simulink to solve the problem parametric optimization of an algebraic objective function. Simulink-scheme should contain blocks for the formation of an algebraic objective function, search for an extremum of an algebraic objective function (solution of the problem of nonlinear programming). In addition, to simplify the work with the scheme, it is planned to develop in the future Simulink-blocks for some typical nonlinear elements. This scheme allows us to see the graph of the algebraic objective function in 2D and 3D form.

ADVANTAGES MATLAB/SIMULINK

J.B. Dabney and T.L. Hartman defines the purpose of Simulink [4]: "The Simulink system can be considered as a combination methods and means automating the process developing modern control systems". In this case, we have in mind the use Simulink [5] for solving problems numerical integration all possible systems differential equations by various methods.

Simulink allows the use of pre-built block libraries for modeling different systems, and also applies a developed model-oriented approach to the development of control systems is integrated into the Matlab environment, which will allow using the built-in mathematical algorithms, powerful data processing tools and scientific graphics.

SEARCH EXTREMUM OF ALGEBRAIC OBJECTIVE FUNCTION IN SIMULINK

In the general case, the nonlinear programming problem consists in finding the extremum of the algebraic objective function for given constraints in the form of equalities and (or) inequalities.

This problem can formally be formulated in the following form: it is required, by varying the components parameter vector system $\bar{A}$, to find the extremum of the algebraic objective function J:

An example setting a algebraic objective function using the "language" of Simulink is shown below. In the case of an algebraic objective function of the form $J(\bar{A}) = k_1 * a_1^2 + k_2 * a_2^2$ its Simulink representation is shown in Figure 1, and the work with the masked function is shown in Figure 2 [6].

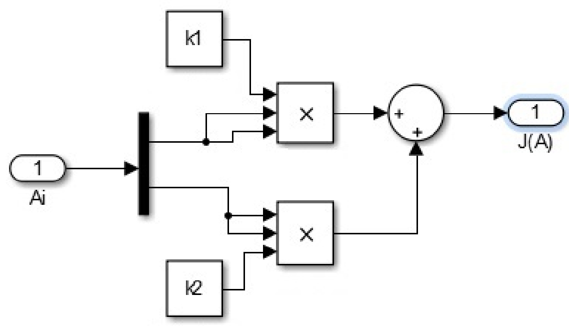

Figure 1. Structural scheme

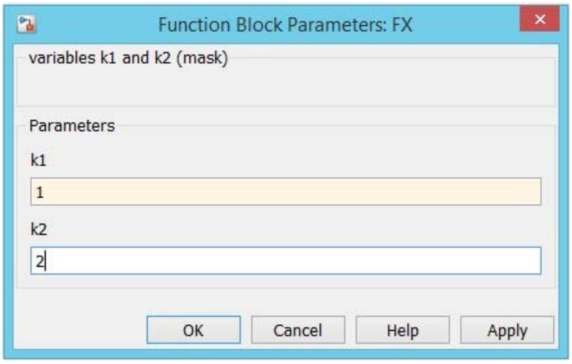

Figure 2. The window of the parameters of the structure diagram

In our case, naturally, the problem of step-by-step (random) enumeration of variable parameters is solved, and not the solution of the problem of integration over time. To implement the search, you must specify the Euler method as a method of "integration" in increments of one second, which will allow us to treat the parameter "integration time" as the number search points for the extremum of the algebraic objective function [7].

The model of the constructed system for finding the extremum of the algebraic objective function is shown in Figure 3.

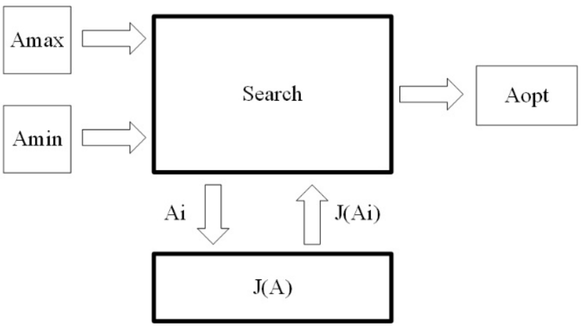

Figure 3. Model of the system for finding the extremum of the objective function

In Figure 4, the following notations are accepted: $\bar{A}$ is a vector of variable parameters and A_{max} and A_{min} are blocks for forming constraints on the vector $\bar{A}$; A_{opt} – the output of the result; The formation of the algebraic objective function is performed in the block $J(\bar{A})$ and the invariable "Search" which searches for the extremum of the objective function.

EXAMPLE

To solve this problem, let's take as an example the simple block diagram of an automatic control system consisting of a first-order aperiodic link and a nonlinear element F(x) "dead zone without saturation" type, which is in feedback. The block diagram is shown in Figure 4.

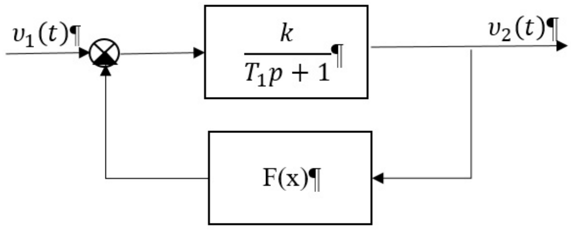

Figure 4. Structural diagram of the automatic control system

It is required to change the parameters T_1 and k to find the extremum of the algebraic objective function, where k is the gain factor, and T_1 is the time constant.

Let's make an example scheme in Matlab/Simulink, shown in Figure 5. It should be noted that with its help it is possible to solve the problem of analysis automatic control systems.

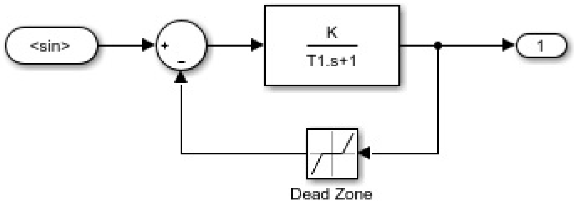

Figure 5. Structural scheme in Matlab/Simulink

First, we form a closed nonlinear system:

$$\begin{cases} v_2(t) = \dfrac{k}{T_1p+1}v(t) \\ v_3(t) = F(x) \\ v(t) = v_1(t) - v_3(t) \end{cases}$$

Then, we obtain the differential equation motion of the system with respect to the output coordinate from a closed nonlinear system [8]:

$$v_2(t) = \frac{k}{T_1p+1}v_1(t) - \frac{k}{T_1p+1}F(x)$$

After obtaining the differential equation motion of the system, the synthesis nonlinear automatic control system is performed by the method orthogonal projections.

Define the input effect as:

$v_1(t) = A_1 \sin(\omega t)$,

where A_1 is the amplitude of the sinusoidal input and ω is the frequency.

The process at the output of the system during the processing of the input sinusoidal influence is taken as:

$$v_2(t) = A_2 \sin(\omega t + \varphi_0),$$

where A_2 is the amplitude of the harmonic signal at the output of the system, φ_0 is the phase shift.

Nonlinear element F(x) of the type "dead zone without saturation":

$$F(x) = \begin{cases} ax - b, \text{при } x \geq b \\ 0, \text{при } -b < x < b \\ ax + b, \text{при } x \leq -b \end{cases}$$

We set the following values of the variables in the input and output actions: A_1=1, A_2=0.8, w=0.7, $\varphi_0 = -0.349$.

We substitute the input and output effects in the differential equation of motion the system with respect to the output coordinate, and also form a discrepancy:

$$\psi(t) = [T_1 p + 1]A_2 \sin(\omega t + \varphi_0) - kA_1 \sin(\omega t) + kF(x)$$

$$p = \frac{d}{dt},$$

where p is the differentiation operator.

As the coordinate function we have chosen $e^{-\alpha_i t}$.

We substitute 2 coordinate functions in the algebraic objective function:

$$\omega_i(t) = e^{-\alpha_i t}$$

We substitute the discrepancy and the coordinate function in the algebraic objective function:

$$J = \sum_{i=1}^{m} \left\{ \int_0^T \psi(t)\varphi_i(t)dt \right\}^2 = \sum_{i=1}^{m} J_i^2,$$

$$\text{где } J_i = \int_0^T \{(T_1 p + 1)A_2 \sin(\omega t + \varphi_0) - kA_1 \sin(\omega t) + kF(x)\} e^{-\alpha_i t} dt$$

Thus, we have obtained an expression for the algebraic objective function:

$$\begin{aligned} J_i = {} & A_2 \frac{-\alpha \sin(\omega T + \varphi_0)e^{-\alpha_i t} + (\alpha \sin\varphi_0 + \omega\cos\varphi_0) - \omega\cos(\omega T + \varphi_0)e^{-\alpha_i t}}{\alpha^2 + \omega^2} + \\ & + A_2 T_1 \times \frac{-\alpha \cos(\omega T + \varphi_0)e^{-\alpha_i t} + (\alpha\cos\varphi_0 - \omega\sin\varphi_0) + \omega\sin(\omega T + \varphi_0)e^{-\alpha_i t}}{\alpha^2 + \omega^2} - \\ & - A_1 k \frac{-\alpha\sin(\omega T)e^{-\alpha_i t} + \omega - \omega\cos(\omega T)e^{-\alpha_i t}}{\alpha^2 + \omega^2} + \\ & + aA_1 \left[\frac{e^{-\alpha t_1}(\alpha\sin\omega t_1 + \omega\cos\omega t_1) - e^{-\alpha t_2}(\alpha\sin\omega t_2 + \omega\cos\omega t_2)}{\alpha^2 + \omega^2} \right. \\ & + \frac{e^{-\alpha t_3}(\alpha\sin\omega t_3 + \omega\cos\omega t_3) - e^{-\alpha t_4}(\alpha\sin\omega t_4 + \omega\cos\omega t_4)}{\alpha^2 + \omega^2} \\ & + \frac{e^{-\alpha t_5}(\alpha\sin\omega t_5 + \omega\cos\omega t_5) - e^{-\alpha t_6}(\alpha\sin\omega t_6 + \omega\cos\omega t_6)}{\alpha^2 + \omega^2} \\ & + \frac{e^{-\alpha t_7}(\alpha\sin\omega t_7 + \omega\cos\omega t_7) - e^{-\alpha t_8}(\alpha\sin\omega t_8 + \omega\cos\omega t_8)}{\alpha^2 + \omega^2} \\ & \left. + \frac{e^{-\alpha t_9}(\alpha\sin\omega t_9 + \omega\cos\omega t_9) - e^{-\alpha T}(\alpha\sin\omega T + \omega\cos\omega T)}{\alpha^2 + \omega^2} \right] + \\ & - b\left[\frac{e^{-\alpha t_1} - e^{-\alpha t_2} - e^{-\alpha t_3} + e^{-\alpha t_4} + e^{-\alpha t_5} - e^{-\alpha t_6} - e^{-\alpha t_7} + e^{-\alpha t_8} + e^{-\alpha t_9} - e^{-\alpha T}}{\alpha} \right] \end{aligned}$$

After this, the algebraic objective function is formed in Matlab/Simulink. We give the graph of $J(T_1,K)$ in 3D shown in Figure 6.

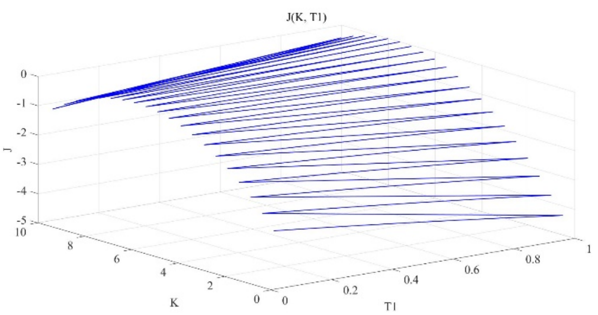

Figure 6. Graph $J(T_1, K)$ in 3D

Then, the extremum of the algebraic objective function is searched for and the corresponding optimal parameters are determined. The minimum of the algebraic objective function is 7,521*10^-6^, with the following values of the variable parameters: K = 6.708, T_1 = 0.4159. It should be noted that the result is close to the desired result and the minimum value of the root-mean-square deviation is 0.05538.

CONCLUSION

A utility is developed to solve the problem optimizing an algebraic objective function using the Matlab/Simulink.

REFERENCES

[1] Анализ и оптимальный синтез на ЭВМ систем управления / Г.А. Дидук, А.С. Коновалов, И.А. Орурк, Л.А. Осипов / Под ред. А.А. Воронова и И.А. Орурка. М.: Наука. Главная редакция физико-математической литературы, 1984. 344 с.

[2] Никитин, А.В. Параметрический синтез нелинейных систем автоматического управления : монография / А.В. Никитин, В.Ф. Шишлаков / под. ред. В.Ф. Шишлакова. СПб.: ГУАП, 2003. 358 с.

[3] Ушаков, В.А. Обзор применения на практике метода ортогональных проекций при разработке систем автоматического управления // Решетневские чтения. 2016. Т. 1. № 20. С. 302-304.

[4] Дэбни, Дж.Б. Simulink 4. Секреты мастерства / Дж.Б. Дэбни, Т.Л. Харман; пер. с англ. М.Л. Симонова. М.: БИНОМ. Лаборатория знаний, 2003. 403 с.

[5] Simulink Documentation URL: http://www.mathworks.com/help/simulink/

[6] Жуков, А.Д. Формирование алгебраической целевой функции с помощью Matlab/Simulink при разработке систем автоматического управления / А.Д. Жуков, В.А. Ушаков // Научная сессия ГУАП. Ч. I. Технические науки / СПб.: ГУАП, 2016 с. 251-255.

[7] Жуков, А.Д. Поиск экстремума алгебраической целевой функции в Simulink / А.Д. Жуков, В.А. Ушаков // Научная сессия ГУАП. Ч. I. Технические науки / СПб.: ГУАП, 2015. с. 235-238.

[8] Ушаков, В.А. Получение дифференциального уравнения движения системы из его структурной схемы в символьном виде / В.А. Ушаков // Современные технологии в задачах управления, автоматики и обработки информации / ИКД «Зерцало-М». М. 2014 с. 99-100.

BIO-WATER MACHINE 2.0

Valenti Susanna Rosaria, Simone Nicola

Computer Engineering and Networks Laboratory – Kore University of Enna - Italy

Email: {nicola.simone;susanna.valenti}@unikorestudent.it

Abstract

Bio-Water Machine 2.0 is a system designed for the purification of citruses in the agro-industrial area. This system is conceived for the softening of water from bacteria and fungi of after harvest citruses. This project promotes the development of innovative sanitization technologies with a multidisciplinary approach, by combining scientific, chemical, biological, electro-technical and engineering skills necessary for the achievement of the product innovation and the advancement of the state of the art. Bio-Water Machine 2.0 has been developed in Matlab, thanks to which it was possible to plan in detail each network component, in order to give a clearer interpretation of the project and its finalizing.

INTRODUCTION

Bio-Water Machine 2.0 is designed in Matlab [1]. By using this software, assisted by Simulink, DBSM, Soft Computing and TrueTime network simulator [2], we have been able to design the machine, the project engine, together with its wireless and wired network for the control of sensors installed within the network, by means of suitable wireless and wired protocols. The project arises from the re-examination and reworking of an already existing and functioning machine, with a suitable network, manufactured by the firm AQANAT [3], which allowed its development and commercialization.

Bio-Water Machine 1.0, currently on the market, uses a solely wired network, while wireless technology is not used. The aim of this machine/network is to integrate advanced technologies of filtration and physical treatment for the sanitization of washing waters without any waste. Our aim is to maintain the key points used in the first machine and to improve the network performances bringing in changes and improvements, so as to further optimize costs and increase its automation.

The project has been developed in the following steps:

- design of Bio-Water Machine 2.0 in Matlab;
- implementation of the purification machine, network engine, of the main tank and decantation tank, by using the DBSM system with suitable modelling of the various machinery components;
- design of the water softening tank sensors by means of TrueTime;
- design of the decantation tank sensors by means of TrueTime;
- control of the alarms related to the network sensors by means of a fuzzy controller.

RELATED WORKS

AQANAT BIOWATER [4], shown in Figure 1, integrates a device with electrodes, which, when undergoing a potential difference, produce locally a mixture of various oxygenated forms, like hydroxyl radical (OH*) in the ppm (mg/L) concentration gamma, highly active against a wide spectrum of pathogens microorganisms, bacteria, and fungi. The high oxidizing power of the electro-physical treatment on propagules of pellicinium spp. and Geotrichum spp. make it particularly suitable for the sanitization of citruses washing waters to the advantage of a lower fruit contamination and infection.

Figure 1: Bio-Water Machine 1.0

The project aims at the recycling of waters and therefore at larger hydric and economic savings for those firms using it, as well as at a higher sustainability. Although these are optimal principles, many processes can be considered out of date from the technological point of view, since technology is by now continuously evolving. The system, developed with a sole wired line, by using PLC, can make the future work obsolete.

The Bio-Water Machine 2.0 project aims at solving the problems of the current machine (1.0), maintaining the key points of water softening while increasing automation, integrating the still not present wireless network, and favoring a higher control and management of the plant.

The firm CSTA Group [5] has worked in a similar way by using reverse osmosis and citruses washing, by means of chlorine dioxide achieving reasonable results, since a decrease both in costs and in after harvest citruses bacteria were noticed. They realized that a water saving of about 40 – 50% could be achieved. These results were certainly excellent, but they were not as regards innovation and technological development. Compared to it, Bio-Water Machine 2.0 uses a more innovative system by using the most of all new technologies. Indeed, apart from achieving a water saving of 70-80% in the industry, thanks to its wireless system, Bio-Water Machine 2.0 allows the highest efficiency and interoperability with the other industrial machines.

SUGGESTED APPROACH

The proposed project consists of a simulation/planning of an industrial network. The project is composed by the following components: machine for water softening, main tank, decantation tank. The idea is to simulate the functioning of the machine carrying out the filtration and the electrolysis processes, and thus the water softening, by means of the StateFlow, highlighting all the inner components which constitute the machine and allow its functioning. The management of both tanks has been implemented by the use of TrueTime network simulator, in which the network inner sensors have been developed with wireless and wired protocols.

The whole functioning of the water softening machine, of the softening tank and of the decantation tank have been implemented/simulated with the MBSD, by the use of Charts. The sensors placed within the computers' network have been managed by implementing the TrueTime logic. Three systems have been managed by wireless IEEE 802.15.4 (Zigbee) and wired CSMA/CD (Ethernet) protocols, in which we have included:

- in network 1-2: conductivity and temperature sensors;
- in network 3-4: main tank sensors of softened water level and pressure;
- in network 5-6: decantation tank sensors of decantation water level and pressure.

thus, allowing the management and control of appropriate tanks, and highlighting the management and the automation of the whole system.

By using a soft computing technique such as Fuzzy Logic, the alarms produced have been managed, after receiving the input values provided, and thus for a possible increase or decrease of values, on the basis of the obtained results. This technique has been used both in wireless and in wired contexts, where sensors manage input and output alarms. In the main tank management, with the first fuzzy block, conductivity and temperature sensors have been managed in input, while the alarm they generate when set standard parameters are exceeded has been returned as output.

The standard parameters actually measured in the input are:

- *Temperature*: ranging from 15 C° to 35 C°;
- *Conductivity*: ranging from 0.5 mS to 2 mS.

The alarm which must be generated in case of exceeding ideal standards has been managed in output: the alarm has been considered with values between 0 and 10 according to the gravity of the alarm which must be generated. After the alarm is generated, values are sent to the appropriate regulator, and, by means of a Matlab-function block, the value is increased or decreased. With the second fuzzy block, both water level and pressure sensors have been managed in input, while in output the alarm which they generate, when the standard parameters are exceeded, is returned.

In this case, the input parameters are:

- *water level*: ranging from 1600 l to 2300 l;
- *pressure*: ranging from 20 to 30.

The alarm which must be generated in case of exceeding ideal standards has been managed in output: the alarm has been considered with values between 0 and 10 according to the severity of the alarm which must be generated. In turn, the value is sent to the regulator of its respective network and is managed by increasing or decreasing the value according to its respective alarm management rules.

In the decantation tank management, the fuzzy logic controller measures the water level and the pressure values in input, while in output it gives the alarm that must be generated in case standard parameters haven't been reached. This control has been created by highlighting the connection with the main tank, since the physical phenomenon of the communicating vessels acts between the two tanks.

The standard parameters measured in input are:

- *water level*: ranging from 250 l to 600 l;
- *pressure*: ranging from 20 to 30.

The alarm which must be generated in case of exceeding ideal standards has been managed in output: the alarm has been considered with values between 0 and 10 according to the seriousness of the alarm which must be generated and the subsequent result has been sent to the respective Matlab-function block for the management of the values.

BACKGROUND

With the MBSD, by using several Charts, the whole functioning of the water softening, of the softening tank and of the decantation tank have been simulated (Figure 2). Within the chart, which regulates the functioning of the softening machine, all the machine components have been managed, considering the time taken by each component to perform its task, so as to have an optimal functioning of the machine itself. By the debounce key, which is input in the machine, a signal of dirty water level and pressure in input, the inner values of the softening machine are managed. When the value given by the debounce is received, the machine is activated, therefore, from OFF state it switches to ON state. When the machine is activated, the valves 1 and 2, which allow dirty water in input to enter the system, can be opened.

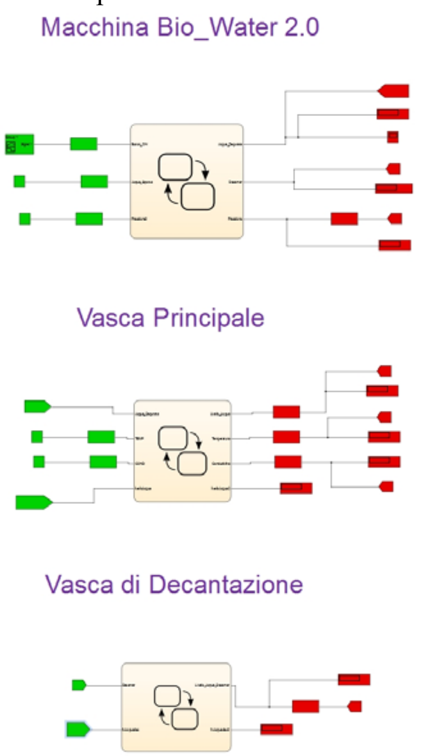

Figure 2: MBSD of the proposed project

After the two valves are opened, the engine, which ideally acts as aspirator of water, can be turned on, and water will go throughout the plant. As soon as the engine is activated, the potentiometer is activated, this is connected to the electrolytic cell and must necessarily be activated soon after the engine activation, and not before it starts to aspirate water.

Subsequently, the control passes to the first filter called sand filter, where the water level to be softened is activated and managed, to which a value corresponding to the decantation water must be subtracted, which will then go into the output. Moreover, it manages the pressure level which will have to decrease, since in real filters, pressure within filters is subtracted in order to have the same potential level in input and output; finally, it will have to save the decantation value it has subtracted. When the first cycle of the first filter has finished, the control passes to the second filter, called AMIAD filter, whose task is to further filter water, thus further softening it. This takes place thanks to the decrease of a value which in turn will be saved as decantation value; as a consequence, pressure is also considered, in turn decreased of a value to reach the same potential difference between input and output.

In the next step, there is the electrolytic cell, where the electrolytic process is simulated, and where, thus, the water cycle is completed. Its value is further decreased and the pressure value is managed as in the ways previously described. The next stage is the separation of values that will go into the output, that is softened water, decantation water, and pressure, which then will be managed by the other network elements.

Considering Figure 2, in a second chart, the main tank is managed, with water from the softening machine in input, the total level of softened water, temperature, and conductivity in output. In a third chart, the decantation tank is managed, with decantation water from the softening machine in input, and total water of the decantation tank in output.

The networks which allow the control of the main tank and decantation tank sensors have been managed by means of TrueTime. The proposed wireless networks are based on IEEE 802.15.4/ZigBee composed by sensors and gateways.

ASSESSMENT OF THE PERFORMANCE

In order to validate the project, several measurements have been carried out. As to performance metrics related to the project, the progression of water level throughout the whole simulation has been measured and the obtained results are depicted in Figure 3. As it is possible to note, the water level varies during a simulation of 1500 seconds. Moreover, it is possible to infer that the water level is varied, in case there is an excess of water and a shortage. Indeed, the water levels never exceed 2300 l, as it was pre-established during planning.

To give a better measurement yield, we decided to measure the system performances, by considering the three main networks individually. We measured:

- the number of packets received and sent;

- the number of packets lost;
- the throughput.

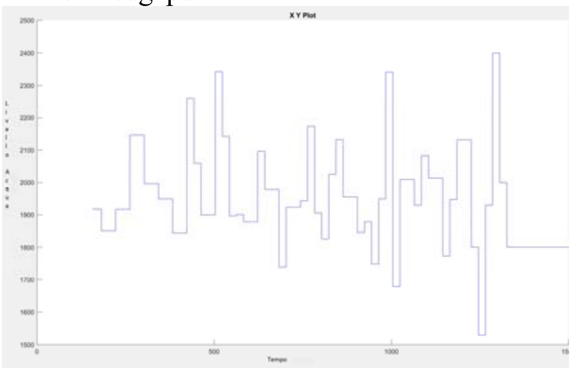

Figure 3: water level

In networks 1-2, in a simulation of 1500 seconds, the following results have been obtained:

- the packets sent from the temperature sensor have been 148;
- the packets received in the Gateway have been 84;
- the packets lost during the simulation have been 64;
- the packets sent from the conductivity sensor have been 148;
- the packets received in the Gateway have been 83.

The average of packets received in a simulation of 1500 s has been 83.5 packets; the average of lost packets has been 64.5 packets. Whereby, in network 1-2 the packets loss has been 43.5%.

Moreover, the throughput of network 1-2 has been calculated:

$$\text{THR} = \frac{\text{number of packages}}{\text{simulation time}}$$

$$\text{THR}=\frac{296\times 272\left[\text{bit}\right]}{1000\left[\text{s}\right]}=80\,\frac{\text{bit}}{\text{s}}$$

In networks 3-4, in a simulation of 1500 seconds, the following results have been obtained:

- the packets sent from the water level sensor have been 124;
- the packets received in the Gateway have been 91;
- the packets lost during the simulation have been 33;
- the packets sent from the pressure sensor have been 124;
- the packets received in the Gateway have been 92;
- the packets lost during the simulation have been 32.

The average of packets received in a simulation of 1500 s has been 91.5 packets; the average of packets lost has been 32.5 packets. Whereby, in networks 3-4 the packets loss has been 26.2%. Furthermore, even in this case, the throughput has been calculated:

$$\text{THR}=\frac{248\times 272\left[\text{bit}\right]}{1000\left[\text{s}\right]}=67\,\frac{\text{bit}}{\text{s}}$$

In networks 5-6, in a simulation of 1500 seconds, the following results have been obtained:

- the packets sent from the decantation water level sensor have been148;
- the packets received in the Gateway have been 84;
- the packets lost during the simulation have been 64;
- the packets sent from the decantation pressure sensor have been 148;
- the packets received in the Gateway have been 83;
- the packets lost during the simulation have been 65.

The average of packets received in a simulation of 1500 s has been 83.5 packets; the average of packets lost has been 64.5 packets. Whereby, in networks 5-6 the packets loss has been 43.5%.

The throughput of network 5-6 has been:

$$\text{THR} = \frac{296\times 272\left[\text{bit}\right]}{1000\left[\text{s}\right]} = 80\,\frac{\text{bit}}{\text{s}}$$

The average throughput of the whole system has been 75 bit/seconds.

CONCLUSIONS

The project presented in this paper concerns the automation of an already existing network such as Bio-Water Machine 1.0. With the introduction of the wireless protocol (IEEE 802.15.4/Zigbee) it has been possible to renew the already existing network while keeping the key points of the original project itself. By means of the system management, we have been able to highlight all the project key points which can be useful for a further physical design of the system and its possible building with a new technology. The advantages achieved for the industry with this project are: improvement of production quality, reduction of after harvesting losses, remarkable water saving, automated control plant, thanks to which there is an advanced technological innovation compared to similar industries. As to the future developments of this system, we thought of planning and creating an application, with graphic interface, to monitor all the system by PC, so as to reduce manual management and allow a complete monitoring of parameters and systems by a computing system.

REFERENCES

[1] https://it.mathworks.com/products/matlab.html
[2] TrueTime Handbook
[3] http://www.aqanat.com/biowater/product.html
[4] Technical documents of AQT300 (machine Bio-Water 1.0)
[5] Azienda CSTA Group analytical and product study, Decco industry

MAGNETIC AND DIELECTRIC PROPERTIES OF LANTHANUM-STRONTIUM MANGANITES AT LOW TEMPERATURES

Vanina Polina
Peter the Great Saint-Petersburg Polytechnic University,
Saint-Petersburg, Russia

E-mail: p.yu.vanina@gmail.com

Abstract

The temperature dependences of the magnetization *M*(*T*) for multiferroic single crystal lanthanum-strontium manganites $La_{0.875}Sr_{0.125}MnO_3$ (LSMO-0.125) and $La_{0.93}Sr_{0.07}MnO_3$ (LSMO-0.07) have been obtained. It is shown that the phase transitions in LSMO-0.07 at T_C = 125.8(1,5) K and in LSMO-0.125 at T_{C1} = 181.2 (1.5) belong to the second order type. The phase transition in LSMO-0.125 at T_{C2} = 157.6 (1.5) K is the first order the phase transitions. From the $M^{-1}(T)$ curves, the values of the magnetic moments have been obtained. Also conclusion was reached that there is not any irreversibility of applying magnetic field of specific values.

INTRODUCTION

A very interesting correlation between doping-induced conductivity and ferromagnetism was discovered at the end of the 20th century for the initially dielectric manganese-containing perovskites LaMnO the so-called manganites, in which the rare-earth metal was replaced by the alkaline-earth one. The composite $La_{1-x}A_xMnO_3$ with quaternary stoichiometry (x ≠ 0, 1) is interesting because of its strong ferromagnetic properties and extremely high values of dielectric permittivity and magnetocapacitance effect even at room temperature [1].

Various practical applications of these manganites are possible thanks to their magnetocapacitance properties. In this case the work the authors [1] attracts attention. They were found extremely high values of dielectric constant and magnetocapacitance effect, already at room temperature. Also it was suggested to influence the properties of the charge inhomogeneities in doped manganites LSMO-x in order to achieve high values of permittivity and magnetocapacitance effect.

Unfortunately, numerous studies of manganites of this type have not answered the question about the microscopic nature, of their giant magnetocapacitance. However, in [2] there is a detailed diagram of the phase of the specified type of manganites in T - x coordinates at concentrations range from 0 to 0.45 at temperatures of 4.2 - 1050 K, and the study of their electric and magnetic properties. Temperature studies of different properties of LSMO-0.07 and LSMO-0.125 [2] have revealed that these compounds have a few magnetic and structural transformations. For example, transition to polaron ordering. According to [3], the polaron phase is an ordered arrangement of the Mn^{3+} and Mn^{4+} ions in which one of the two alternating atomic layers of the (001) plane contains, as in pure LMO, only the Mn^{3+} ions, while the second one contains both types of ions, i.e., holes [2].

Nevertheless, the temperatures of these transitions, the magnetic moments of the materials, the type of phase transitions (PT), and the practical effect of the application of a strong magnetic field remain unclear.

The goal of this study was to obtain the information on the temperature evolution (4–240 K, i.e., exactly where the unusual macroscopic properties of these materials are observed) of the magnetic properties of the LSMO-0.07 and LSMO-0.125 compounds and look for dielectric properties evolution under applying different regimes of magnetic field.

EXPERIMENT

The studies were carried out on a vibration magnetometer in the International Laboratory of High Magnetic Fields and Low Temperatures (Wroclaw, Poland). The weight of single-crystal samples was 121.95 mg for LSMO-0.125 and 152.8 mg for LSMO-0.07, respectively. The magnetic field was applied along the c axis; the measuring field for magnetic properties evolution was 0.2 T and from 0 to 8 T for dielectric ones. The temperature dependences of the magnetization of the samples were obtained in the 4–240 K temperature range and for capacitance measurements it depended on the value of capacitance of samples under specific temperature.

RESULTS AND DISCUSSIONS

Figure 1 shows temperature dependences of magnetization for samples with the LSMO-0.07 composition under cooling (black) and their approximations in the high-temperature (blue) and low-temperature (red) regions.

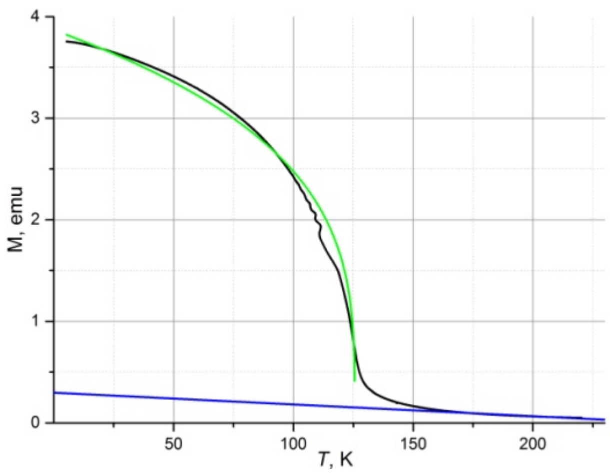

Figure 1

Temperature dependence of magnetization for the LSMO-0.07 sample under cooling is shown in Figure 1. The black curve changes its tendency near 130 K. According the phase diagram from [2] this temperature fit with PT from the high-temperature paramagnetic phase to the low-temperature non-collinear one, accompanied by the emergence of spontaneous and residual magnetization. So we can conclude that this magnetic structure is weakly ferromagnetic rather than purely antiferromagnetic [2].

Therefore we can use such a power function for approximating temperature dependence of magnetization M(T):

$$(T_C - T)^{\beta}, \quad (1)$$

where T_C is the PT temperature, β is the critical exponent.

As you can see in Figure 1 such approximation (green curve) satisfactory describes the experimental curve (black one). In this way were gained parameters of function (1): T_C = 125.8(1.5) K, β = 0.280(8).

For comparison with calculated value of parameters we obtained the PT temperature by graphic method. We found the intersection point of two types of approximation of magnetization – at low and high temperature range – its value matches with calculated value of T_C within ± 0.5 K.

Figure 2 shows temperature dependences of magnetization for samples with the LSMO-0.125 composition under cooling (black) and their approximations in the high-temperature (blue) and low-temperature (red) regions.

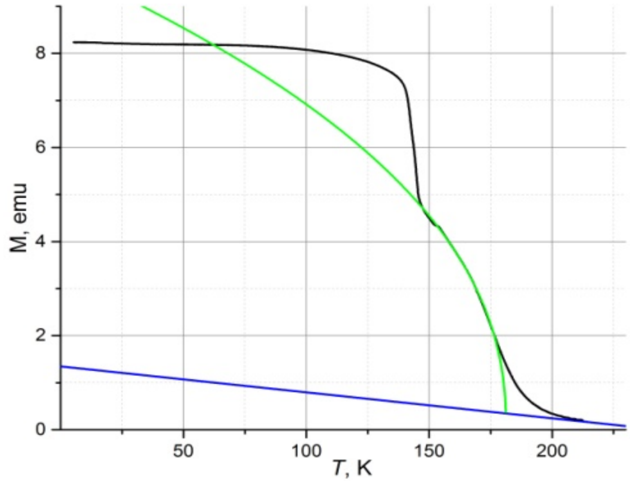

Figure 2

Temperature dependence of magnetization for the LSMO-0.125 sample under cooling is shown in Figure 2. As far as the magnetization temperature evolution curve has two points where it changes tendency (near 180 K and 157 K) we can conclude that two magnetic phase transitions are observed in the LSMO-0.125 sample. The M(T) temperature dependence between these two points was described by the same function (1) and corresponding parameters: T_{C1} = 181.2(1.5) K and β_1 = 0.440(13). The value of the critical exponent is close enough to value 0.5 for the mean field theory. Also value of T_{C1} obtained from the graphic method matches with calculated value too and it is in good agreement with the result obtained in [2].

The second PT was approximated by a step function with T_{C2} =157.6 (1.5) K. This transition apparently corresponds to the transition to the polaron or the polaron-ordering phase [2, 3].

Thus, based on the character of the temperature dependences of M(T), and the values of the critical exponents obtained for the LSMO-0.07 and LSMO-0.125 samples, it can be assumed that the PT at 125.8 K in the first sample and at 181.2 K in the second one are the second order phase transitions, while the PT in the second sample (LSMO-0.125) at 157.6 K is the first order phase transition. Preliminary results were presented in [4].

Figure 3 shows temperature dependence of LSMO-0.07 sample capacitance in the low-temperature range under different values of applied magnetic field.

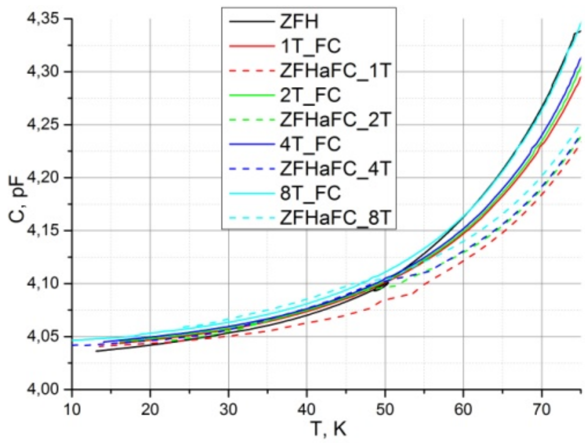

Figure 3

At the next stage of our study we have constructed the temperature dependence of the reverse magnetization 1/M for both samples, approximated them in high-temperature region (paramagnetic phase) and estimated the values of the magnetic moments of manganese ions in both samples. They were as follows: $\mu_1 = 2.47(1)\ \mu_B$/Mn and $\mu_2 = 2.82(1)\ \mu_B$/Mn for LSMO-0.125 and LSMO-0.07, respectively.

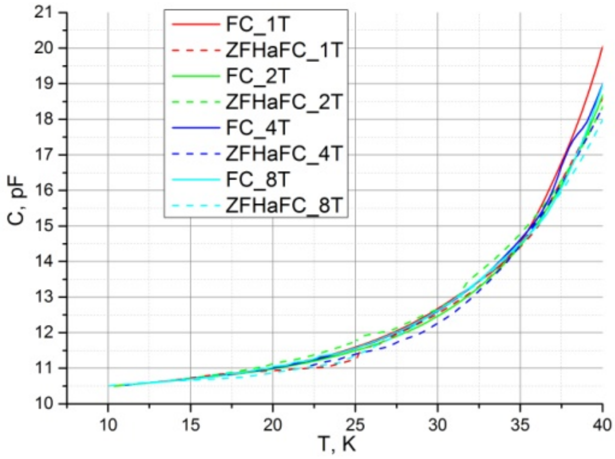

Figure 4

Figure 4 shows temperature dependence of LSMO-0.125 sample capacitance in the low-temperature range under different values of applied magnetic field.

We have studied the experimental temperature dependence of the capacitance depending on consequence of applying magnetic field (Figure 3, 4)) at temperature range 10-70K for LSMO-0.07 and 10-40K for LSMO-0.125. Regime of applying magnetic field was following: we cooled sample under magnetic field of different values (field cooling - FC) and then heating it up without field (zero field heating after field cooling - ZFHaFC). It is seen that application of magnetic field make very small differences in values of capacitance in both samples and there is no any irreversibility at these processes at mentioned low temperature range.

CONCLUSION

We have studied the temperature evolution of magnetization in the single crystals of the LSMO-0.07 and LSMO-0.125 compositions and have established that a single magnetic phase transition has been observed at $T_C = 125.8(1.5)$ K for the first compound, and two magnetic transitions – at $T_{C1} = 181.2(1.5)$ K и $T_{C2} = 157.6(1.5)$ K for the second one.

We have determined the values of the critical exponents $\beta = 0.280(8)$ for LSMO-0.07 and $\beta 1 = 0.440(13)$ for LSMO-0.125.

We have figured out that observed phase transitions at mentioned above temperatures (T_C and T_{C1}) are the second order phase transitions, and the first order phase transition (T_{C2}).

We have estimated the magnetic moments of studied compounds: $\mu 1 = 2.47(1)\ \mu B$/Mn and $\mu 2 = 2.82(1)\ \mu B$/Mn for LSMO-0.125 and LSMO-0.07, respectively.

On the final stage of our study we have conclude that there is not any irreversibility of applying magnetic field of specific values.

REFERENCES

[1] R.F. Mamin, Giant dielectric susceptibility and magnetocapacitance effect in manganites at room temperature / R.F. Mamin, [et. al.] // Journal of Experimental and Theoretical Physics Letters. – 2007. – Vol. 86. – P. 643–646.

[2] E. Dagotto Colossal magnetoresistant materials: the key role of phase separation / E. Dagotto, T. Hotta, A. Moreo // Phys. Rep. – 2001. – Vol. 344. –P. 153.

[3] A.A. Mukhin Magnetic and structural transitions in $La_{1-x}Sr_xMnO_3$: Phase $T-x$ diagram / A.A. Mukhin [et al.] // Phys. Rev. Lett.. - 1998. Vol. 68, N 4. – P. 356-362.

[4] Vanina P.Yu., Temperature evolution of lanthanum-strontium manganites magnetic properties / Vanina P.Yu., Naberezhnov A.A., Nizhankovskii V.I., Mamin R.F. // St. Petersburg Polytechnic university journal: Physics and mathematics. – 2016. – Vol. 2, Issue 3. – P. 175-180.

This work was supported by the Russian Science Foundation (Project № 14-22-00136).

PRACTICAL RESEARCH OF THE ANALYSIS AND AUTOMATION OF THE WORK OF THE AIRPORT SYSTEMS ON THE BASIS OF MATHEMATICAL MODELS AND SIMULATION MODELING

Vershinina M., Okhremenko A.

Saint- Petersburg State University of Aerospace Instrumentation
Saint-Petersburg, Russia

E-mail: marusenitsa@gmail.com
aaohremenko@gmail.com

In modern world the fastest and the safest way to get the destination is air transportation. People are traveling for business or personal goals.

At any airport there is a luggage system which is responsible for transportation and baggage allowance. Sometimes luggage may lag behind a passenger or remain unidentified. In this case, suitcases are sent to special areas, where luggage will be manually identified by airport employees.

Each airline strives to ensure that passengers are delivered to the destination in the most effective way. Achieving of this goal is closely connected to the precise organization of the airport. Modern conditions of market of the air transport require airport enterprises to improve the quality of services provided to carriers and users of airport. The main objective is to reduce the time spent on servicing and meeting the requirements for safety and regularity of traffic. The main goal is to reduce the time that aircraft spent on service and requiring the rules for safety and regular of traffic. This goal may be achieved by using information technologies [1,2,8,9]. The peculiarity of the aviation industry is that every airport has its own distinctive features. One of the directions of practical solutions is the development of perspective mathematical models and the use of simulation computer simulation.

The purpose of this paper is to describe the mathematical model for calculating the reliability of the luggage system of the airport and the construction of a simulation model for the technological processes at parking sites of servicing aircraft.

Figure 1 - The geography of flights from airport (based on openflights.org data)

Technology service flights have been considered as part of the proceedings of the research. Also scheduling ground-handling services including critical path operations equitable for the vast majority of types of aircraft has been examined and an analysis parameters of the technological processes of aircraft ground handling had been made, stochastic models of technological operations included in the technological schedule was constructed.

Simulation model of technological processes of ground handling includes:

1) Algorithm for the implementation of the aircraft maintenance process, describing the sequence and relationship of the operations forming it;

2) Models of individual technological operations, including statistical distributions of the basic parameters of operations such as time duration, the number of special vehicles used. Restrictions on model details require that the model created reflects only that set of technological operations, which is fundamentally important in the optimization of the transportation service process and that meets IATA requirements [8,9].

As a result of the simulation has been processed, visualized and interpreted the results of a computer-assisted computer experiment. The simulation was conducted for the full range of services provided by airport for this aircraft, using largest number of special equipment.

The aircraft model Boeing 737 that was chosen for the research is currently one of the most popular type of passenger aircraft. Boeing 737 and its modifications are represented in aircraft parks of all major airlines of the world. The simulation model has based on the aircraft maintenance schedule, in accordance to which operational planning and preparation for flight management are carried out[3,4,5].

Modeling was performed using the software package AnyLogic [2,5]

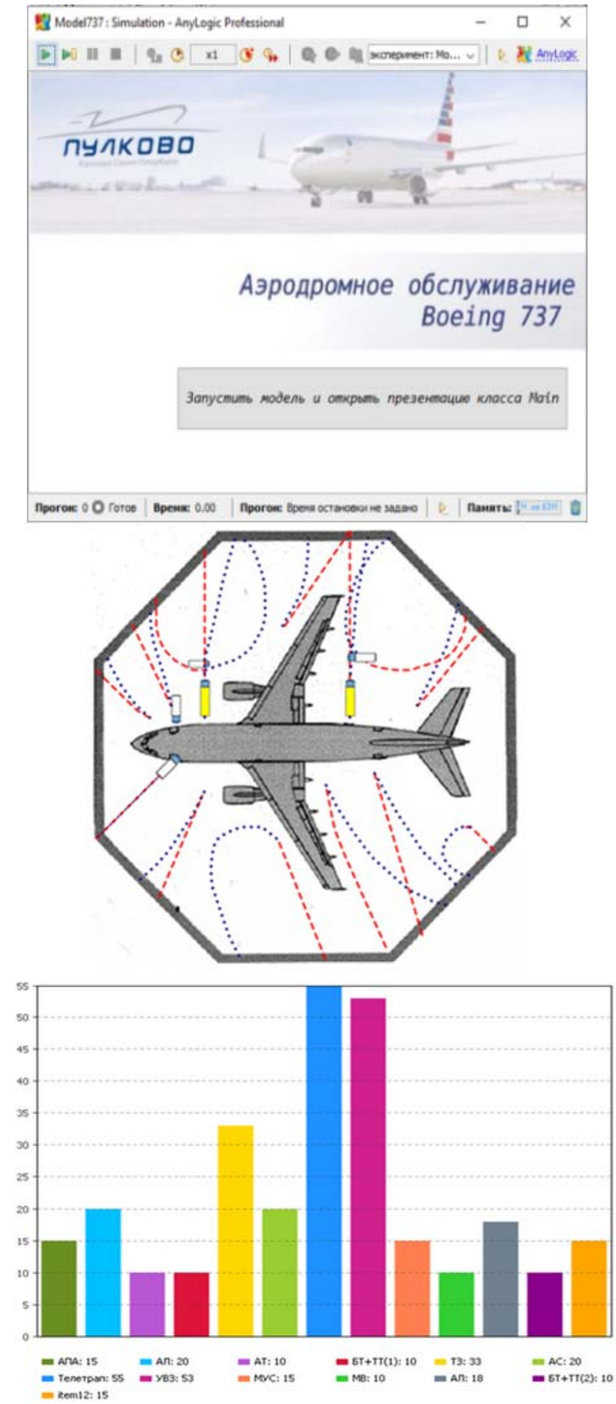

Figure 2 - The result of the simulation. Time diagram of aircraft maintenance

This approach allows organizing the realization of operations of the maintenance of flights, and monitoring the implementation of these operations. This is achieved by splitting one process into elementary components - technological operations.

The model also helps to solve the tasks of operational planning and automation of decision making aircraft handling.

The advantage of the model is that it allows to analyze the processing process by adjusting the model parameters, in other words, state of the system while changing the route of movement of each vehicle, duration of one of the operations or entire process, makes possible to predict the behavior of the system.

In practice, this method will significantly improve the level of flight safety, operational efficiency due to well-coordinated interaction of services, which will increase the efficiency of the ground handling system at the airport, help to avoid malfunctions and reduce the risk of collision of special vehicles.

The conclusion from the simulation results is that, with proper implementation of the norms and maintenance instructions, the system works in a coordinated manner, ensuring efficient allocation and utilization of airport resources. These units of special vehicles and equipment not interfere with the operation of neighboring maintenance facilities, while driving through the service area they do not create congestion or collision between themselves. The problem zones in the ground handling area of this aircraft haven't been found, which confirm the rationality of using the current aircraft maintenance schedule. On the basis of this software tool, it is possible to play various possible non-regular situations.

Another important key step is the airports' luggage system. Duaring of this research, the baggage system of the airport was studied; the mathematical model of the system was selected.

During the research the scheme of baggage transportation at the airport was clarified. The majority of passengers hand over their luggage to the cargo holds of the aircraft at the check-in counters. At one of the four so called "islands" of registration all of the bags are registered and weighed, and also receives an individual code mark. At the system bags are scanned and inspected by the means of various apparatuses several times. If the suitcase does not cause suspicion, it is getting to the sorter for delivery to the aircraft. If there are some doubts, then suitcases get additional inspections, and even may be pass a manual search.

The baggage system of the airport consists of many elements. It includes conveyors, elevators, inspection devices, x-Rays, scanners (different scanning angles), sorters, vertisorters and much more [3,6,7]. Each of these elements can fail, it is important to organize such a scheme of the system, so that the luggage system does not interrupt while doing through. Figure 2.1 shows the general scheme of moving baggage through the system: 1 - check-in counter; 2 - scanning of suitcases and bags; 3- examination of luggage for explosiveness and radiation background; 4 - manual examination of baggage; 5 - baggage sorter; 6 - the luggage yard; 7- the formation of luggage for delivery to the flight; 8 - baggage forwarding area.

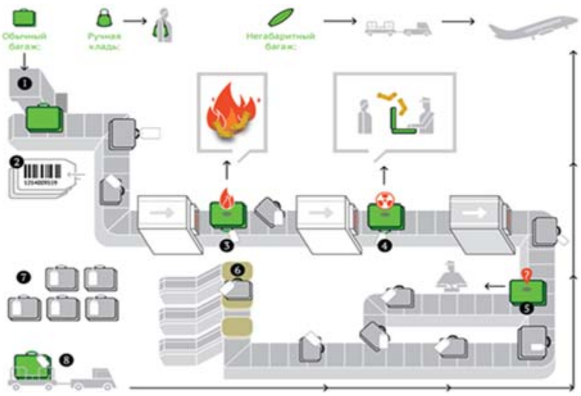

Figure 3. Overall plan for moving baggage through the system

Some of the conveyors of the system have a reversible movement in order to switch the movement of luggage to another direction.

Regardless from which “island” the baggage arrived from, received from the arrived plane or from the reception of oversized baggage, it passes through all stages of inspection and processing and is sorted in the direction. All goods at the system pass through an identical path through similar links in the system.

The baggage system of airport is a system with permanent redundancy [2,4,6]. Analyzing the layout of the baggage system at airport, the elements of the system were identified and some of them were combined into blocks. For example, the check-in counters of each “island” are connected in parallel to each other and are integrated by a connecting conveyor. Each “island” has two exits, so it’s advisable to divide the “islands” into two parts. Two parts of the “island” are connected to each other in parallel - the goods from one half can always be transferred to the other with the help of a reverse conveyor.

Computation of the reliability of the system is calculated on the basis of the construction of the structural diagram. Each block can contain only those elements that correspond to one statistical distribution. The structural scheme of reliability is a graphic representation or representation in the form of logical relationships, the conditions when the system and the object are working. When for the functioning of the system it is necessary that all the units are working, then this corresponds to a block diagram in which all blocks are connected in series. Calculation of the reliability of the circuit with a serial connection of elements is carried out by the multiplication of reliability. There is also a parallel block diagram in which the elements are connected in parallel way.

As a result reliabilities of the system at the outputs of the sorters. “P” is the reliability of different groups of elements:

$$PEX1 = 1-(1-P10)(1-P23) \tag{1}$$

$$PEX2 = P9 \tag{2}$$

$$PEX3 = 1-(1-P15)(1-P21) \tag{3}$$

$$PEX4 = P11 \tag{4}$$

$$PEX5 = 1-(1-P8)(1-P22) \tag{5}$$

$$PEX6 = 1-(1-P20) \tag{6}$$

The final formula of reliability (outputs to the sorter are connected in parallel):

$$P = 1-(1-PEX1)(1-PEX2)(1-PEX3)$$
$$(1-PEX4)(1-PEX5)(1-PEX6) \tag{7}$$

At the end of the journey, luggage aredelivered to the sorter, connected in series to all outputs.

The probability of failure-free operation according to statistical data on failures is estimated by the expression described by formula (8):

$$P_c(t) = e^{-\lambda_c t} \tag{8}$$

$n(t)$ is a number of elements that have not failed by the time; N is the number of all products involved in the process; $P(t)$ is the statistical estimation of the probability of failure-free operation of the product.

The failure rate according to statistical data on failures is determined by the expression indicated in formula (9):

$$\lambda(t) = \frac{\Delta n(t)}{N\Delta t}, \tag{9}$$

$\Delta n(t)$ is the number of failed elements on the time interval $(t, t+\Delta t)$; F (t) is the statistical estimate of the failure rate of the elements; Δt is the time interval.

The baggage system of airport consists of 934 elements. Statistical data on the number of failures of elements for 157 days are substitute to developed mathematical model. The final reliability of the system is 0.41. The baggage system existing at the airport has sufficient reliability to ensure efficient work of the airport.

The model developed in this research can be used in the future to appraisal the reliability and efficiency of the baggage system existing at the airport, as well as to identify the most susceptible elements in the system.

REFERENCES

1. Fetisov V. A., Maiorov N. N. Prakticheskie zadachi modelirovaniia transportnykh sistem [Practical Problems of Modeling of Transport Systems]. Saint-Petersburg, GUAP Publ., 2012. 185 p. (In Russian).

2. Rusinov I. Ia. Organizatsiia vozdushnykh

perevozok [Organization of Air Traffic]. Moscow, Transport Publ., 1976. 184 p. (In Russian).

3. Afanas'ev V. G. Kommercheskaia ekspluatatsiia mezhdunarodnykh vozdushnykh linii [Commercial Operation of International Air Services]. Moscow, Transport Publ., 2002. 325 p. (In Russian).

4. Ignat'eva A. V., Maksimtsov M. M. Issledovanie system upravleniia [Research of Management Systems]. Moscow, IuNITI-DANA Publ., 2003. 157 p. (In Russian).

5. Maiorov N. N., Fetisov V. A., Gardiuk A. N. Tekhnologii i metody modelirovaniia passazhirskikh perevozok na vozdushnom transporte [Technology and Modeling Techniques Passenger Air Transport]. GUAP Publ., 2014. 215 p. (In Russian).

6. Maiorov N. N., Fetisov V. A. Modelirovanie transportnykh protsessov [Modeling of Transport Processes]. GUAP Publ., 2011. 165 p. (In Russian).

7. Pravdin N. V., Negrei V. Ia., Podkopaev V. A. Vzaimodeistvie razlichnykh vidov transporta (primery I raschety) [The Interaction of Different Modes of Transport (Examples and Calculations)]. Moscow, Transport Publ., 1989. 208 p. (In Russian).

8. IATA. Web. 6 March. 2017 .<www.iata.org >

9. ICAO. Web. 6 March. 2017 <www.icao.int >

MATHEMATICAL MODELS OF LOCATION SIGNALS REFLECTED FROM THE UNDERLYING SURFACES OF THE EARTH AND THE SEA MODELING SAR IMAGES FOR ECOSYSTEM MONITORING TASK

Wattimena Gysberth Maurits
Polytechnic of Ambon State,
Ambon, Indonesia

E-mail: mauritswattimena@gmail.com

Abstract

When testing onboard equipment of aircraft using navigation radar maps for navigation, there is a need for mathematical models of signals reflected from the earth's surface and the sea surface.

Traditionally, using theoretical constructions, such models were models of stochastic signals, the envelope fluctuations were described by the laws of Rayleigh and Rayleigh-Rice. These models were used both for simulating signals reflected from the earth's surface, and for signals reflected from the sea surface. With low resolution of airborne radars, these models described the statistical characteristics of fluctuating signals quite well. Modern onboard locators have high resolving power and the Rayleigh and Rice models can no longer be used in the synthesis and modeling of modern on-board navigation systems.

In this paper, we propose an approach to the construction of models of location signals that uses both theoretical construction and experimental data, which allows us to take into account the features of the reflection of the location signals from small parts of the underlying surface of the earth and the sea, while taking into account both the correlation between the individual sections and the anisotropy of the reflections when observing areas from different angles. Reflections from the sea surface are approximated by a log-normal law, reflections from the terrestrial, in view of the variety of surface types, Beckman and Weibull laws, particular cases of which are the laws of Rice, Hoyt and Rayleigh.

These models can be used for high-precision mapping, monitoring environmental pollution, testing the operating modes of aircraft equipment.

INTRODUCTION

In recent years, the requirements for resolving power for the tasks of high-precision mapping of the earth's surface have been increasing every year. Therefore, the topic of mapping the terrain by synthesizing the aperture of the antenna from the aircraft's side remains relevant today, where it is necessary to achieve high resolution of the generated radar image.

This high resolution is determined by many factors, and in particular one of these factors are the fluctuations of the signal reflected from the underlying surface, by the characteristics of which we obtain information for the formation of the radar image. Known works that are devoted to synthesizing the antenna aperture are mainly based on the average properties of the reflecting surface.

In calculating these properties, the average power of the re-reflected signals are calculated from the basic radar equation. In fact, depending on the type of surface, signal fluctuations occur, which can worsen these characteristics. How much they get worse can be seen after the equipment is created. It is desirable for developers to have in advance a set of distribution laws for different types of surfaces and information on how they impair the potential characteristics of the elements of the resolution of the generated radar image, calculated in a theoretical way.

There is a considerable list of problems solved by radar survey. Important tasks of radar monitoring, performance solutions which due to improving prospects for radar image equipment includes the following: assessment of the characteristics of the environment and ecosystems (from regional to global), description of forest, agricultural and fishery ecosystems; Determination of the state of forest ecosystems, assessment of growth and condition of forest lands, detection of legal and illegal logging, assessment of the area and consequences of forest fires and floods, pyrogenic and post-identification of the size, nature and volume of water surface contamination, determining the area of leakage of combustible and liquid chemicals in disaster areas; Identification of zones of flooding and shallowing of the coasts of the seas and lakes; Monitoring in polar regions, including assessing the state of coastal ecosystems, assessing the state of marine areas; Production of cartographic works by land, sea surface, shelf, compilation, maintenance and updating of the land cadaster; Carrying out the cartography of sea ice and the evaluation of the ice deformation; Topology and lithological measurements;

The successful solution of this list of monitoring tasks is determined by the capabilities of information radio-electronic (primarily radar) systems capable of extracting information about the objects of observation contained in power engineering, the structure and polarization of the signal, and functioning in many frequency ranges of the electromagnetic spectrum.

METHODS FOR MODELING THE ECHO SIGNAL FOR THE FORMATION OF SAR IMAGES

There are two approaches to modeling the echo from the earth's surface. The first approach is the electrodynamic model, when the re-scattered signal is calculated by the Maxwell equations.

The second model, which has found application in practice and which describes the fluctuations of the echo, uses a statistical approach.

The first approach uses all possible approximations depending on the type of surface roughness, for example, small perturbation approximation, by the Kirchhoff method, by Rayleigh methods.

Another method, using the Feynman diagram method, requires cumbersome and complex mathematical computations and it is necessary to have a lot of prior information: about the reflecting properties of the signal, about the channel, etc.

In the second approach, which is used for designing systems, in which a statistical model of the echo signal on a computer is modeled. Computer simulation uses all possible laws for the distribution of signal fluctuations of the elements of the resolution of the underlying surface, which do not contradict the experimental data.

The simplest kind is a stable echo signal. The second kind, when there are many elements of the underlying surface or a digital map of the terrain in the simulation, fall into the elements of the resolution of the beam, then the fluctuations correspond to the Rayleigh distribution law. If there is a stable element in the signal, then Rayleigh-Rice. If the conditions of geometrical optics are not met, and there is a correlation between the elements, then there may be other laws. In particular, it very well approximates the experimental data - the Weibull distribution law, and for the sea surface the log-normal law. In some cases, the log-normal law is also used for hilly or undulating types of earth's surface. Other laws are also used, but we will limit ourselves to the following:

- Log-normal
- Weibull
- Rayleigh

Some laws are rarely found in the literature, or the amplitude of the echo is calculated at average power, but there is no information on how many fluctuations in the envelope amplitude of the echo, coordinated with a certain distribution law, affects the quality of synthesis, the resolving power of the radar.

Some of these laws follow from physical representations, and some laws are observed in practice and do not contradict real data. But in order to compare them one should calculate the signal-to-noise ratio (in terms of power) for each of the above distribution laws, which should be the same. In addition, since these are two-parameter laws, and the signal-to-noise ratio should be equivalent for all types of laws, it is necessary to show clearly how to specify the equivalence.

THE METHOD OF FORMING A RANDOM MATRIX WITH A GIVEN CORRELATION FUNCTION

We have an algorithm of a random signal with a given correlation function, we will form an algorithm for the random matrix.

1) We form the vector $\eta_{i,j}$ - the matrix of normally distributed independent random variables with zero means and unit variances $\eta_{i,j}\ V\ N(0,1), i = 1,..,n\ \ j = 1,\dots,m$

$$\eta_{i,j} = \begin{bmatrix} \eta_{1,1} & \eta_{1,2} & \eta_{1,3} & \cdots & \eta_{1,n} \\ \eta_{2,1} & \eta_{2,2} & \eta_{2,3} & \cdots & \eta_{2,n} \\ \eta_{3,1} & \eta_{3,2} & \eta_{3,3} & \cdots & \eta_{3,n} \\ \vdots & \vdots & \vdots & \ddots & \vdots \\ \eta_{m,1} & \eta_{m,2} & \eta_{m,3} & \cdots & \eta_{m,n} \end{bmatrix}$$

2) From the matrix $\eta_{i,j}$ we form $X_{i,j}$ - the matrix of normally distributed random variables, also with zero means and unit variances, but with an exponential correlation over the columns. The following are the recurrent form of the formula of each j-th column of the matrix $X_{i,j}$

$$\eta_{i,j} \Rightarrow X_{i,j} = \begin{bmatrix} x_{1,1} & x_{1,2} & x_{1,3} & \cdots & x_{1,n} \\ x_{2,1} & x_{2,2} & x_{2,3} & \cdots & x_{2,n} \\ x_{3,1} & x_{3,2} & x_{3,3} & \cdots & x_{3,n} \\ \vdots & \vdots & \vdots & \ddots & \vdots \\ x_{m,1} & x_{m,2} & x_{m,3} & \cdots & x_{m,n} \end{bmatrix}$$

3) From the matrix $X_{i,j}$ we form $Y_{i,j}$ - the matrix of normally distributed random variables, also with zero means and unit variances, but with the addition of exponential correlation in rows.

$$X_{i,j} \Rightarrow Y_{i,j} = \begin{bmatrix} y_{1,1} & y_{1,2} & y_{1,3} & \cdots & y_{1,n} \\ y_{2,1} & y_{2,2} & y_{2,3} & \cdots & y_{2,n} \\ y_{3,1} & y_{3,2} & y_{3,3} & \cdots & y_{3,n} \\ \vdots & \vdots & \vdots & \ddots & \vdots \\ y_{m,1} & y_{m,2} & y_{m,3} & \cdots & y_{m,n} \end{bmatrix}$$

4) Form two matrices $Y_{[n,m]}$ And from them to form two quadratures:

$$Y_{[n,m]} \Rightarrow U_{[n,m]} \text{ and } Y_{[n,m]} \Rightarrow V_{[n,m]}$$

$$U_{i,j} = \begin{bmatrix} u_{1,1} & u_{1,2} & u_{1,3} & \cdots & u_{1,n} \\ u_{2,1} & u_{2,2} & u_{2,3} & \cdots & u_{2,n} \\ u_{3,1} & u_{3,2} & u_{3,3} & \cdots & u_{3,n} \\ \vdots & \vdots & \vdots & \ddots & \vdots \\ u_{m,1} & u_{m,2} & u_{m,3} & \cdots & u_{m,n} \end{bmatrix}$$

$$\text{and } V_{i,j} = \begin{bmatrix} v_{1,1} & v_{1,2} & v_{1,3} & \cdots & v_{1,n} \\ v_{2,1} & v_{2,2} & v_{2,3} & \cdots & v_{2,n} \\ v_{3,1} & v_{3,2} & v_{3,3} & \cdots & v_{3,n} \\ \vdots & \vdots & \vdots & \ddots & \vdots \\ v_{m,1} & v_{m,2} & v_{m,3} & \cdots & v_{m,n} \end{bmatrix}$$

5) Set the variance matrices for two quadratures $\sigma_U = \sigma_V = \sigma$, where $\sigma_{i,j}$ – is the isotropic surface, with no shiny spots.

$$\sigma_{i,j} = \begin{bmatrix} \sigma_{1,1} & \sigma_{1,2} & \sigma_{1,3} & \cdots & \sigma_{1,n} \\ \sigma_{2,1} & \sigma_{2,2} & \sigma_{2,3} & \cdots & \sigma_{2,n} \\ \sigma_{3,1} & \sigma_{3,2} & \sigma_{3,3} & \cdots & \sigma_{3,n} \\ \vdots & \vdots & \vdots & \ddots & \vdots \\ \sigma_{m,1} & \sigma_{m,2} & \sigma_{m,3} & \cdots & \sigma_{m,n} \end{bmatrix}$$

6) Form a random Rayleigh field using two normally distributed quadratures, taking into account the dispersion matrix.

$$A_{[n,m]} = \sqrt{(\sigma U)^2 + (\sigma V)^2}$$

RESULTS OF COMPUTER MODELING

There are different modes of mapping, we will consider the telescopic view mode, in which the selected portion of the earth's surface is irradiated multiple times and a high resolution is obtained from the angular coordinate. In this telescopic mode, there are difficulties. For example, if the aircraft is moving fast enough, it is possible to accumulate enough probing pulses, but the elements of the underlying surface are shifted from the pulse to the probe pulse. Then we need to take into account their correlation properties. Therefore, we assume that the velocity of the carrier is such that the displacement of the elements of the underlying surface is insignificant when viewed from pulse to pulse.

We confine ourselves to mathematical modeling of the mapping process under different types of distribution laws and visually compare them. The modeling algorithm is implemented in the MATLAB package. And there is an appropriate interface, which allows you to set all kinds of mapping modes (side, line and telescopic), set the initial parameters of modes and select the type of echoshi.

We will simulate the mapping process by synthesizing the antenna aperture using a telescopic view. During the observation of the site by the earth's surface, the center of the beam shifts to the center of the observation zone, at each radiation period of the probe signal pulse.

Now, in order to observe the characteristics of the elements of the radar image resolution after the synthesis, we introduce a test image where the echo from the elements of the underlying surface will fluctuate according to the equivalent distribution laws or will be stable.

RESULTS OF COMPUTER MODELING

It is necessary to simulate a random field distributed according to the Rayleigh law arbitrary size by the algorithm given above. The results can be represented as:

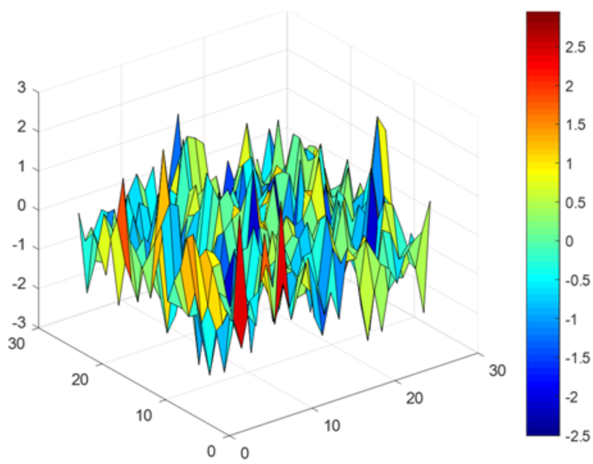

Figure 1- Random normal field

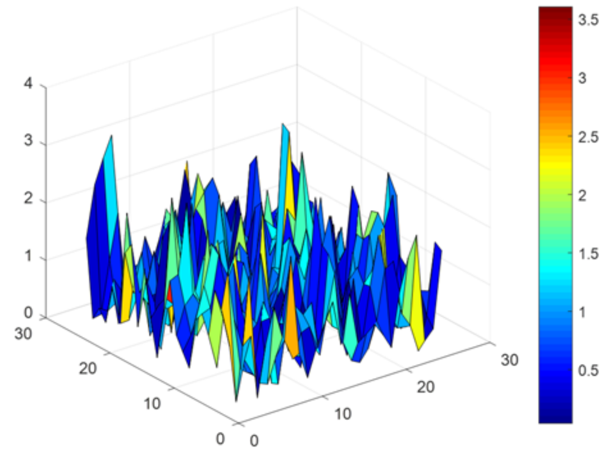

Figure 2 - The random Rayleigh field corresponds to reflections from the earth's surface

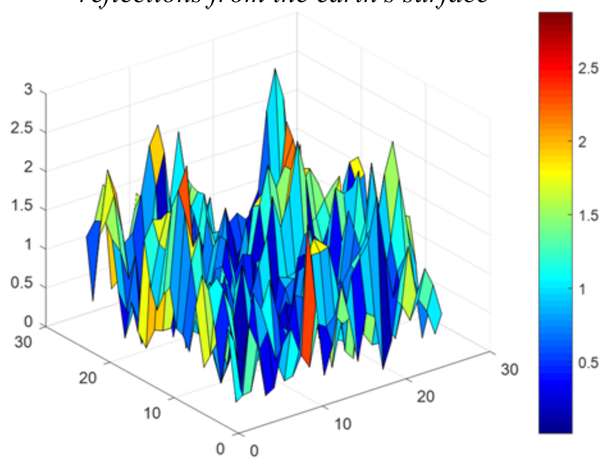

Figure 3 - The random log-normal field corresponds to reflections from the sea surface

According to the results of computer simulation, it is visually evident that the stable characteristics of the resolution elements after the operation of the radar image formation algorithm have been obtained with fluctuations of the echo signal according to the Rayleigh-Rice and Weibull distribution laws, and the worst resolution characteristics were obtained with the log-normal distribution law. Under the Rayleigh law, the results of the study were of a satisfactory nature.

CONCLUSION

Based on the results obtained, two conclusions should be drawn. From the first conclusion, it follows that the worst result is obtained with the log-normal distribution law, the best with a stable signal, whereas under the Weibull law, the particular case of which are the laws of Rayleigh and Rayleigh-Rice, the resolving characteristics are approximately the same.

Therefore, if a person wants to calculate his mapping system without even knowing the synthesizing algorithms, simulating an echo signal according to the log-normal law knows that this will give him the worst result of the radar image resolution performance, because the dispersion law is large, but it will be better if there will be other distribution laws of its characteristics.

The second conclusion is that, since some of the laws give the same result, and the Weibull law has invariance under reflections from the ground, the Weibull distribution is an excellent model for describing the echo signal.

REFERENCES

[1] V.A. Nenashev, A.A. Sentsov, G.V. Kuyumchev. Simulation of the process of formation of a high-resolution radar image in airborne radars with synthesized aperture. Questions RLT. Series of general technical № 20, 2013 year

[2] Shepeta A.P. Synthesis of nonlinear shaping filters for simulation of input signals of location systems. // Proceedings of the International Scientific and Technical Conference (reports), May 1994. - Kiev: Ukrainian Academy of Sciences, NGO Kvant. - Issue 1, p.81-85.

[3] Nenashev V. A., Shepeta A. P., Modeling algorithm for SAR image based on fluctuations of echo signal of the Earth's surface / V. A. Nenashev, A. P. Shepeta// Proc. of SPIE Remote Sensing, Vol. – Toulouse, France, 2015. – P. 96420X-1 - 96420X-8.

[4] VV Izrantsev, DA Shepeta Modeling of external signals of onboard instrument complexes of fifth generation aircraft // Izv. Higher education / Instrument making. - 2000, number 2, with a .76-83.

[5] Kondratenkov GS, Frolov A.Yu. Radio broadcasting. Radar systems for remote sensing of the Earth. - M: Radio Engineering, 2005.

[6] P.I. Dudnik, A.R. Ilchuk, B.G. Tatar. Multifunctional radar systems. - M: Drofa, 2007.

THE MODELING ALGORITHM OF ADAPTIVE KALMAN`S FILTER

Yudin Ivan

Saint-Petersburg State University of Aerospace Instrumentation,
Saint-Petersburg, Russia

E-mail: ivan-yudin@mail.ru

Abstract

Any measuring instrument has some inaccuracy, it may impact a large number of external and internal influences, which leads to the fact that obtained information will be noisy.

There are two ways of solving this problem: increasing the accuracy of measuring instruments and improvement of accuracy by statistical processing of the redundant number of measurements, which get a rating of the measured value. Improving the accuracy of measuring instruments requires a significant investment, while the statistical processing of the measurements in the presence of the computer is cheap and fast enough.

Today there are many methods of statistical processing of measurements. For dynamical systems in addition to Kalman`s filtering using filters of Wiener, Wiener-Hopf, etc. the Main advantage of Kalman`s filter is that it solves the problem in time domain, and not the frequency domain, also it is filter solution for multidimensional problems. The adaptive Kalman`s filter is currently used in many electronic and telecommunication systems. In this article, we consider the algorithm of Kalman`s filtering for estimating coordinates of the mobile object according to the navigation data from the accelerometer**.**

STATEMENT OF THE PROBLEM

Consider the problem when the data must be processed sequentially at a time on a rolling values. It is supposed to do with adaptive Kalman`s filter (picture 1).

If the random process obeys the Gauss law, the Kalman`s filter minimizes the mean square error for the extrapolated value estimates the position of an object in space. The Kalman`s filter can be generated for the coordinates of the movable object in one, two or three coordinates in one-, two - or three-dimensional measurements from the sensors the position of an object in space (gyroscope, accelerometer, and digital magnetic compass). For simplicity, further we consider the problem of filtering measurements with one sensor. Model of target movement is described as

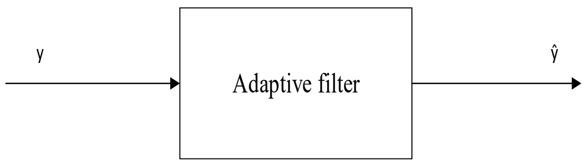

Figure 1- Schematic representation of the filter where: y – the measured value, ŷ– estimate the required values

The problem of filtering in discrete time can be solved without too much difficulty. First, we present the problem formulation in phase space:

$$\begin{cases} x(k+1) = A(k) * x(k) + v(k), k \geq k_0 \\ y(k) = C(k) * x(k) + w(k) \end{cases} \qquad (1.1)$$

where: x(k0)– not subject to direct observation, the phase vector of dimension n, x(k) – the initial value vector x(k) given the covariance matrix P(k0), y(k)– measurable vector of dimension m, A(k) and C(k) – are known matrices of appropriate dimension, v(k) – a vector of disturbances of dimension n, w(k)– error of measurements of dimension m.

Visualize in details a scheme of the filter (figure 2).

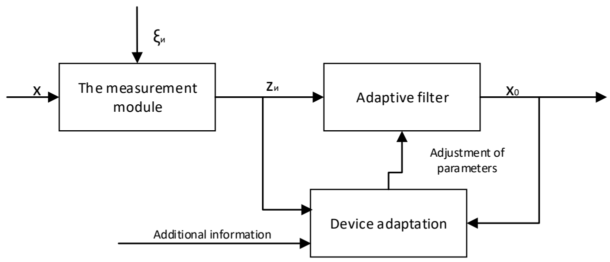

Figure 2 - Detailed view of filter

It is necessary to construct a linear unbiased estimate of x(k) based on the sequences of measurement results y(k0), y(k0+1),…, y(k). This estimate is denoted by ŷ(k).

Error estimation we define as the difference x(k) and ŷ(k):

$$\tilde{x}(k) = x(k) - \hat{y}(k) \qquad (1.2)$$

To solve the problem, it is additionally necessary to assume that there is no a priori information about the initial state of the system (P(k0)→ ∞). Then in the beginning, starting with the time instant k0, make measurements as long as the total number of separate observations will not be more than n. After that, one can make an assessment.

$$P(k_0) = \mathrm{cov}(x(k_0)) = E((x(k_0) - \\ -Ex(k_0)) * (x(k_0) - Ex(k_0))), \tag{1.3}$$

where: P(k0) - the covariance matrix of the initial state vector.

For the solution assume that the value ŷ(k) and $\hat{P}(k)$ at time k is known. Make an extrapolation of k thus the unknown disturbance ν(k) remain unaccounted for.

$$x*(k+1) = A(k) * \hat{y}(k) \tag{1.4}$$

Make an extrapolation of the value represents the totality of knowledge about the vector x(k+1). To identify the relationship between these two variables, replace

$$\hat{y}(k) = x(k) - \tilde{x}(k) \tag{1.5}$$

$$A(k) * x(k) = x(k+1) - \nu(k) \tag{1.6}$$

Get:

$$x^*(k+1) = x(k+1) - \\ -A(k) * \tilde{x}(k) - \nu(k) \tag{1.7}$$

The value representing an error $A(k) * \tilde{x}(k) + \nu(k)$ can be combined into a covariance matrix, we denote it P*(k+1).

$$P^*(k+1) = \mathrm{cov}(A(k) * \tilde{x}(k) + V(k)) = \\ = \mathrm{cov}(A(k) * \tilde{x}(k)) + \mathrm{cov}(V(k)) = \\ = A(k) * \tilde{P}(k) * A'(k) + Q(k), \tag{1.8}$$

where: P(k)– the covariance matrix of estimation errors, Q(k)– the covariance matrix of the error disturbances.

Then P*(k+1) can be interpreted as the error matrix extrapolation:

$$P*(k+1) = \mathrm{cov}(x^*(k+1) - x(k+1)) \tag{1.9}$$

Making multiple transformations, obtain the following 3 equations filter.

$$\hat{y}(k) = x^*(k) + K(k) * (y(k) - C(k) * x^*(k)) \tag{1.10}$$

$$P^*(k) = \tilde{P}(k) + K(k) * C(k) * P^*(k) \tag{1.11}$$

$$K(k) = P^*(k) * C'(k) * (C(k) \\ * P^*(k) * C'(k) + R(k))^{-1}, \tag{1.12}$$

where: R(k)– the covariance matrix of the measurement errors, K(k)– matrix gain.

Thus the goal is achieved. The result is identical to the algorithm of Kalman\`s filter.

THE USAGE OF THE KALMAN\`S FILTER

Numerical implementation of the filtering algorithm consists of the following steps:

- At the first stage existing estimate and its covariance matrix are extrapolated to the next interval.

$$x^*(k+1) = A(k) * \hat{y}(k), \tag{2.1}$$

$$P^*(k+1) = A(k) * \tilde{P}(k) * A'(k) + Q(k). \tag{2.2}$$

- The following calculates the optimal gain matrix K and design estimation is improved using the new observations.

$$\hat{y}(k) = x^*(k) + K(k) * \\ *(y(k) - C(k) * x^*(k)). \tag{2.3}$$

$$K = \frac{P^*(k) * C'(k)}{C(k) * P^*(k) * C'(k) + R(k)} \tag{2.4}$$

- The last stage is determined by the covariance matrix of the new modified assessment.

$$\tilde{P}(k) = P^*(k) - K(k) * C(k) * P^*(k) \quad (2.5)$$

The initial conditions are defined as follows. In the initial time k0 is the first observation of y(k0). Before constructing a first assessment

$$\hat{y}(k_0) = \frac{C' * R^{-1}}{C' * R^{-1} * C} * y(k_0) \tag{2.6}$$

and determines a value of the covariance matrix $\tilde{P}(k_0)$:

$$\tilde{P}(k_0) = \frac{1}{C' * R^{-1} * C}. \tag{2.7}$$

These expressions form the initial conditions for the recurrence formula.

The biggest advantage of the Kalman\`s filter to estimate the coordinates of the movable object is that it guarantees a regular calculation of the gain of the filter. The main disadvantage is that when calculating the gain factor model of target movement is allowed with random linear measurements. In real situations the movement of the object may differ from a linear model of motion. In these cases, the Kalman\`s filter is adjusted by adjusting the covariance matrix Q for an unknown random maneuver of the object.

A RESEARCH OF THE REAL PRECISION

Using of simulation, computer modeling studies of the real accuracy of the estimates of phase coordinates of the tracked object. Simulation on a computer is a simulation of the input signals zи(k) and the processing of these signals by using algorithms. Simulation input zи(k) represents a change of the phase coordinates of the true and noise observations ξи. Noise monitoring ξи simulated with random numbers. Knowledge of the real error filtering allows us to assess the capacity of the developed filter algorithms in conditions close to real. Real accuracy is assessed by standard deviation estimates of phase coordinates by the number at least 100 realizations of formula

$$\sigma_{x_p}(k) = \sqrt{\frac{\sum_{j=1}^{N}(x(k) - x_{oj}(k))^2}{N-1}} \qquad (3.1)$$

where: $\sigma_{x_p}(k)$ - the average quadratic error of estimation of the phase coordinates of the target; $x_{oj}(k)$ - estimated values of the phase coordinates of the target j-th realization; N – number of realizations.

SIMULATION MODEL AND RESULT OF KALMAN`S FILTER

To study the algorithm performance in the Matlab/Simulink program was developed for simulation modeling. The program consists of 3 units: a sensor simulator (model of the accelerometer), the Kalman`s filter, the block of determining the accuracy of measurements.

The first block simulates the movement of the target relative to the stations, calculating the current values of range, bearing and elevation angles of the target. Values are summed with noise, thus simulates the work of the respective channels of observations. The statistical processing unit is designed to assess the quality of the filter when multiple implementations of the session measurements. The data obtained in the simulator, and the evaluation algorithm compares and calculates the root mean square error of estimation.

The core in the simulated system is considered as inertial system consisting of the accelerometer and Kalman`s filter. Determine the impact of sensor noise on the output of the system and evaluate the performance of the filter.

We show the algorithm of Kalman`s filtering, for example. Suppose that a sensor should produce a clean sine wave with amplitude equal to 5, and frequent 50 rad/sec. Let the variance of the white noise is 9. Then the resulting values will be the following:

Simulate the system (Picture 3) and check its performance.

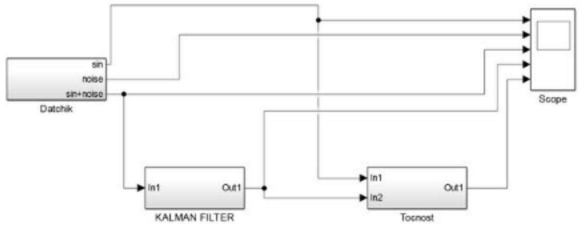

Figure 3 - Diagram of the Kalman filter in Matlab/Simulink

The simulation diagrams (figures 4 - 9):

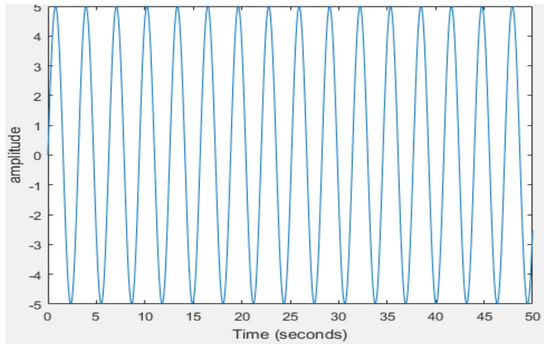

Figure 4 – signal sin coming from the sensor

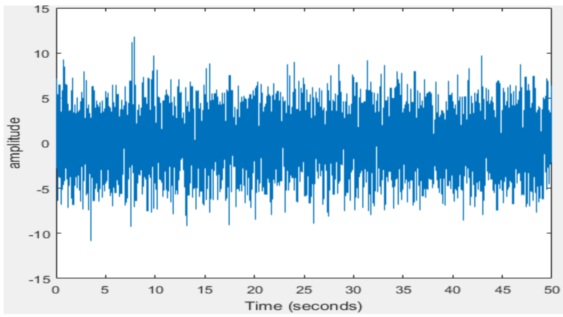

Figure 5 – white noise, which will be mixed with the desired signal

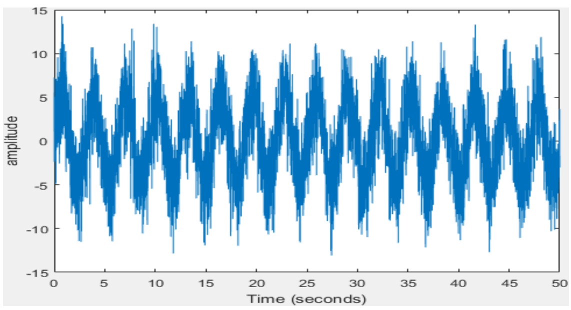

Figure 6 – desired signal along with noise

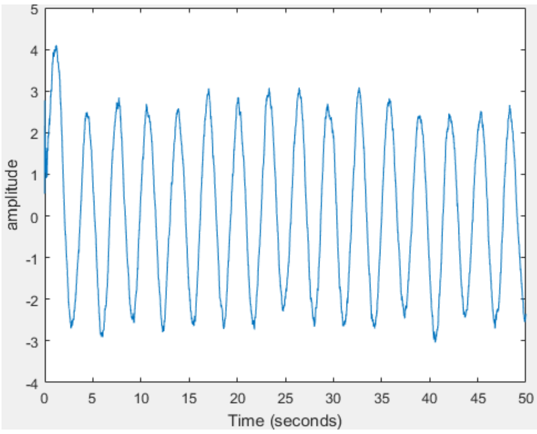

Figure 7 – the signal obtained at the output of the filter

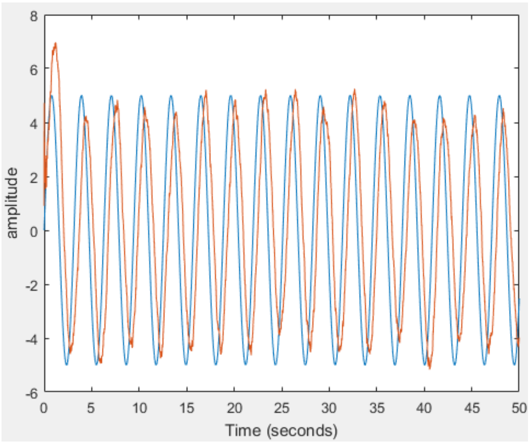

Figure 8 – the output signal amplified by 1.7 times, superimposed on the input

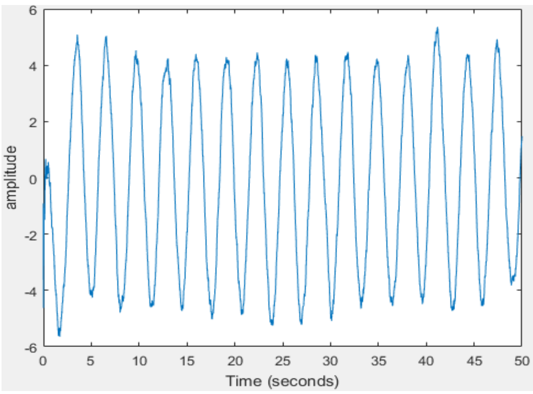

Figure 9 – the difference between the input and output signal

As can be seen from the graphs, the filter adequately removes the noise signal. When calculating standard deviation, its value was 3.75.

PROSPECT FOR THE DEVELOPMENT OF THEM

The first possible development of the theme is to use multiple Kalman`s filters. This approach of using the interactive multi-model filters, each tuned to a predetermined model of the movement of the object in interactive multimode models operate at the same time; however, they are not used independently. Is it the mixing of the values of estimated for each model movement. The update equation for each model movement depends not only on the i-th model state but also from condition of all other motion models. These results are mixed with using the calculated probabilities of transition from one model to another.

The second branch of development in the refinement of estimates of the measured coordinates are the methods of aggregation.

CONCLUSION

The expediency of using Kalman filtering has been shown in navigation systems. The presented results provide the necessary processing algorithms and measurement data of inertial sensors that can directly be used by developers of Autonomous systems high-precision positioning of a person on the ground.

According to the results of the developed set of programs it is possible to formulate recommendations on changes to the software signal processing system for Autonomous navigation. The model can be easily adapted for testing the algorithms in real time

REFERENCES

[1] A. Yu. Gorbachev Criteria for the evaluation of algorithms for optimal filter // Aerospace instrumentation, No. 6, 2008

[2]Dan S., Baojun Zh., Linbo T. A Tracking Algorithm Based on SIFT and Kalman Filter // In Proceedings The 2nd International Conference on Computer Application and System Modeling. 2012.

[3] Greg Welch, Gary Bishop, «An Introduction to the Kalman Filter», 2001

[4] M.S.Grewal, A.P. Andrews, «Kalman Filtering — Theory and Practice Using MATLAB», Wiley, 2001

[5] Stratonovich, R.L. (1959). Optimum nonlinear systems which bring about a separation of a signal with constant parameters from noise. Radiofizika.

MODELING AND INVESTIGATION OF THE COMPRESSION CHARACTERISTICS OF LFM AND NLFM SIGNALS

Zhuravlev Artemij

Saint-Petersburg State University of Aerospace Instrumentation,
Saint-Petersburg, Russia

E-mail: artemijzhuravlev@yandex.ru

Abstract

The purpose of this article is to investigate the effect of compression of NLFM and LFM signals. Compression algorithms in the frequency and time domains are considered. A comparative analysis of compression characteristics is carried out.

INTRODUCTION

Using radar stations with pulse compression makes it possible to have high accuracy in measuring radar target parameters, high energy potential, and also high resistance to passive interference. Using NLFM and LFM signals makes it possible to simplify the digitization of radar data.

Due to this, they can be used in radiotomography. The main task of radiotomography is a remote, non-contact study of hidden objects and their internal structure. radiotomography systems can be used in security systems for screening people in order to prevent the transport of prohibited items.

Also radiotomography can find application in systems of quality control and integrity of industrial products. Radio wave methods are relatively safe for humans and allow us to detect a wide class of objects, including dielectric ones. However, it is generally not possible to completely get rid of the interfering effects, therefore, usually they talk about different quality indicators, in turn, the compressed signal (shown in Fig. 1) customary estimated by the ratio of the main lobe level / side lobe level and the main lobe width.

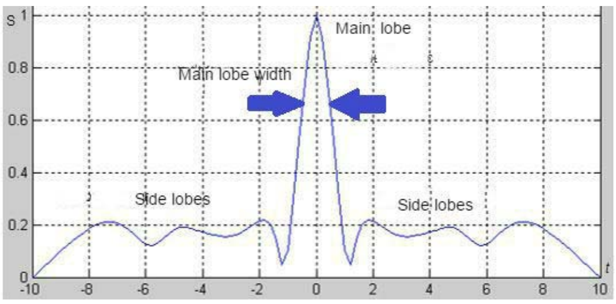

Fig. 1 – Characteristics of compressed signal

FORMULATION OF THE PROBLEM

Let us study the characteristics of the compression of LFM and NLFM pulses. To do this, consider their mathematical models and compression algorithms in the frequency and time domains.

MATHEMATICAL MODELOF LFM AND NLFM SIGNALS

Model of signal generation with linear frequency modulation:

Linear frequency modulation can be represented as:

$$s(t) = A*cos\ (2\pi f_c t+\pi*B/\tau*t^2+\varphi_0) \qquad (1)$$

where A – the amplitude of the signal, $f_c - the$ carrier frequency , B – the width of the partial pulse band, τ – the pulse width, φ_0 – the initial phase.

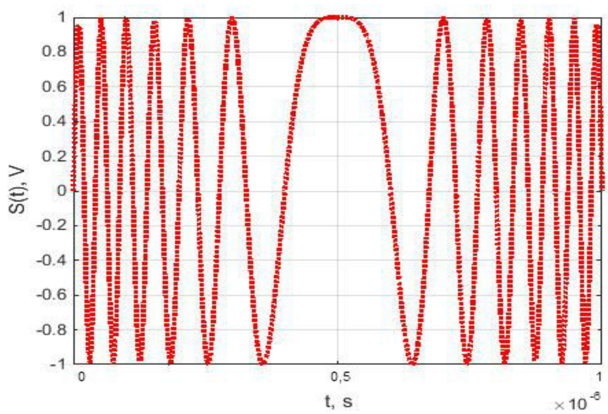

Fig.2– LFM-signal

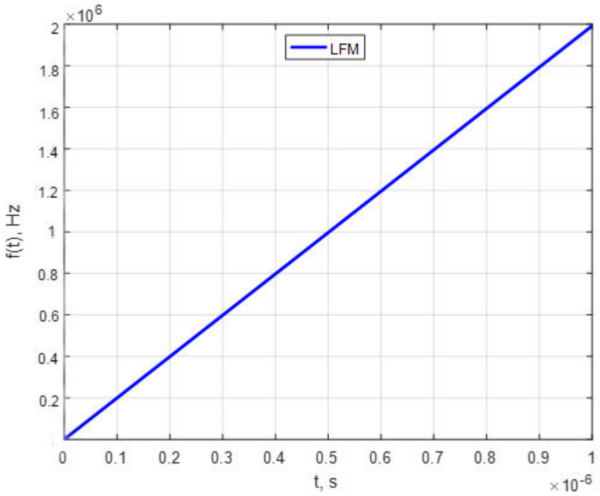

Fig.3 – Law of frequency variation for LFM

Model of signal generation with non-linear frequency modulation:

There are different versions of the laws of nonlinear frequency modulation. In this paper, we investigate the harmonic law of NLFM, defined by the following equation:

$$\omega(t) = \omega_0 + \beta t + \Delta\omega \sin \Omega t, \qquad (2)$$

where $\omega_0 = 2\pi f_0$ – Initial circular frequency, f_0 – Initial linear frequency, $\beta = \omega_d / t_u$ – rate of change of the circular frequency, $\omega_d = 2\pi f_d$ – circular frequency deviation, $\Delta\omega$ – the value of the maximum increment to the law of frequency variation, Ω – frequency of change in the law of intrapulse modulation. While changing the frequency in accordance with the positive speed β, the phase is change according to the law:

$$\varphi(t) = \omega_0 t + \frac{\beta t^2}{2} - \frac{\Delta\omega}{\Omega} \cos \Omega t \qquad (3)$$

By adopting $m = \dfrac{\Delta\omega}{\Omega}$ rewrite expression:

$$\varphi(t) = \omega_0 t + \frac{\beta t^2}{2} - m \cos \Omega t \qquad (4)$$

When the signal phase changes, the LFM pulse will be described by the expression:

$$S(t) = \begin{cases} S_m \cos\left(\omega_0 t + \dfrac{\beta t^2}{2} - m \cos \Omega t\right), 0 > t > t_u \\ 0, t_u > t \end{cases} \qquad (5)$$

As a result of the simulation, a NLFM signal is synthesized, it is depicted in Fig. 4

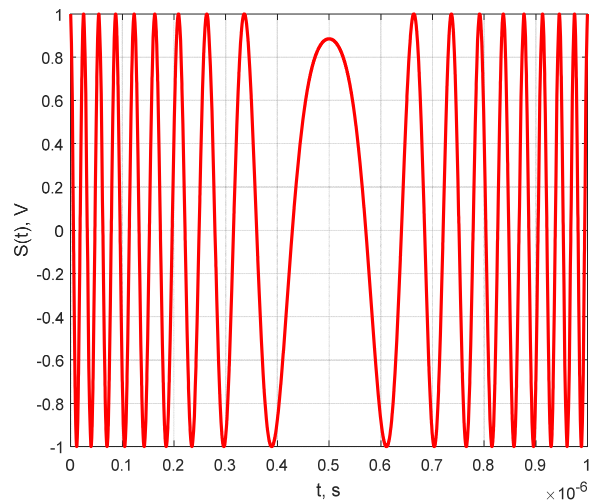

Fig. 4 –NLFM-signal

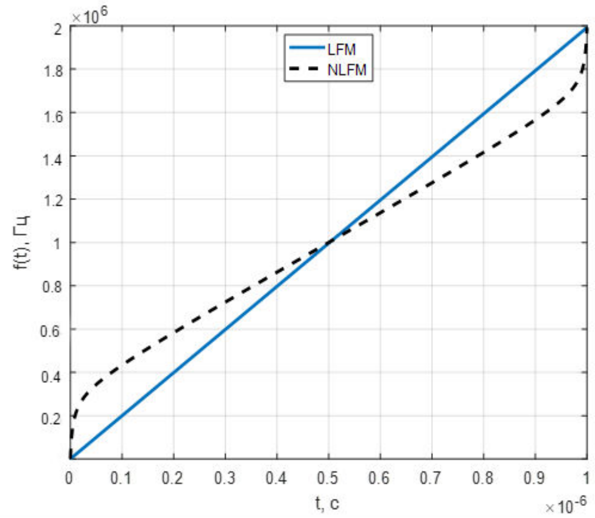

Fig. 5 – Law of frequency change for NLFM

COMPRESSION ALGORITHMS

Figure 6 shows two approaches in digital signal processing to implement a matched filter that provides signal compression. In these cases, the input signal is a sequence of samples of a complex envelope formed using either a digital down-conversion or an analog multiplier followed by an analog-to-digital conversion in each baseband channel.

Figure 6a shows the implementation of a digital process providing convolution of signals in the time domain, which determines the efficiency of the matched filter for any signal used in the radar station. In this case, the discrete convolution is performed in the time domain by convolution of the input sequence of samples of the complex envelope after the digital down conversion of the frequency and the sequence of samples of the impulse response of the matched filter.

Convolution in the time domain can be associated with laborious calculations, so a more cost-effective approach from the point of view of computational complexity is shown in Figure 6b, in which processing in the frequency domain is used to perform the convolution. The digital signal compression process in the frequency domain operates based on the properties of the Fourier transform, according to which the convolutions of two time sequences are equivalent to the product of the discrete Fourier transforms of each of the sequences.

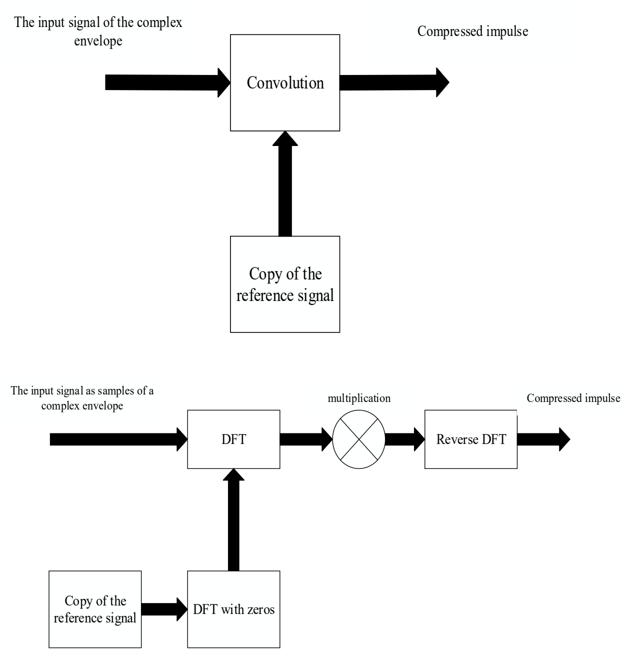

Fig.6: a – Digital time-domain pulse compression processor; b - The digital pulse compression processor in the frequency domain

SIMULATING RESULTS

Let's begin to investigate the impact on the LFM signals. LFM signals have an interesting property. If the signal is applied to a frequency-dependent delay line whose signal delay time is large at low frequencies (in the initial part of the LFM signal) and decreases as the frequency increases in the chirp signal, then the output of such a line "compresses" the signal in one period High-frequency oscillation by summing the amplitude values of all signal periods. In this case, the amplitude of the output signal increases and the statistical noise decreases, since the noise, which are simultaneously summed for the same periods, is not correlated.

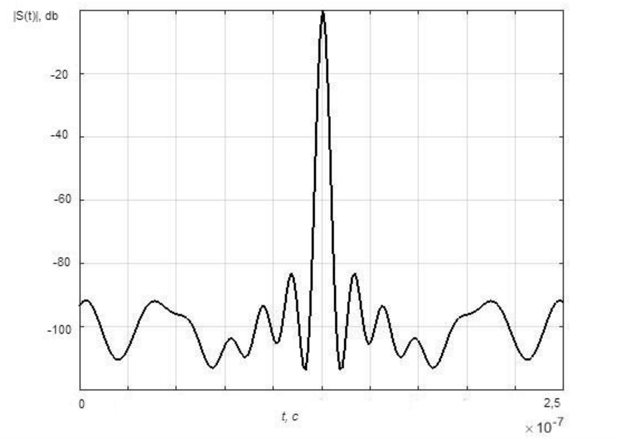

Fig.7 – LFM signal after compression

Next, we will investigate the characteristics of the NLFM signal:

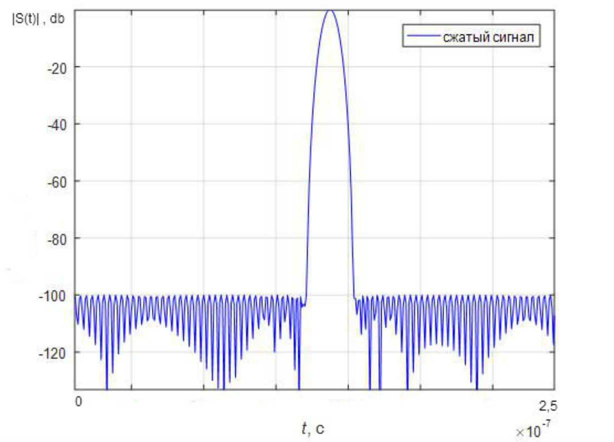

Fig.8 – NLFM signal after compression

RESULTS

Table 1

Signal	LFM	NLFM
Main lobe / side lobes	85 Db	100 Db
The width of the main lobe, at -80 dB	$0{,}11*10^{-7}$	$0{,}3*10^{-7}$

CONCLUSION

The models of Frequency Modulated signals, as well as models of compressed LFM and NLFM, are obtained.

The main characteristics of signals after compression, their comparison are considered. Based on this comparison, we can say that these signals differ little with such parameters, however, the NLFM signal shows itself better than LFM according to the results of table 1. The simulation results obtained in this work are of great importance in studies related to noise immunity of transmitted information in communication channels, interference prediction and the choice of the characteristics of communication systems under disturbing conditions.

REFERENCES

[1] Беседа .А.Л., Бестугин А.Р., Гладкий Н.А., Король М.В. и др. под редакцией Синицына Е.А. «Цифровые методы формирования и обработки сигналов в РЛС управления воздушным движением» 2011, 186 стр.

[2] Дудник П.И., Ильчук А.Р., Татарский Б.Г. «Многофункциональные радиолокационные системы». Изд-во «Дрофа» , 2007, 283 стр.

[3] Сколинк М.И., перевод Вербы В.С. «Справочник по радиолокации.Книга 1» Москва:Техносфера, 2014, 672стр.

[4]Свистов В.М. «Радиолокационные сигналы и их обработка». Изд-во «Советское радио», 1977,448 стр.

CONTENTS

The scientific edition

BULLETIN OF THE UNESCO DEPARTMENT
“DISTANCE EDUCATION IN ENGINEERING” OF THE SUAI

Collection of the papers
Issue 2

Computer imposition

Papers are publish in author's edition

Подписано в печать 10.04.2017. Формат 60x84 1\8.
Усл. печ. л. 14,4. Тираж 150 экз. Заказ № 135.

Редакционно-издательский центр ГУАП
190000, Санкт-Петербург, Б. Морская ул., 67

Department of operative polygraphy
SUAI
190000, St. Petersburg, st. B. Morskaya, 67